Environmental Monitoring of Jharia Coalfield, Jharkhand, India, using Multi-polarization SAR and Interferometric SAR data

Thesis submitted to Andhra University
In partial fulfillment of the requirements for the award of
Master of Technology in Remote Sensing and Geographic Information System

ANDHRA UNIVERSITY

Submitted By:

Ritwik Majumdar

Supervised By:

Dr. R.S. Chatterjee

Geosciences Division

iirs

Indian Institute of Remote Sensing

Indian Space Research Organization
Dept. of Space, Govt. of India,
DEHRADUN – 248001
UTTARAKHAND, INDIA

May, 2013

Abstract

In the present study, an attempt has been made to detect and delineate land subsidence phenomena due to coal fire and or mining related activities and also the various environmental parameters said to be affecting the environmental hazard in the Jharia coalfields, using high resolution space borne optical and synthetic Aperture Radar data. Microwave remote sensing has an unique capability to detect the surfacial features in terms of terrain sensitivities and scattering properties of the radar wave from the terrain features. It can also able to detect slow surface movement in terms of uplift or subsidence. Various ground based techniques, such as differential GPS and optical leveling study for land subsidence has also been utilized for evaluation and validation of space borne measurements.

Among the various space-borne techniques available till date, to detect and delineate ground deformation, Differential Interferometric SAR (D-InSAR) is considered to be the most efficient technique for measuring spatially-continuous ground deformation. In this work, satellite-based D-InSAR technique has been employed to identify the areas affected by land subsidence and to measure precisely the rate of land subsidence in order to prepare a spatially continuous land subsidence map for the 2003-2007 time period.

The precision and feasibility of D-InSAR technique is largely controlled by the quality of InSAR data pairs, wavelength of the SAR signal as well as the changes in the terrain over the time. In the present study, ENVISAT ASAR C-band data has been used for differential InSAR processing. SRTM 90m resolution Digital Elevation Model of the study area has been used for topographic phase compensation for generating the differential interferograms. From InSAR based observation during 2003-2007 period over Jharia coalfield, it has been observed that the land subsidence along Jayrampur, Barora, Govindpur, Dobari, East Bassuriya areas, are mostly due to surface or sub-surface coal-fire. There are few instances of subsidence caused by depillaring of the old and abandoned underground mines e.g. Sudamidh. Ground based differential GPS and optical leveling observation of the selected four test sites (Dobari, Bassuriya, Jayrampur & Sudamdih) confirms horizontal and vertical land movement in terms of subsidence or uplift and horizontal strain.

For geo-environmental hazard monitoring, identification of the environmental parameter for a typical opencast coal mining area, were selected and using high resolution optical and InSAR based digital elevation model and their derivatives were used to delineate the said parameters.

It has been observed that the InSAR based digital elevation model though coarser than the high resolution optical stereo DEM, is very useful for delineation of opencast, abandoned coal mines, overburden dump‘s boundary due to its high sensitivity towards the terrain parameters. Optical stereo digital elevation model due to its high spatial resolution, were very useful to delineate the smaller features like coal dumps.

Mapping of environmental parameters using alternate-polarization C-band space borne ENVISAT ASAR data, based on their scattering properties, randomness of the scattering process (entropy) in different polarizations (HH-, VV- and HV-) has been studied, comparing the standard deviation values of backscattering coefficient for different environmental parameters reveals that the overall backscattering response of the environmental parameters in co-polarizations (HH and VV) is closely similar, however settlement and vegetation shows fresnel type surface scattering and overburden dumps, coal dumps, abandoned/closed mines shows dominantly *bragg* type surface scattering. In cross polarization (HV-), the mean backscattering response is high in case of settlements, vegetation and functional opencast mines; moderate in case of agricultural land, barren land and functional opencast mines followed by fallow land and coal washeries; and low in case of water body and abandoned/closed opencast mines. The backscattering strength in cross-polarization is due to two main scattering processes: volume scattering as a function of dielectric inhomogeneity and multiple (surface) scattering as a result of strong variation in surface geometry or terrain ruggedness.

Keywords: Differential SAR interferometry (D-InSAR), ENVISAT ASAR, land subsidence, differential GPS, optical leveling, geo-environmental parameters, digital elevation model, alternate polarization, scattering mechanism, Jharia coalfield, India

Acknowledgements

I would like to thank all the people without their support, this project work would not have been successful.

Firstly, I am grateful to Dr. Y.V.N. Krishnamurthy, Director, Indian Institute of Remote Sensing Dehradun (IIRS), Dr. P.S. Roy, former Director, Indian Institute of Remote Sensing(IIRS) Dr. S.K. Saha, Dean-Academics, Indian Institute of Remote Sensing Dehradun (IIRS) & Dr. V.K. Dadhwal, Director, National Remote Sensing Centre (NRSC),Hyderabad for giving me an opportunity to undertake M. Tech. course at IIRS. I also express my strong gratitude for their kind support, timely guidance and facilities provided to me for carrying out the project successfully.

I express my sincere thanks to Dr. R .S. Chatterjee, Scientist 'SF', IIRS for his constant encouragement and close guidance that added a new dimension to my knowledge in SAR technology for detecting & delineating ground deformation & its limitations. His continuous support and assistance have indeed proved to be the guiding force in all my endeavors.

My sincere thanks are due to Dr. P.K. Champatiray, Head, Geosciences Division & Prof. R. C. Lakhera (former Head, Geosciences Division), IIRS for permitting me to use the lab facilities throughout the project and their continuous support and guidance regarding all the technical and non-technical issues during this tenure. I also like to thank other faculty members of Geosciences Division, of IIRS, late Prof. V.K Jha (former faculty, Geosciences Division), Dr. S.K. Srivastav, Dr. I.C. Das, who have directly or indirectly helped me in course of time.

I like to thanks Dr. Shefali Agarwal, Head, Photogrammetry & Remote Sensing Division, IIRS, Dr. Anil Kumar & Sri Ashutosh Bharadwaj for their continuous help & support in learning the intricacies of DEM generation and DGPS processing.

I also take this opportunity to express my sincere and humble thanks to Dr. Varun kumar and his team from Survey Of India, Dehradun for carrying out the DGPS survey during the field work and also their guidance to learn DGPS data processing technique & survey methods. I would also like to convey my special thanks to Dr. K. V. Singh of Central Mining & Fuel Research Institute, Dhanbad and his team to carry out optical leveling during the fieldwork. I am indebt to Shri K. V. R. Raju and his team of Bharat Coking Coal Limited, Dhanbad for providing the logistic support and also for providing the mine surface plans for different mine areas.

I would like to acknowledge the help provided by Geological Survey of India, Coal wing, Kolkata personnel for providing the relevant technical document on coal mining and exploration in Jharia coalfield.

I like to express my sincere gratitude to my parents & Vidya, for their continuous persuasion and encouragement to complete the thesis.

Last but not the least, I like to thank the entire Geosciences family of National Remote Sensing Centre, Hyderabad for their continuous encouragement and pursuance to complete my thesis.

Place: Hyderabad
Date: May,2013

Ritwik Majumdar

CERTIFICATE

This is to certify that Mr. Ritwik Majumdar has carried out the dissertation entitled "Environmental Monitoring of Jharia Coalfield, Jharkhand, India, using Multi-polarization SAR and Interferometric SAR data" for the partial fulfillment for the award of degree of Master of Technology (M. Tech.) in Remote Sensing and GIS. The project has been carried out in Geosciences Division under the guidance of Dr. R.S. Chatterjee, Scientist 'SF' at Indian Institute of Remote Sensing, Dehradun, India.

Dr. R.S. Chatterjee
Project Guide

Dr. P.K. Champatiray
Head, Geosciences Division

Dr. S.K. Saha
Dean (Academics), IIRS

Dr. Y.V.N. Krishnamurthy
Director, IIRS

Contents

3. Principle of land subsidence

4. Land subsidence: measuring tools and techniques

5. Materials and Methods

CHAPTER 1

INTRODUCTION

1.1 Introduction

Land subsidence is lowering of the land-surface elevation from changes that take place underground. The exploitation of subsurface resources has increased many fold during the last century and related to this, a large number of subsidence occurrences have occurred in various parts of the world. This phenomenon involves the settlement of the ground surface and affects wide areas. Civil structures built on these areas must withstand these vertical (and sometimes horizontal) ground deformations, and widespread damage occurs when differential settlements cannot be accommodated beneath their foundations. Land subsidence has become a global environmental and economic problem which specifically includes: (1) changes in elevation and slope of streams, canals, and drains; (2) damage to bridges, roads, railway tracks, storm drains, sanitary sewers, canals, and levees; (3) damage to private and public buildings; and (4) failure of well casings from forces generated by compaction of fine-grained materials in aquifer systems. Even if land subsidence does not have the same catastrophic impact as other more sudden natural events like flooding or earthquakes, the environmental and economic impacts cannot be neglected.

Recent developments in satellite geodesy techniques, by using spaceborne Differential Interferometric Synthetic Aperture Radar (D-InSAR), introduced a new tool to detect and measure subtle vertical displacements (cm to sub-centimeter level). Various workers has used this technique for monitoring long-term land subsidence phenomenon (Zebker *et al*., 1986, 1992; Gabriel *et al* 1989;Goldstein *et al.,* 1993,1995; Rosen *et al*., 1996: Galloway *et al*., 1998; Massonnet *et al*., 1993,1997,1998; Strozzi. *et al* 2001; Amelung *et al*., 1999,2000; Franceschetti et al 1999; Ferretti et al.,1999.2000,2001,2005;Rosen *et al*., 2000;Usai 2001; Colesanti *et al*., 1999,2001; Hansen *et al*., 2001,2002,2005; Fruneau and Sarti, 2000; Berardino *et al*., 2002; Crosetto *et al*., 2002,2003; Lanari *et al*., 2004; Chatterjee *et al*., 2006, Raucoules *et al*., 2007;Hooper *et al*., 2007 & 2008;). Among the various space-borne techniques available till date for measuring ground deformation, D-InSAR technique is considered to be the most efficient way for measuring spatially-continuous ground deformation with higher precision. The precision and feasibility of D-InSAR technique is largely controlled by the quality of InSAR data pairs, in terms of baseline and wavelength of the SAR signal.

In this study, an integrated measurement and monitoring approach has been attempted using space-borne D-InSAR technique, along with differntial GPS and optical leveling based measurements. A satellite-based Differential Interferometric Synthetic Aperture Radar (D-InSAR) technique has been employed to identify the areas affected by land subsidence and an attempt has been made to measure precisely the rate of land subsidence phenomenon in order to prepare a spatially continuous land subsidence map during the 2006 and 2008 for Jharia coalfield, India.. SRTM 90m resolution DEM of the study area has been used for topographic phase compensation for generating the differential interferograms. Differential GPS-based measurements were carried out by Geodetic division of Survey of India, Dehradun and the optical leveling based measurements were carried out by the Central Mining & Fuel Research Institute (CMFRI), Dhanbad. Bharat Coking Coal Ltd (BCCL), Dhanbad has provided logistic support and ancillary data regarding the colliery boundary, mining parameters and construction of survey monument for the four test areas where subsidence is taking place due to coal fire, underground mining, depillaring of the old underground mines respectively.

1.2 Study area

Jharia Coalfield is located in Dhanbad district of Jharkhand state, India and lies between latitudes 23°35′ and 23°55′ N and longitudes 86°05′ and 86°30′E. The coalfield is about 40km long from west to east and 25 km in width from north to south with an aerial coverage of about 450 sq km. the details about the Jharia basin is discussed chapter 2.

1.3 Relevance of the study

Mining history goes back to the last century in Jharia coalfield (JCF), which is one of the richest coal reserve in India. There are number of environmental hazard which has incorporated due to the coal mining in the area, e.g. coal fire, ground subsidence, acid drainage.

There are number of studies carried out by Central Mine & Fuel Research Institute (CMFRI), Central Mine Planning & Development Ltd. (CMPDL) as well as Bharat Coking Coal Ltd. (BCCL) to monitor and mitigate these environmental issues from ground based observation.

The current project is an integrated approach to detect and delineate ground subsidence from both space and ground based observation. Geosciences division of Indian Institute of Remote Sensing, Dehradun was responsible for analysis Interferometric SAR data using DInSAR technique for detection and delineation of ground subsidence, whereas CMFRI and Survey of India (SOI),Dehradun were responsible to carry out optical leveling and DGPS survey in the four selected test sites of BCCL colliery for vertical and lateral movement respectively of the ground over time.

1.4 Objectives

The main objective of the present research are as follows:

1. Detection and delineation of ground subsidence using DInSAR technique and result validation from ground based DGPS and Optical levelling results.
2. Digital elevation model generation using high resolution optical stereo data as well as interferometric data, for terrain characterization and validation of result from available ASTER and SRTM data.
3. Characterization of different environmental parameters and their response to the active microwave backscatter in terms of scattering mechanism.

1.5 Environmental Indicators

The concept of sustainability /sustainable development in respect of the use of environmental resources includes the notion that the outputs derived, whether they are from land, water or air can be produced continuously over time, and that a balance can be achieved between the rate of economic growth, their use & environmental quality, which minimizes the risk of long term degradation. A sustainable development practice is one which is sensitive to ecological constraints and seeks to minimize the undesirable effects of exploitation and use which might impact negatively on the longer term viability of a resource. It is also one, in which the full economic and environmental replacement costs associated with the use of a resource should be met.

Remote sensing measures of many physical aspects of the environment and therefore can play a role in the measurement of Sustainable Development Indicators (SDI). Becker's (1997) approach to providing criteria/definitions for developing indicators in terms of time and space shown in table 1, which have been compiled with reference to the work of a number of scientists, are very relevant to develop SDI for physical aspects of the environment, that can be determined by remote sensing and that should be suitable for contributions to a frameworks approach to SDI's in the future. The complexity of defining the sustainability indicators is revealed by the sets of criteria shown in the Table 1.

Table 1. :Criteria for the selection of Sustainability Indicators (after Becker 1997) and adapted for their relevance to remote sensing

1. Scientific Quality	2. Ecosystem relevance	3. Data Management	4. Sustainability Paradigm
• 1.1 Indicators really measures what it is supposed to detect • 1.2 Indicators measures significant aspect • 1.3 Problem specific • 1.4 Distinguishes between causes and effects • 1.5 Can be reproduced over time • 1.6 Uncorrelated, independent • 1.7 Unambiguous	• 2.1 Changes as the system moves away from equilibrium • 2.2 Distinguishes agro-systems moving away from sustainability. • 2.3 Identifies key factors leading to unsustainability. • 2.4 Warning of irreversible processes • 2.5 Proactive in forecasting future trends • 2.6 Covers full cycles through time • 2.7 Corresponds to aggregation level • 2.8 Highlights links to other system levels • 2.9 Permits trade-off detection and assessment between system components and levels • 2.10 Can be related to other indicators	• 3.1 Cost effective • 3.2 Data availability • 3.3 Quantifiable • 3.4 Representative • 3.5 Transparent • 3.6 Geographically relevant • 3.7 Relevant to users • 3.8 User friendly • 3.9 Widely accepted • 3.10 Easy to measure • 3.11 Easy to document • 3.12 Easy to interpret • 3.13 Comparable across borders over time	• 4.1 What is to be ' sustainable? • 4.2 Participatory definition • 4.3 Adequate rating of single aspects • 4.4 Resource efficient • 4.5 Carry capacity • 4.6 Health Protection • 4.7 Target values • 4.8 Time horizon • 4.9 Social welfare • 4.10 Equity

It is well known that in many cases remote sensing, due to the regional & temporal coverage of the data, can measure these variables more economically than other field based or manual methods. It is necessary to identify those indicators/ parameters that can be measured reliably on a regular basis by remote sensing, without bias and truly reflect the characteristics of the environment when it is changing.

CHAPTER 2

JHARIA BASIN

2.1 Geology

The Jharia coal basin is the second coalfield in the chain of Damodar Valley coalfield, roughly elliptical in shape and extends over an area of approx. 450 sq. km (Fig. 2.1.1).

The coalfield consists of four major sedimentary formations namely Talchir, Barakar, Barren Measures & Ranigunj. The lowermost Talchir is devoid of any coal bearing formation and lies outside the mining area of the coalfield. The Barakar and the Ranigunj are the only two coal bearing formations, of which the former is exposed all along northern and north-eastern part of the sedimentary basin (Fox.1930). In Barakar Formation, the extraction of coal is being carried out mostly by opencast method. Thus the discontinuity between Barakar & Barren Measures is easily demarcated as two different clusters which are not only differ from one another by its geological sequence but also in the method of mining. Some of the underground mines situated in the central and south-eastern part of the basins are worked in the Barakar, overlained by Barren Measures. The deposition of the coal seams, their characteristics and nomenclature in the Barakar formation follows the sickle shape of the coalfield, varying from WSW-ENE on the western part to E-W in the central and N-S in the eastern side with a varying dip of 10-15º (Mukhopadhyay 1981).

Jamunia, Khudia, Katri, Elra Kari Jore ad Chatkari Jore are the six major river/drainage flowing from north to south over the basin and enters into the Damodar river, which flows west to east . All these streams are seasonal and gets dried up during the summer season. There are also some smaller nalah/jores which are tributaries of the aforesaid streams.

2.2 Structural lineament

Lineament is an important geological feature in coal field areas, as it has an important role in guiding mine planning and safety. In fire affected coal fields like Jharia Coalfield, the nature of lineament-fault pattern is of particularly important to understand possible nature of fire propagation.

The sediments of Jharia Coal Basin bears signatures of different deformational structures like fold and faults which have a greater influence in understanding the coal mining techniques.

.

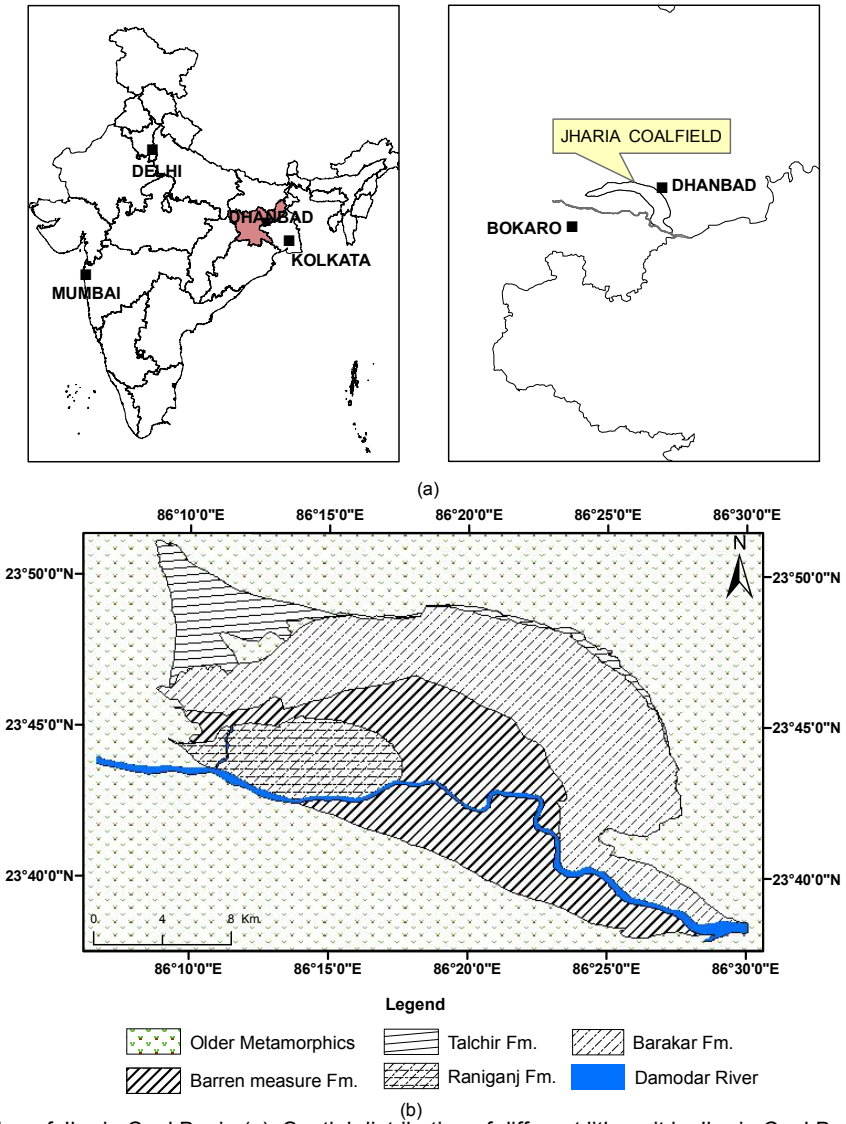

Fig. 2.1.1 Location of Jharia Coal Basin (a); Spatial distribution of different lithounit in Jharia Coal Basin (b)

The basin slopes very gently (5-10º) towards south near the Southern boundary, the slope of the basin becomes steeper and then the direction reverses towards north (slope amount (20º-30º). The broad structure within the basin is that of a large scale elongated doubly plunging open syncline (Chandra & Chakraborty 1989). There are number of smaller domes and basins within the larger structure. These are very open and somewhat elongated and trends E-W parallel to the trend of the major basin. On either side of the oval outcrops of the sediments, long, narrow horsts of pre-cambrian gniess are exposed with the basin itself. The most important are Dugda high and Durma inlier in the north-east and the Pathardih high in the east.

The Gondwana sediments are in the nature of tectonic troughs, placed linearly and having faulted boundaries. Often the magnitude of down throw of the faulted boundaries varies greatly resulting in the strata dipping towards the faults with a E-W trend and the strata dip towards the southern boundary is itself a fault, called the Southern Boundary Fault (Fox, 1930).

Faults :

Southern Boundary Fault :

Most prominent fault, trending roughly WNW-ESE along the southern edge of the basin, and is not a single fracture line but a zone of parallel fractures. A number of interbasinal faults, which are both inter and intraformational in nature, have been identified. The fault angle varies from 45°- 65° with the horizontal, and throw in all cases are normal (Sengupta,1980). The important among these are :

(1) E-W trending fault system
(2) NW-SE and NNW-SSE trending faults
(3) NE-SW fault systems
(4) Low angle faults

The low angle normal faults have been encountered in Sudamdih mine. The faults have varying through ranging from a few centimeters to more than 50 metres (Sengupta, 1980). These low angle faults in the Sudamdih area have created problems in mining. From the surface and subsurface data now available it is quite evident that all the major faults of the Jharia basin were initiated as contemporaneous faults. Many of the major contemporaneous faults developed in short segments and extended their strike lengths in subsequent times (Ghosh and Mukhopadhyay, 1985). The major intra-basinal contemporaneous faults of the Jharia basin occur in systems of close spaced, nearly parallel faults which sometime branch into two to three forks, some of which may coalesce again.

2.3 Coal Reserve & Resources

Coal resources of India are being continuously unveiled through systematic exploration. Geological Survey of India (GSI) is carrying out the task of updating the National Inventory for Coal since 1972 following the ISP norms, which was first formulated in 1956 and modified later. Year wise updating of the inventory is being done since 1988 by meaningful compilation of subsurface data accrued from regional as well as detailed exploration carried out by GSI, Central Mine Planning and Design Institute, Singareni collieries Company Limited, Mineral Exploration Corporation Limited and different state Government Agencies. Accordingly the inventory was finalized as on 01.01.2007 and the total geological coal resource of the country was estimated to be 2,55,172.4 million tonnes. In pursuance of the decision of the 44th sub-committee meeting on Energy Minerals (Gr. III of CGPB), henceforth the National Inventory of Coal will be updated financial year wise from 2008 onwards and will be published on 1st May of each year.

State wise distribution of Indian coal (Table 2.3.1) shows that Jharkhand tops the list with 74.4 billion tonne (b.t) followed successively by Orissa (63.2 b.t), Chattisgarh (41.6 b,t), West Bengal (28.3 b.t), Madhya Pradesh (20.3 b.t), Andhra Pradesh (17.7 b.t) and others.

Table 2.3.1: State wise break up of Indian Coal resource (figures in million tonne) BCCL report :2008

State	Resource
Jharkhand	74392.15
Orissa	63233.58
Chhatishgarh	41450.48
West Bengal	28334.84
Madhya Pradesh	20346.23
Andhra Pradesh	17714.46
Maharashtra	9669.53

Categorization of coal resource into 'proved', 'indicated' and 'inferred' is based on the degree of confidence level of exploratory data. The updated proved resource of the country is 99,060.39 million tonne, while that of 'indicated' and 'inferred' categories are 120177.39 million tonne and 38143.77 million tonne respectively. (Table 2.3.2)

Table 2.3.2: Depth wise resource for Jharia Coal Field (BCCL report : 2008)

Jharia Coalfield		Depth	Proved	Indicated	Inferred	Total
Prime Coking			4039.41	4.01		4043.42
		600-1200	574.94	694.70	0.00	1269.64
		0-1200				
	Total Prime Coking		**4614.35**	**698.71**	**0.00**	**5313.06**
		0-600				
		600-1200	4064.18	2.82	0.00	4067.00
		0-1200	296.30	1800.70	0.00	2097.00
		0-600				
		600-1200	**4360.48**	**1803.52**	**0.00**	6164.00
		0-1200	5606.74	495.26	0.00	6102.00
			496.00	1355.00	0.00	1851.00
	Total Medium Coking		**6102.74**	**1850.26**	**0.00**	7951.00
Total for Jharia			**15077.57**	**4352.49**	**0.00**	**19430.06**

2.4 Land use pattern

Land use/ land cover map of the study area has been prepared from IRS LISS III Pan merged data aided by digital image enhancement and visual image analysis. The methodology adopted to map the land use/ land cover units is given in the Fig. 2.4.1

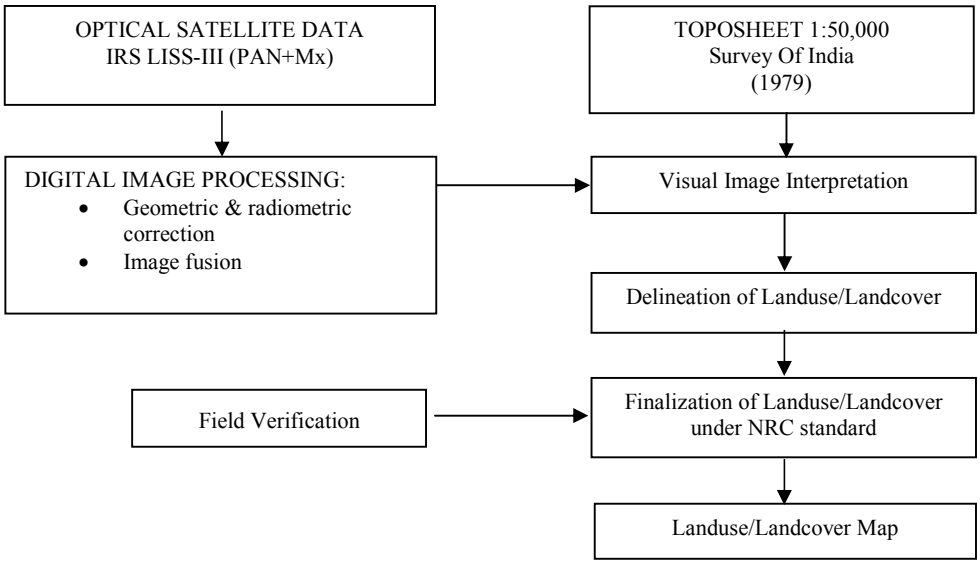

Fig. 2.4.1 Flow diagram landuse/landcover mapping from satellite data (IRS LISS III Pan Merged data)

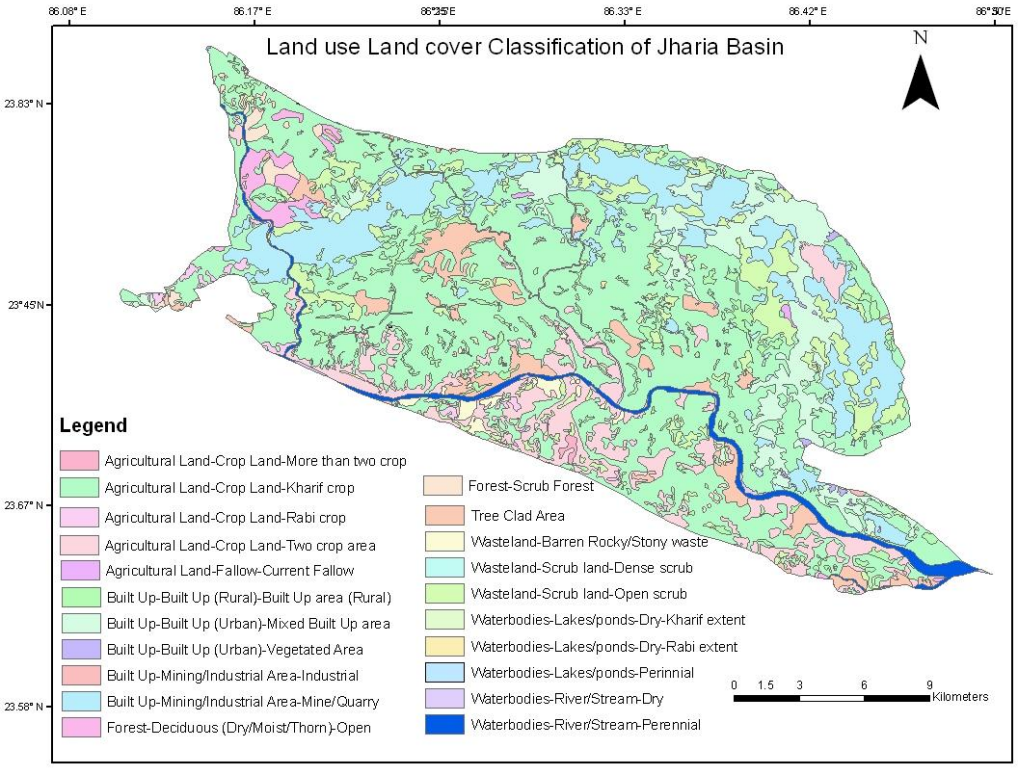

Fig. 2.4.2 Land-use Land cover map of Jharia coalfield under NRC LULC standard :Courtesy NRSC 2007 (prepared using IRS P6-LISS III image)

As discussed earlier, majority of the area is classified as built-up, mining, quarry and industrial area, along with that are different types of agricultural area forest land, waste land and water bodies respectively. The classification scheme adopted from Natural Resources Census (NRC) standard for land use land cover (LULC) classification delineated from IRS-P6 LISS-III data on 1:50,000 scale. The LULC map of the Jharia basin is shown in Fig. 2.4.2.

2.5 Mining scenario

Jharia coalfield has about 100 years history of coal mining and has 40 seams in Barakar and 10 seams in Ranigunj measures (Saxena & Singh 1980). The present day mining situation in the coalfield is briefly described below:

1. Old workings - The yester-year mining practices in the field have left a legacy of unapproachable abandoned underground mine workings standing on small pillars in a large number of places. With the passage of time these workings have become waterlogged and the accurate mine plans are generally not available. Many of these workings are below and by the side of important surface properties. About a dozen of the unapproachable old workings have subsided in recent past causing severe damages on the surface in the form of wide - cracks, large depressions, sinkholes (potholes), blockage of roads and rails, damage to buildings and other surface properties. The main characteristics of these subsidences were that - indications on the surface are seen only a few hours in advance, they do not follow any pattern, they cause marked depressions with wide cracks and steppings, and they are associated with rumbling sound.

2. Extraction thickness - Generally seams less than 1.2m in thickness are considered unworkable. The maximum extraction thickness may be upto 4.8m in one lift. In case of multi-lift and multi-section mining the extraction has been up to about 12m.

3. Depth - The underground workings in the coalfield are generally at depths less than 250m. Only about 20% of the workings are at greater depths. The maximum depths of the workings may be around 500m while the minimum may be about 15m.

4. Multi-seam extraction - As stated earlier there are 40 coal seams in Barakar measures and 10 in Ranigunj measures in the coalfield and the total thickness of seams is on average 12% of coal measures. In these conditions almost everywhere multi-seam mining has been done. In some situations two or three seams are standing on developed pillars.

5. Multi-section extraction - The maximum thickness of coal seams in the coalfield is around 20m. In the seams, more than 6-7m in thickness, multi-section development has been extensively done on room and pillar pattern. Suitable methods of exploitation of the thick seams developed in two to three sections are being looked for.

6. Method of underground extraction - About 80% of production from underground mining is obtained by bord and pillar system and the remaining 20% from longwall mining.

7. Percentage of extraction - The percentage of extraction from the panels in workings without longwall system varied greatly from about 60 to 80 in both caving and stowing cases.

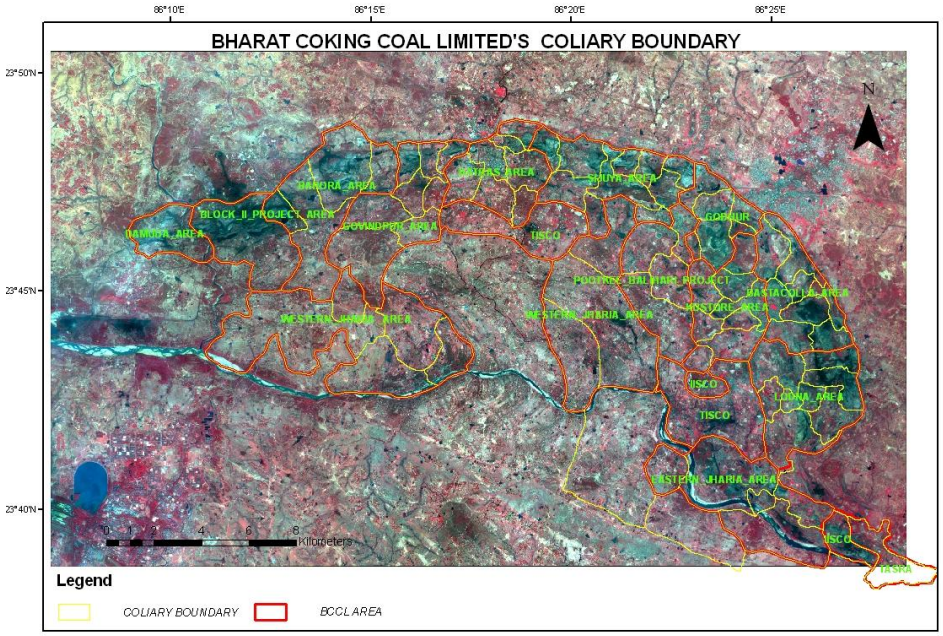

Fig. 2.5.1: BCCL 's area and Colliery boundary in Jharia coalfield, draped on IRS P6 LISS-IV –CARTO merged product.

After independence, Coal Authority of India (CIL) has taken up major part of the collieries and Bharat Coking Coal Ltd. (BCCL) have around fifteen area offices (Fig. 2.5.1) which controls the mining activity and environmental monitoring in connection with CMPDIL. TISCO and ISCO are the two private body present in Jharia coalfield having both opencast and underground mining areas.

2.6 Subsidence in Jharia coal field

Jharia coalfield is facing subsidence problems due to the presence of old workings, which are generally waterlogged and about a dozen of them have subsided in recent times, causing severe damages to surface topography and properties. Coal fire related subsidence is also an important parameter to be mentioned herein.

Fig. 2.6.1: SH road (Jharia-Sindri) affected by fire near Indira chowk, Jharia.

Fig.2.6.2: Sagging of ground due to mine fire near Simlibahal village.

Fig.2.6.3: Land subsidence and generation of cracks at East Bassuriya area (Gwalapatti village).

Salient points of subsidence parameters in the coalfield after subsidence studies by previous workers (e.g. Saxena *et al* 1980)) are described below:

1. Visual impacts of subsidence in Jharia coalfield over different categories of surface properties are stated below:

(a) Subsidence upto about 500 mm were generally not visually felt in barren areas.
(b) Subsidence upto a magnitude of about 650 mm over hydraulically sand stowed workings did not cause any visual distortion in the surface topography or impact on surface vegetation.
(c) Over caved workings at depths upto about 100m discontinuous subsidence has taken place with stepping.
(d) Over caved workings at depths less than 50 m sinkholes/pot-holes were also developed.
(e) Subsidence over unapproachable workings also caused pot holes, discontinuities and steps.
(f) Discontinuities were more prominent over the workings (both current and old) in thick seams and at a few place stepping was of the order of 2m and more.
(g) The width of cracks on the surface varies and the maximum observed was over 1000 mm due to extraction of 8m thick seam at a depth of about 70m.
(h) In general the impact of subsidence on surface topography was very prominent over caved workings at shallow to very shallow depths.
(i) Subsidence of the order of 600 mm and more caused severe disturbances in sub-surface and underground water regime resulting in loss of water from aquifers and water tables.
(j) Subsidence with cracks retarded growth of vegetation on the surface due to loss of water from top-soil.
(k) Subsidence over unapproachable old workings and also over current workings at depths upto about 100m were generally sudden (taking place within a few hours to a few days of initial indications).
(l) Damage to buildings took place even with subsidence as low as 300-500 mm over workings at a depth of about 300m.
(m) Water logging of central portion of subsided areas is very commonly seen.
(n) All major cracks over underground workings were generally within extraction perimeter, i.e, the angle of break was inside the *goaf*.

2. Maximum subsidence over hydraulically sand stowed underground workings in the coalfield is not more than 6.5% of extraction thickness even with multi-lift and multi-seam extractions at depths ranging from about 35 to 400m. Over caved workings the subsidence varied but is less than 60% of extraction thickness at depths upto about 480m. Non-settlement of overlying old workings at a few places caused an increased subsidence due to settlement of both the seams. In general the magnitude of subsidence was more over the areas having rock mass disturbed due to previous underground mining activities.

2.7 Coal fire in Jharia Coalfield

Coal fire has been found to be a serious problem worldwide in coal mining processes. Coal fire burns valuable coal reserve and prevents access to proven reserve in the affected area. Moreover, it leads to severe environmental degradation of the region by an overall increase of the ambient atmospheric temperature, by the emission of obnoxious gases (e.g., SO_2, NO_x, CO_x, CH_4) along fissures and cracks and by causing land subsidence and collapse.

Jharia Coalfield, Jharkhand, India, is known for being the exclusive storehouse of prime coking coal as well as for hosting the maximum number of known coal fires among all the coalfields in the country.

Apart form the ground observation to detect surface- sub-surface fires and its dynamics, aerial and space based remote sensing is one of the useful tool for detection of this phenomena in both spatial and temporal domain.

Various workers (e.g. Bhattacharya *et al* 1992, Reddy *et al* 1993, Mansor *et al* 1994, Saraf *et al* 1995, Zhang *et al* 1997 & 2004, Prakash *et al* ,1995,1997,1998 & 1999, Barsi *et al* 2003, Chatterjee, 2006) have used aerial and space based (Landsat TM-5, ETM-7, ASTER) thermal remote sensing observation for detection of thermal anomalies and thereby mapped and modeled the surface and sub surface coal fire dynamics for Jharia as well as other basin in the world affected by coal fire. As the objective of the thesis does not include thermal anomaly mapping and modeling surface and sub surface fires, the discussion is restricted here in. In stead, based on the information available from the field survey, literatures and also BCCL, on the effects of coal fire in Jharia Coalfield (JCF) has been addressed.

In 1971, the Indian coal industry was nationalized under Coal India (CIL) and Bharat Coking Coal Ltd. (BCCL), a subsidiary of CIL, was formed. BCCL, headquartered in Dhanbad, a major metropolitan center and home of the Indian School of Mines, was intended from its inception to operate exclusively within the 450 km^2 Jharia Coalfield, India's principal source of domestic coking coal. The fledgling company did not start off in an enviable position. BCCL inherited from previous private ownership about 396 poorly operated collieries, of which many of the mined coal seams were on fire (Bharat Coking Coal, 2008) (Fig. 2.7.1).

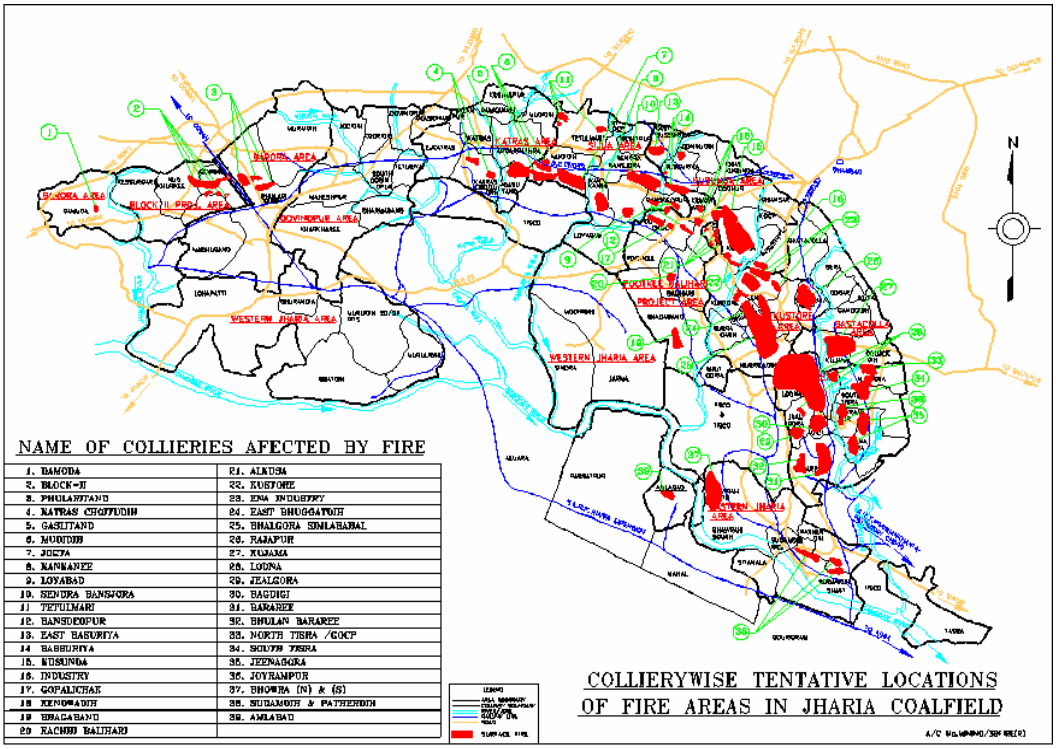

Fig. 2.7.1 : Mine fire location in Jharia coalfield (BCCL,CMPDIL 2008)

Efforts to extinguish the fires have been partially successful. About 59 fires continue to burn in the coalfield as of 2008 (Fig. 2.7.1). This is likely the largest complex of above and underground coal fires in an actively mined area in the world. From the initial fires in 1916 at Bhowrah through the present, the fires have spread and grown to affect coal production, the environment and the health, safety and well being of over one million people living in the region (Chandra & Srivastava 1977 & Schori et al., 1997; Michalski 2001,2004).

Table 2.7.1 Seams affected by fire in Jharia coalfield (Chandra & Srivastava 1977)

	Name of locality	**Seams affected by fire**	**Remarks**
1.	Albion	V-VI-VII	Fire area west of Jamnia river and proceeding along the strike (e.g. west -east) the barrier between Bokario –Jhaira and Albion is under the effect of fire
2.	Nadkharki	XI-XII	Fires in the debris of the seam at the top
3.	Madhuban	XI-XII	Under extreme fire
4.	Dura Khas	VII	Debris fire
5.	Pure Dharmuband	VII	Debris fire
6.	Selected mandara	VII	Debris fire
7	Barwa Bera	VIII	Half earth blanketed
8.	Barwa Bera	X	
9.	Barwa Bera	X	
10	Barwa Bera	X	Western half of the fire area has been sand blanketed to save the railway line-Mahuda-Gomoh section of the SE railway
11	Ganeshpur (Phularitand)	X-XIII	Fire in Goaf connecting all the seams
12	Dharamaband coliary	XVIII	Debris fire in the overburden of the carbonaceous shale

13	Lakarka	XIII-XIV	Spontaneous heating in quarry debris
14	Gazlitand	XV	Spontaneous heating, sand blanketed
15	Muridih, (Sijuya)	XII-XIV,XV	Spontaneous heating controlled by sand blanketing
16	Jagta	XIII-XIV	Spontaneous heating
17	Jagta	XV	
18	Kankanee	XIII-XIV	An extension of Jagta fire
19	Angarpatra	XI-XII	Underground fire began as debris fire
20	Diamond Anganpatra	X	Due to Goaf heating
21	Tetulmaree	VII-VIII	Outcrop fire quenched by water
22	Sendra, Banshjora	XI-XIV	Outcrop fire
23	Bansdeopur	XIII-XIV	Sand blanketed
24	Gopalichowk	XV	Spontaneous heating
25	Gopalichowk	XVI	Elicit distillation quarry fire
26	W. Godhar colliery (Dheriajoba fire area)	XI-XII	Quarry fire, flooded to quench
27	Kusunda colliery	X-XII-XIII	Sand blanketed
28	Industy colliery	XI-XII	
29	Ena colliery	XIV	
30	Bhatdih colliery	XI-XII	
31	Ena colliery	XV	
32	Simlabahal colliery	XV	Debris fire
33	Standard colliery	XV	
34	Ena collary	XIV	Packed with soil
35	Rajapur colliery	X	Active fire
36	K.P. Dobari & pure Jharia	X	Active fire bulldozed
37	N, Barakar, Benihir & Suratand area	XV-XIV A- XIV	Sand packed
38	Bagdih/Lodna	XV-XIVA	Clay blanketing and safety trench`
39	Kujama	XI	Debris fire
40	N. Tesra colliery	VII-VII	Outcrop fire
41	D.D. Tesra colliery		Outcrop fire
42	Kalithan, Jinagara	X	Sand blanketed
43	New Jinagarea	X	Sand blanketed
44	Central Jinagara	X	Sand blanketed
45	S. Tesra	XI-XII	Outcrop fire
46	Jayrampur	XIII-XIIIA-XIIIB	
47	Buland bararee		The dyke burnt with the overburden
48	Bararee	XV-XIVA-XIV	Seam fire sealed underground by stopping
49	Bhaunra	XII	Active seam fire
50	Bhaunra	XIV	Active fire, seam burning underground. Sealed and partly controlled by surface blanketing
51	Pathardih	IX-X	Active fire
52.	Sudamdih	XIVA-XIV	Soil blanketed and bulldozed
53.	Pathardih-hugudih link fire	XI-XII	Fire localized and quenched by water jet
54.	Sudamdih	XV	Prior to fire s4eam has largely been converted to Jhama due to dolerite dyke
55.	Chashnala	XI-XII-XII-XIV	Active fire

The table 2.7.2 shows an account of human casualty from 1990-2008 in the different mines of Jharia coalfield due to fire/subsidence related effects.

Table 2.7.2: fire/ subsidence related casualty in jharia coalfield (*source: BCCL 2008)

Year	Name of the Mine	Casualties
1989-90	Begunia	
1994-95	East Katras, Gopalichowk, Loyabad	1 girl died on 19.01.1995 at E. Katras
1995-96	Industry, Bansdeopur, east. Bhuggatdih, Kendwadih	1 person died on 26.09.1995 at Kendwadih
1996-97	East Bhuggatdih, Bagdigi, Rajpur	
1997-98	Simlibahal, east. Bhuggatdih	1 girl died on 14.08.1997 at Simlibahal
1998-99	Godhur, Bararee, Ena	
1999-2000	Kujama, Simlibahal, Mudidih, Borira, OCP of Damgoria OCP, Lodna, E. Bhuggatdih,Lodna	
2000-01	Rajpur OCP, Ghanoodih, E. Bhuggaatdih, , Bhowrah(S), Lodna	
2001-02	DB road linking Jharia-Dhanbad, east. Bassuriya, east Bhuggatdih, Mudidih, Rajapur OCP	1 woman died on 08.07.2001 at East Bassuriya
2002-03	Kendwadih	
2004-05	Begunia, Kendwadih, Ena	1 woman died on 26.07.2003 at Kendwadih
2006-07	Gopalichak, Block IV OCP, East Katras, Kusunda	10 person died & 5 injured on 15.03.2007 at Kusunda
2007-08	Basseriya, Patherdih,N. Tisra,Lodna	

Surface and sub surface coal fire in Jharia coal field resulted in crack developments in the ground- buildings, damaging, roads, bridges and other infrastructures. Extensive field work in the fire affected areas revealed the effect of coal fire related hazard which is illustrated in the figures (Fig. 2.7.2-2.7.10).

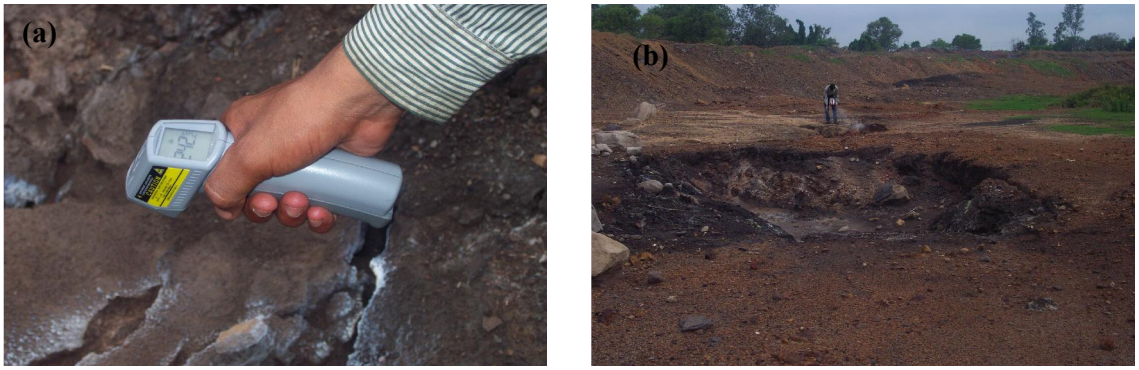

Fig. 2.7.2a,b): Land subsidence due to underground fire in Jayrampur test site
(IR thermometer reading 242°C for underground fire)

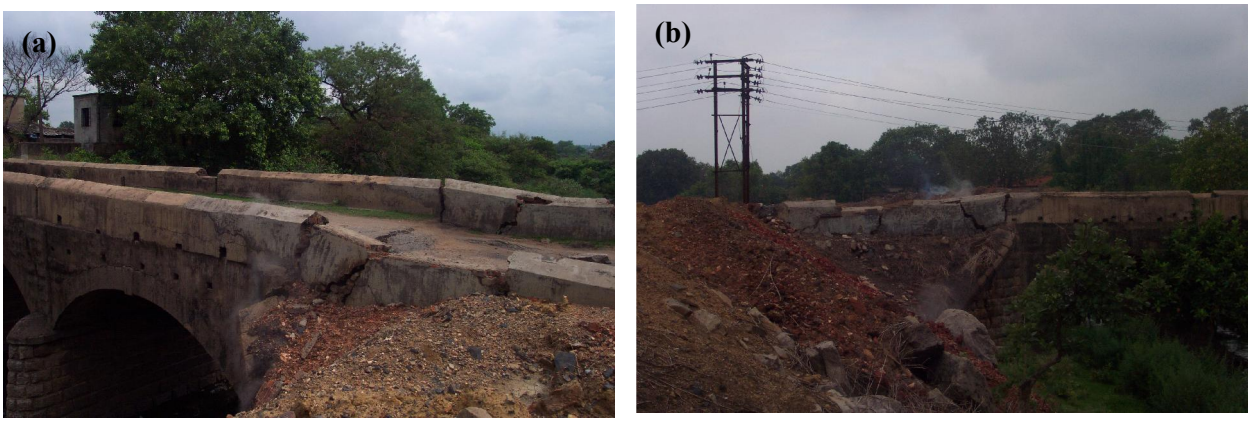

Fig.2.7.3 (a,b): Damaged foot bridge due to coal fire in Jayrampur area

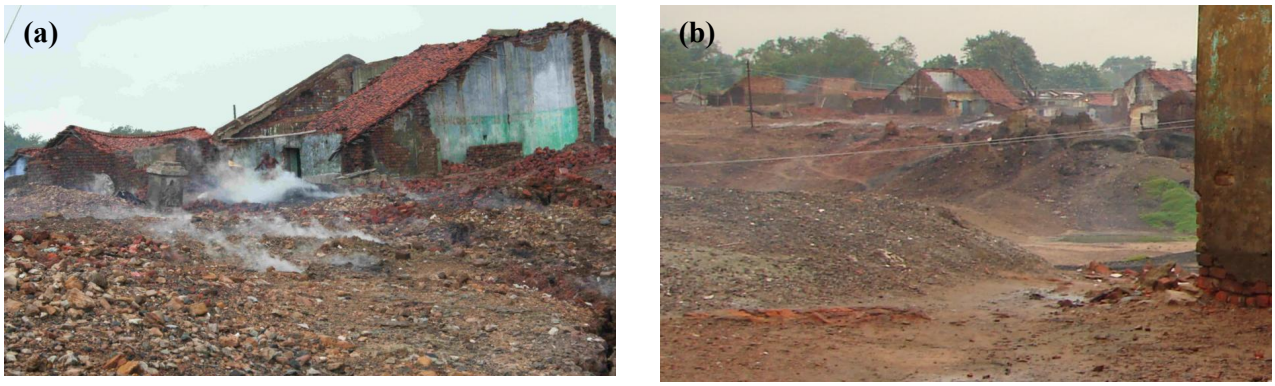

Fig.2.7.4. a,b: Huts damaged due to subsidence related to coal fire in Kendwadih village

Fig.2.7.5.: Cracks developed in the floor of a house in Ena-Islampur due to coal fire

Fig.2.7.6. a: Hutments damaged (demolished) in Kusunda area due to subsidence
b: Land subsidence in Bokapahari due to advancing fire

Fig. 2.7.7(a),(b): Huts damaged due to subsidence related to fire in Kendwadih village

Fig. 2.7.8 a: Fire and smoke in Kukurtoopa; b: Dwelling endangered by fire at Bagdigi

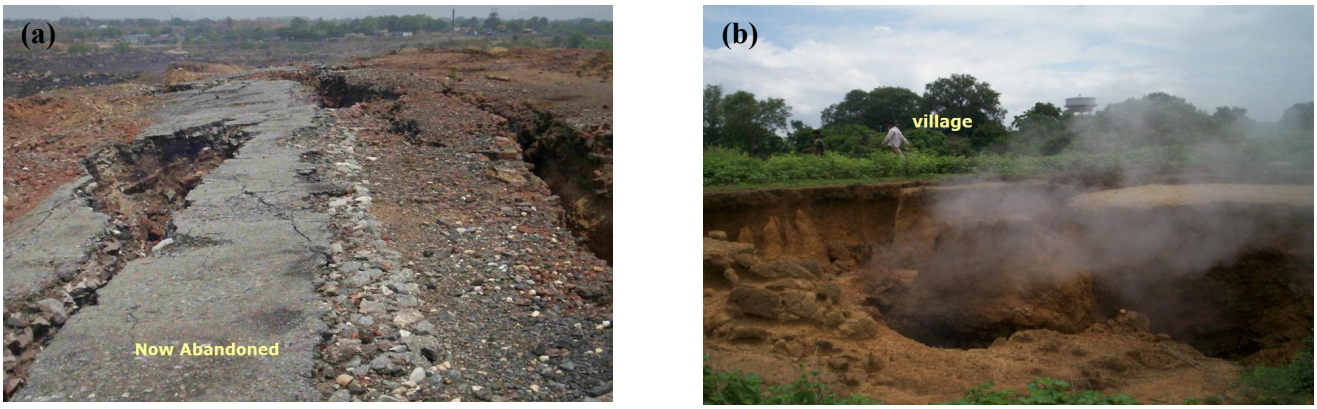

Fig. 2.7.9 (a): Cracks/fissure development in the main road in East Katras due to fire (now abandoned)
(b): fissure development in Gwala basti (E.ast Bassuriya)

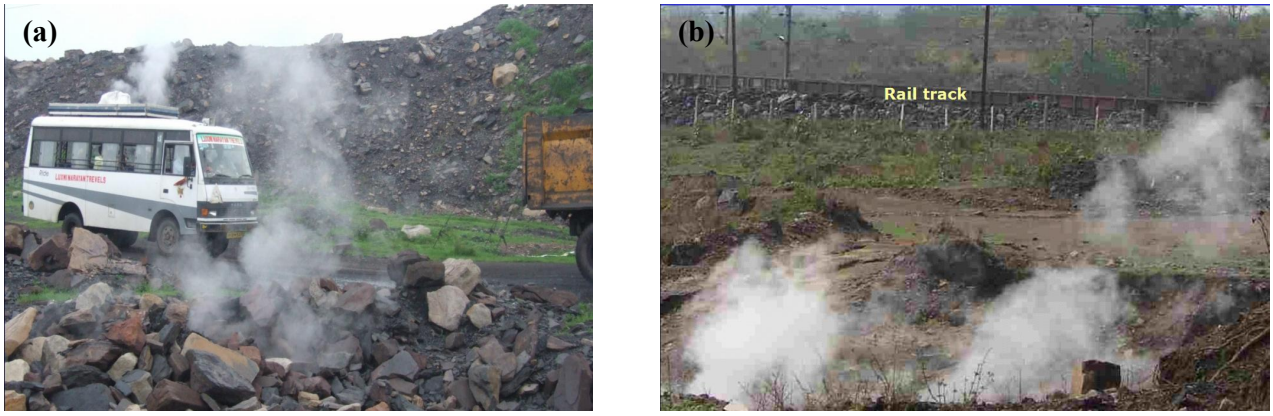

Fig.2.7.10 (a): D.B. road in Goluckdih (Jharia to Baliapur) affected by fire
(b): Railway track endangered by fire at Bansjora area

2.8. Environmental Indicators in Jharia coal field:

As discussed earlier about the criteria for environmental indicators and their role in monitoring the sustainable development of an area over time. In this section, we will discuss about various land features that can be treated as environmental indicators in a typical opencast coalfields and their role in geo-environmental monitoring.

The history of mining in the Jharia coalfield is more than a century old. However, it had no mark on the environment upto 1926-28. It is known that during these years C.S. Fox had to map the coalfield riding on elephant as the whole basin was deeply forested. Within the last 50 years, the coalfield has been reduced to a barren land. The landscape has taken a weary dismal dirty look with marks of old workings and existing mining activities covered with coal dust. The old topography has totally changed. now only an artificial topography has been created with excavations here and there and mounds of torn up overburden rocks dumped haphazardly. This was all due to unplanned and indiscriminate mining by the private mine owners, who never cared about the environment and its effect on future generation.

Besides the voids formed due to underground mining, have added a great deal to environmental hazards in terms of subsidence. Underground fire due to spontaneous combustion of coal has caused further subsidence causing considerable loss to lives & property. Communications have snapped in several places due to subsidence of railway lines and roads. Presently the Jharia town is in severe danger as it is lying on smouldering fire below. Within the total mining area of 300 sq. km in this field, more than 100 mine fires are reported of which 70 are active (Prasad et al 1984). These have resulted in loss of about 37 million tonnes of prime coking coal and blocking up of another 48 m tonnes (Sinha 1986). The fire besides causing damage to coal, has caused damage to vast stretches of lands, buildings and road-rail networks. In some parts of the field, water from the old waterlogged unfilled

goafs has erupted causing many major accidents. The total lives claimed by such accidents between 1969-2000 were more than 800 in 20 accidents of which a single disaster of Chasnala colliery in 1975, caused death of about 375 persons. (Chandra & Sinha 1988). In order to find out the effect of mining in the Jharia coalfield, Ghosh 1988 has prepared a map marking the areas affected by fire, collapse, querry, overburden dump, coal dump and washery in the Jharia coalfield. According to the assessment by Ghosh (1987a & b) out of 300 sq. km of mining area in the coalfield 10.8 sq. km is under fire.

Mapping and monitoring the environmental indicators of opencast coal mining can help immensely for efficient planning and management of mining operations, assessment of environmental impacts on land use, and execution of reclamation measures. Research on the utility of mapping and monitoring mining-related environmental indicators for planning and management of mining operations, assessment of environmental impacts due to mining, and the establishment of appropriate reclamation measures is presently ongoing.

An opencast mining related environmental indicator includes the total area of opencast mining (also known as opencast project area or OCP), unreclaimed abandoned or closed opencast mines, and overburden and coal dumps, barren land/fire affected areas/subsiding areas. Optical multi-spectral data are efficient for delineating the total area of opencast mining (Ghosh and Ghosh, 1990; Rathore Chatterjee et al., 1994; Prakash and Gupta, 1998).

During opencast mining, the overlying soil is removed and the fragmented rock is heaped in the form of overburden dumps (Ghosh, 2002). Dump materials are left over the land in the form of overburden dumps. These occupy large amount of land, which loses its original use and generally gets soil qualities degraded (Barpanda et al., 2001). As the dump materials are generally loose, fine particles from it become highly prone to blowing by wind. These get spread over the surrounding fertile land and plants, disturbing their natural quality and growth of fresh leaves. It has been found that overburden dump top materials are usually deficient in major nutrients. Hence, most of the overburden dumps do not support plantation.

Fig. 2.8.1: Side view of overburden dump in Barora area

Due to similar spectral signatures of various mining-related environmental indicators, namely abandoned or closed opencast mines (may or may not be water logged), active opencast mines, overburden dumps, and coal dumps, it becomes difficult even in the high resolution satellite data (e.g. CARTOSAT-1, IRS P6 LISS IV) for delineation of these features.

In the present work the attempt has been made to map the aforesaid environmental parameter/indicators and to understand the scattering properties using multi-polarization SAR data. With the available detailed surface plans (1:4,000;1:8,000;1:12,000 scale) of the opencast mining areas of the Jharia coalfields, provided by BCCL, a map composition is made showing spatial distribution of all the ten environmental indicators in Jharia coalfields in Fig. 2.8.2

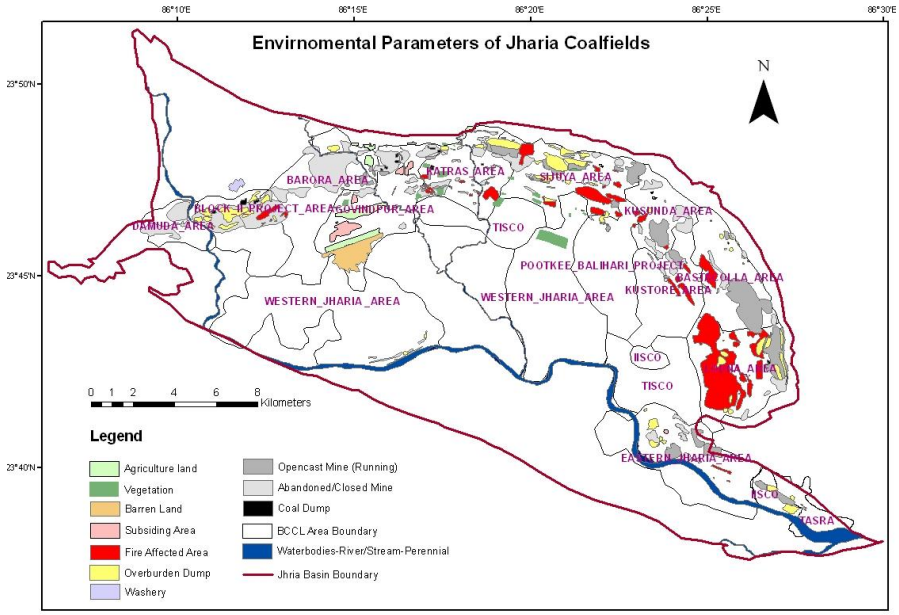

Fig. 2.8.2: Spatial distribution of different environmental indicators in Jharia coalfields (JCF)

CHAPTER 3

PRINCIPLE OF LAND SUBSIDENCE

Subsidence is an inevitable consequence of underground mining— it may be subtle and localized or extend over large area at an alarming rate. It may be immediate or delayed for many years. During recent years, with the expansion of urbanization and increased concern for the environment, it is no longer possible to ignore its aftermath. In the United States, mining companies have, therefore, begun to devote attention to the subject and study it in a methodical manner. Appropriate regulations have also been promulgated by various government agencies, depending on the needs of the region, in order to protect the public interest.

The major mining induced ground movements and subsidence parameters that are used to assess impacts of subsidence are discussed in the following sections. The classification system for impact levels due to subsidence induces ground movements are also discussed herein.

Mining induced ground movements:

Vertical subsidence: Vertical, rigid body, subsidence has little or no effect on buildings or other surface structures where the subsidence occur uniformly. The structures are naturally, left at a lower level but normally this has little or no adverse effect upon them. Drainage systems and services to a building normally subside with the building and impact only results when differential subsidence occurs.

Although the mining of all underground minerals may not result in subsidence, most studies to date have concentrated on the extraction of flat bedded deposits-primarily coal. Hence throughout this discussion, references to coal mining has been given more emphasis. The information presented herein is, therefore, most pertinent to coal mining, although it generally applies to other bedded deposits. The principles may be also extrapolated to other mining methods, but the conclusions need validation by actual experience.

The term *subsidence,* implies the total phenomenon of surface effects associated with the mining of minerals and not only the vertical displacement of the surface as is sometimes inferred in the literature.

3.1 Principle of subsidence

Whenever a cavity is created underground, due to the mining of minerals or for any other reason, the stress field in the surrounding strata is disturbed. These stress changes produce deformations and displacements of the strata, the extent of which depends on the magnitude of the stresses and the cavity dimensions. With time, supporting structures deteriorate and the cavity enlarges, resulting in instability. This induces the superjacent strata to move into the void. Gradually, these movements work up to the surface, manifesting themselves as a depression. This is commonly referred to as subsidence. Thus *mine subsidence* may be defined as ground movements that occur due to the collapse of the overlying strata into mine voids. Surface subsidence generally entails both vertical and lateral movements.

Surface subsidence manifests itself in three major ways:

1. Cracks, fissures, or step fractures.
2. Pits or sinkholes.
3. Troughs or sags.

Surface fractures may be in the form of open cracks, stepped slips, or cave-in pits and reflect tension or shear stresses in the ground surface.

When the mine void is of larger size due to longwall mining or eventual collapse of pillars, the collapsed strata fall into the excavation and bulk (i.e., broken material occupies a larger volume than in situ rock). This process continues until a height is reached of about three to six times the mined seam thickness (Singh and Kendorski, 1981), unless the material spreads or is transported to other parts of the mine by water. Cyclical wetting and drying of the debris could also induce greater compaction.

When the cavity is essentially filled with broken rock, the debris offers some support to the superjacent beds (Fig. 3.1.1). As these strata settle or sag, bed separation may occur because of the tendency for lower strata to subside more than the higher beds. Overall, as the various strata settle or subside, they sag rather than break and produce a dish or trough shaped depression on the surface. This type of feature normally covers a larger area than sinkholes, and is referred to as *trough* or *sag subsidence.*

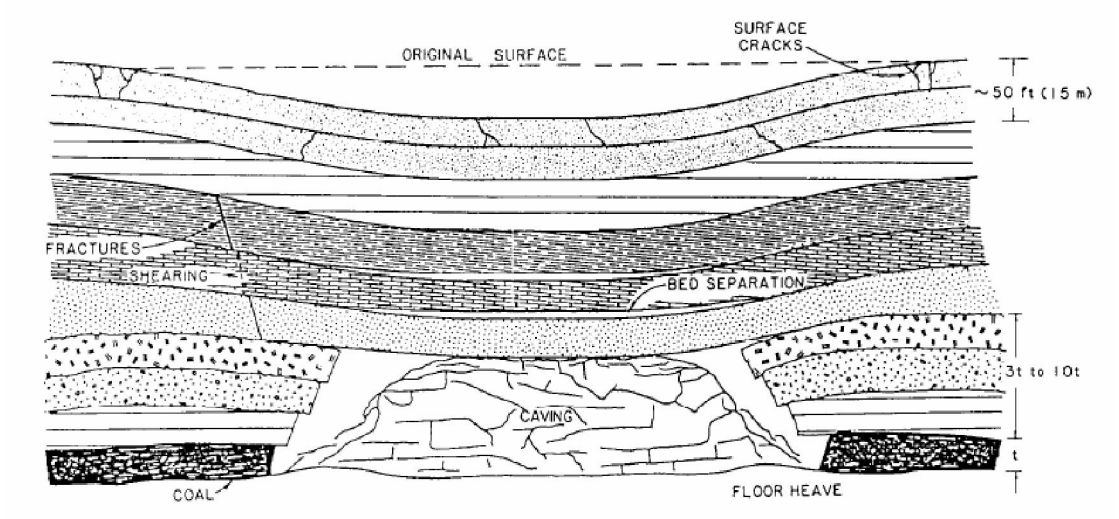

Fig 3.1.1 Strata disturbance and subsidence caused by mining (Singh and Kendorski, 1981).

Trough subsidence may occur due to mining at any depth. The overall movements of the ground around the opening are depicted in Fig.3.1.2; the direction of motion is not only vertically downward but also horizontal and in some locations, upward.

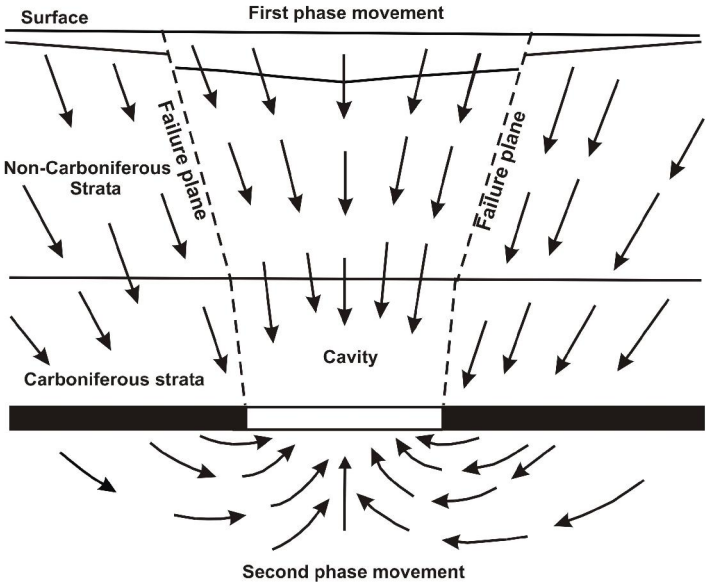

Fig. 3.1.2 Schematic representation of ground movements due to subsidence (Singh, 1985).

The mining of a single point 'P' (Fig. 3.1.3 a) at seam level will affect a circular area on the surface, defined by the base of an inverted cone with P as the apex and the limit angle *g* as the semi-angle of the cone. If this cone is turned upright, then the mining of any part of its base will influence the subsidence of its apex 'P' (Fig. 3.1.3b). Hence, this circular area is termed the *area of influence.* This implies that the diameter of the area of influence is given by 2*D* tan *g,* where *D* is the depth of the seam below the surface and *g* is the limit angle. (It may be noted that some authors use the complement of the limit angle, often termed the "angle of major influence"). This diameter also defines

the *critical width* of the workings, which is the minimum width that needs to be mined before the maximum possible subsidence is observed at the centre of the trough. If the mined width is less than critical, it is termed as *sub-critical,* and the amount of subsidence that occurs will be less than the maximum. If a *super-critical* (i.e., larger than critical) width is excavated, the central portion of the trough will attain maximum subsidence, and a flat-bottomed depression will be produced Fig. 3.1.4).

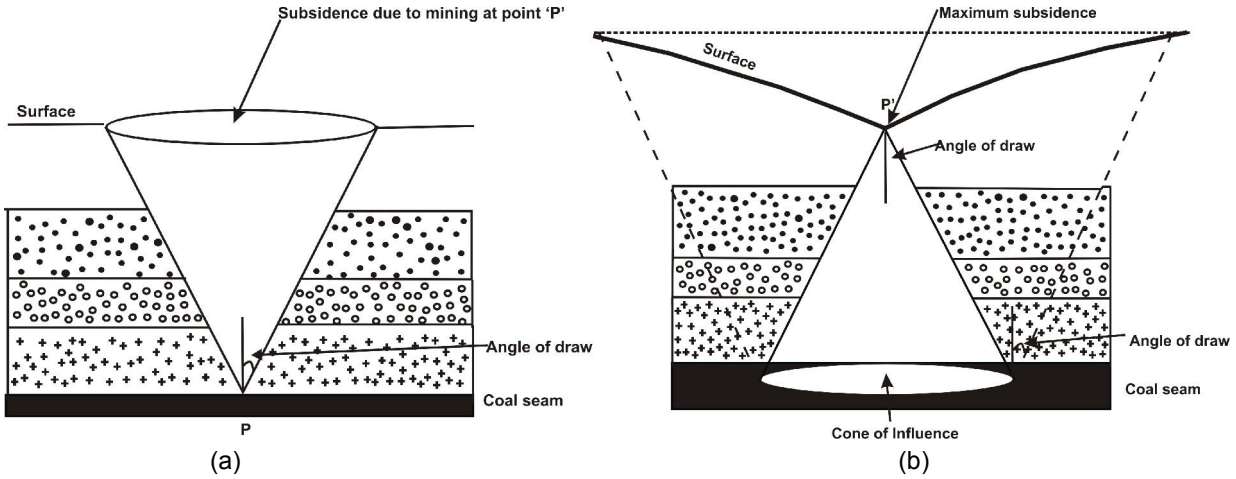

Fig. 3.1.3: (a) Sketch depicting area of influence (a) Effect on surface by mining at 'P'.
(b) Maximum subsidence at P′ by mining entire area of influence. (Singh, 1985).

If the vein being extracted is relatively flat and nearly horizontal, as is generally the case with coal and potash, the overburden and surface collapses, forming a *depression* or *trough.* The surface area affected by mining is generally larger than the vein area excavated. Hence the angle of inclination between the vertical at the edge of the workings and the point of zero vertical displacement at the edge of the trough is termed as *limit angle* or *angle of draw.*

As subsidence occurs, a movement of surface points towards the centre of the mined area occurs. The amount of vertical displacement experienced is the greatest at the centre while the horizontal displacements are least at the centre and maximum at or close to the edges of the mined area.

Since these lateral movements are not uniform, there are changes in the lengths per unit length (i.e., strains) along any cross section of the mined panel. These strains tend to stretch the surface near the edges of the trough (i.e., these are tensile), and push inward within the boundaries of the extracted area (compressive strains; see Fig. 3.2.2). Both the tensile and compressive horizontal strains disappear at the centre of the subsidence trough in the case of critical- and supercritical-width workings. Fig. 3.2.2a shows the progressive development of the mine working and the sub-critical, critical, and supercritical widths being formed. As the mine workings progress, the horizontal tensile and compressive strain regions also move along (Fig. 3.2.2b). Hence these are also referred to as travelling strains.

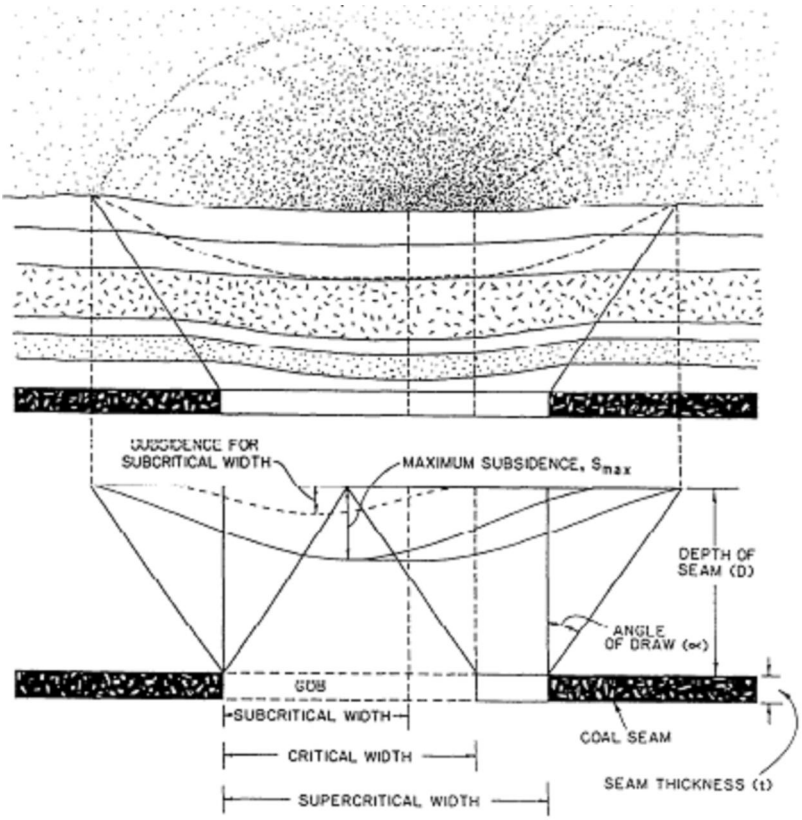

Fig. 3.1.4: Influence of extraction width on subsidence. (Singh et al 1981)

The inclination to the vertical of the line connecting the edge of the mined area with the surface point exhibiting the maximum tensile strain is called the *angle of break* or *angle of fracture* (Fig. 3.2.3). These terms should not be confused with the draw or limit angle defined earlier. Generally, the angle of break is somewhat higher with sub-critical-width workings than with critical or supercritical-width workings for a given region.

3.2 Components of subsidence

Subsidence consists of five major components, which influence damage to surface structures and renewable resources (see Fig. 3.2.3):

1. Vertical displacement (settlement, sinking, or lowering).
2. Horizontal displacement (lateral movement).
3. Slope (or tilt), i.e., the derivative of the vertical displacement with respect to the horizontal.
4. Horizontal strain, i.e., the derivative of the horizontal displacement, with respect to the horizontal.
5. Vertical curvature (or flexure),

Vertical curvature may be approximated by the derivative of the slope, or the second derivative of the vertical displacement with respect to the horizontal.

Uniform horizontal movements of the ground surface also cause little damage to structures. But breaks in pipes, electric or communications lines, roads, and other features may occur.

Surface horizontal strains cause most of the damage to structures located above mined areas. They cause tensile or shear cracks and buckling. Masonry structures withstand compression much better than tension. Strains may induce distortion, fractures, or failure. The weaker parts of the structure (e.g., openings) and the lower part of the frame are the first to show tension cracks.

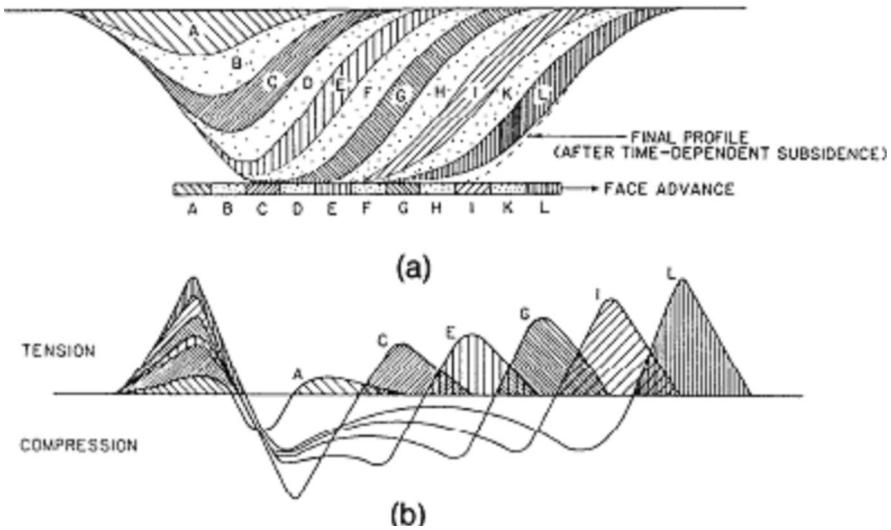

Fig. 3.2.1 Development of subsidence trough and strains with face advance (Rellensman and Wagner, 1957). (a) Subsidence development. (b) Traveling strain curve.

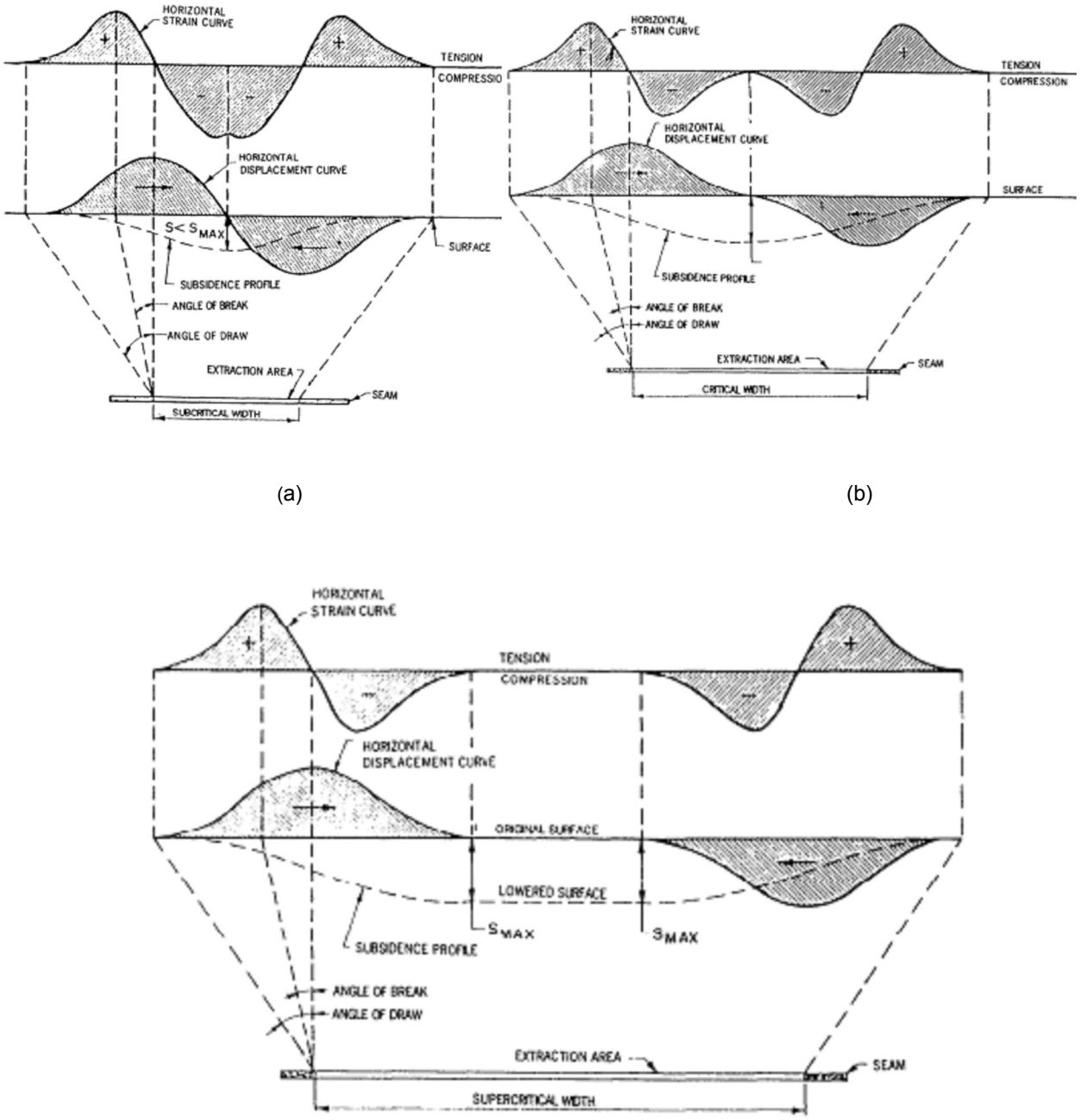

Fig.3.2.2 Schematics of displacement and strain curves for various working widths. (a) Sub-critical width. (b) Critical width. (c) Supercritical width. (Singh, 1985).

Curvature causes two types of distress on structures: (a) *shear strain,* which induces angular changes and tends to distort buildings out of square (distortion is generally proportional to structure height): and (b) *flexure* or *bending,* which causes strains in long load-bearing members. Concave curvature

causes tension along the bottom and compression along the top of the building. The dimension of curvature is the inverse of length.

Hence generally, the reciprocal of the curvature (i.e., radius of curvature) is quoted. For mine subsidence, this normally varies between 3200 ft (1000 m) and 6600 ft (2000 m), and seldom falls below 1600 ft (500 m) (Brauner, 1973).

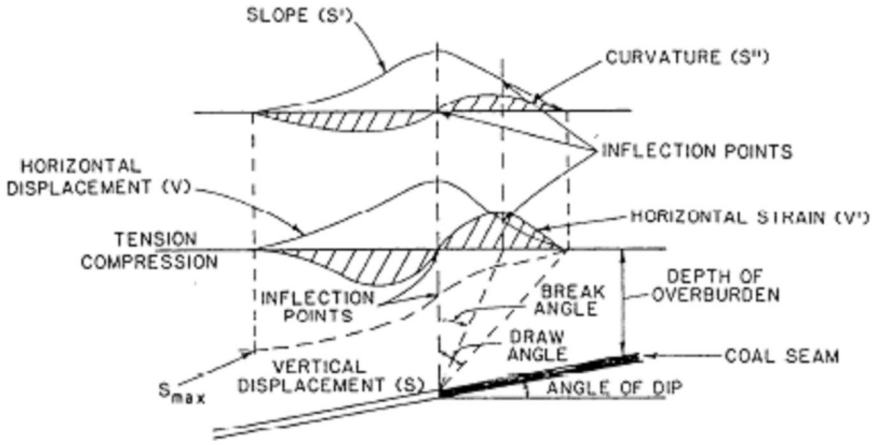

Fig. 3.2.3 Schematic of ground movements caused by subsidence (Singh et al, 1985).

There are several geologic and mining parameters and the nature of the structure affect the magnitude and extent of subsidence that occur due to coal mining (Brauner, 1973).

Effective seam thickness: The thicker the seam extracted, the larger the amount of surface subsidence that is possible. In some cases, the entire seam may not be mined or some pillars or other non-minable coal may be left in place. Hence the effective seam thickness should be considered. In thick beds, the slenderness (height-to-width ratio) of the pillars is higher for a given extraction ratio. Slender pillars are normally more prone to failure.

Multiple seams: Where multiple worked-out mining horizons exist, collapse could be initiated from any one of several levels, thereby increasing the likelihood of subsidence events, because the adjacent strata are disturbed. This is especially true when the prior mining was in an overlying seam.

Seam depth: A school of thought exists that at greater depths, an arch is formed over the mine cavity, preventing surface subsidence. In recent years, this has been gradually refuted.

Perhaps the time period that elapses before subsidence effects are observed at the surface is prolonged, but the total amount of subsidence does not appear to be changed; that is, subsidence is independent of depth. Pit depths generally do not exceed certain limits.

Dip of seam: When the coal seam being mined is inclined, an asymmetric subsidence trough is formed that is skewed toward the rise; that is, the limit angle is greater on the dip side of the workings.

The strains are also smaller toward the dip direction. Pillars in steeply dipping seams tend to be less stable.

Competence of mine roof and floor: Since subsidence propagates from the mine level, the characteristics of the mine roof and floor are vital in the initiation of subsidence movements. Soft fireclay floors, especially if susceptible to further weakening due to moisture, induce pillar punching or heave. Weak roofs, composed of shale, siltstone, and limestone, permit falls that are accentuated if punching also occurs. Competent roof beds tend to support the overlying strata longer and hence delay the subsidence. Also, when these fracture, they occupy a greater bulk volume than weaker strata (which compact more). When both the roof and floor are strong, the pillars tend to spall and crush.

Nature of overburden: Strong massive beds above the mine level tend to prop the overburden for a prolonged period and defer the occurrence of subsidence.

Near-surface geology: The soils and unconsolidated rocks near the surface tend to accentuate subsidence effects. The geologic materials are less homogeneous and isotropic than the underlying strata, and often behave in an inconsistent manner. Cracks and fissures may initially form in a 50-ft (15-m) thick layer from the surface (Singh and Kendorski, 1981). Later, these may be filled by plastic deformation or material transportation by water. Occasionally, however, water flow may accentuate these fissures and form gullies. Structures and renewable resource lands are thereby adversely affected. The composition of the rock/soil cover is important; if the material is of a fine, sandy nature containing large amounts of water, it may flow to a rock fracture and drop into the underground workings. Besides, water accumulating in the abandoned mine may seep upwards into the unconsolidated strata above through natural fissures and cracks in the rock and increase the potential for soil collapse.

Geologic discontinuities: The existence of faults, folds, and the like may increase subsidence potential. Mining disturbs the equilibrium of forces in the strata and may trigger movement along a fault plane, due to ease of slippage, causing either settlement or upthrust at the surface, which may appear as a series of step fractures. The effects of the other parameters may need to be discounted in areas of adverse geological conditions.

Lateral movements concentrate near the fault, but the strains may become immeasurable on either side. Structures that straddle fault planes tend to be severely damaged, but nearby buildings remain relatively intact. Joints and fissures in the strata affect subsidence behavior in a manner similar to faults but on a smaller scale.

Fractures and lineaments: Natural fractures and lineaments affect surface subsidence, but a strong correlation has not been established to date.

Degree of extraction: Lower extraction ratios tend to delay subsidence. It is less prevalent in areas superjacent to first mining, since sufficient pillar support is generally available without crushing of pillars. In second mining, the cross section of the pillars is reduced by splitting and slicing. Localized stress build up, promote crushing and excessively wide roof areas exposed between pillars stimulate roof failure. Third mining is almost invariably followed by roof collapse in the workings. Surface manifestations are a function of time, dependent on the rate of upward propagation of settlement.

Surface topography: As may be anticipated, sloping ground tends to emphasize downward movements because of gravity. Tensile strains may become more marked on hilltops and decrease in valleys. Surface effects are influenced accordingly.

Groundwater: Deformation of the strata around mined areas may alter drainage gradients, resulting in the formation of surface or underground reservoirs (in aquifers). Low-lying areas, such as in central Illinois, may become flooded. Rocks may be weakened by saturation. Erosion patterns could change, and in limestone areas, caverns or karst areas may be created over a period of time. Where surface runoffs from precipitation or water from leaky mains are allowed to accumulate, water may percolate down through the soil to the fractures and fissures in the bedrock, and finally into the mine openings. The erosion and lubrication effects induce failure.

Water level elevation and fluctuations: Water reduces the strength and stiffness of pillars and the roof and floor markedly. Periodic changes in mine humidity promote deterioration of all these members. Floor softening permits punching, resulting in instability and subsidence. Flow through fissures cause seepage pressures, endangering the stability of the rock mass. Cleavage and bedding planes are lubricated by water, inducing movements.

Mined area: The critical width needs to be exceeded along both the lateral and longitudinal axes to achieve maximum subsidence. This is especially important if competent strata present in the overburden tend to bridge across the panel and decrease subsidence when the panel width is less than the critical width, even though the length of the panel is greater.

Method of working: The type of initial subsidence experienced, namely pit or trough, depends on whether room and pillar or longwall mining is being practiced. With room and pillar mining, the eventual collapse of pillars may lead to trenching or sagging of the surface. The displacements and strains over short distances, when they start appearing on the surface, are significant. Nearly immediate but predictable subsidence occurs with longwall mining. Harmonic mining, either by working adjacent longwalls in the same seam or superposed panels in different seams, can be effectively utilized to neutralize compressive and tensile strains and thereby protect surface structures. However, the method is not readily applied and is restricted for use only where mining costs become subservient to historical or social demands.

Backfilling of the *Gob*: Partial or complete backfilling of the *gob* reduces, but does not eliminate, subsidence. The amount of subsidence that occurs depends upon the type and extent of backfilling

adopted. Thus, for example, hand packing is not as good as pneumatic stowing or hydraulic backfilling.

Time elapse: The amount of subsidence observed is a function of time. In room and pillar operations, no surface effects may be noted for some time after the mining is complete until the pillars deteriorate or punch into the floor. In longwall mines, the surface may start sagging almost immediately after the face passes below an area. However, the occurrence of massive beds in the overburden could delay this. With longwalls, surface movements are complete within a few years, but when pillars are left intact for support, this may take decades. Room and pillar mining with removal of pillars may produce surface effects similar to longwall mining, with the degree of similarity dependent upon the amount of coal left as fenders or stumps.

Structural characteristics: The extent of damage to a structure is dependent on the type of structure and its size, shape, age, foundation design, construction materials and techniques used, standards of maintenance and repair, and purpose. The surcharge due to building loads may induce soil compaction, generating instability. Tall structures cannot tolerate much tilt, poorly constructed or older buildings are more readily damaged, and a large edifice is more liable to crack because of the strains and curvature induced by subsidence.

3.3 Temporal effects of subsidence

The duration of subsidence resulting from mining is composed of two distinct phases:

(1) active and

(2) residual.

1. Active subsidence

Active subsidence refers to all movements occurring simultaneously with the mining operations, while residual subsidence is that part of the surface deformation that occurs following the cessation of mining (or in the case of longwall mining, after an underground excavation has reached its critical width). The duration of residual subsidence is of particular importance from the standpoint of structural damage at the surface as well as from a legal perspective.

The latter involves evaluating the extent of liability of underground mine operators for post-mining subsidence. Time spans during which surface subsidence may occur vary markedly with the mining method being used. Longwalls induce subsidence rapidly, beginning almost immediately after mining. With room and pillar systems, major occurrences of surface subsidence may be delayed for decades until the support pillars have substantially deteriorated and collapsed. The actual time involved depends on a number of factors such as the strengths of coal, roof, and floor; extent of fracturing; presence of water; depth of workings; pillar size; and percentage extraction. Hence prediction of when or how much damage may occur becomes difficult.

Longwall mining: The duration of residual subsidence movements above longwall panels is relatively short, typically varying between a few weeks and about 10 years. Further, the magnitude of these movements rarely exceeds about 10% of the total subsidence.

There are numerous empirical relations proposed to estimate the duration of residual subsidence but none of them are applicable as a generalization due to site specific constants contained within each expressions.

Room and pillar mining: In room and pillar mining without pillar recovery, the magnitude of active subsidence is generally small, and the ground surface may experience a variable frequency of subsidence incidents during this period. The coal pillars and the surrounding rock are usually relatively sound at this time with only minor deflections of the roof being transmitted to the surface.

Some time after mining, however, complete collapse of the abandoned pillars and the adjacent strata may occur as a result of natural causes or human activities. These processes are likely to continue until all the voids created by mining excavation have been filled by the caved strata. Consequently, in the case of room and pillar mining, the residual subsidence can be the major subsidence measured on the surface.

Recent studies, however, have shown that no matter how well-designed a room and pillar layout might be, the additional weight transmitted to the pillars due to excavations will cause measurable deformation on the pillars, and these movements will eventually be transmitted to the surface. Depending upon the extent of pillar loading and the characteristics of the pillars and the super-incumbent material, the surface deflection may vary from considerable to negligible, and sometimes is nearly undetectable. The long-term stability of mine pillars is extremely difficult to determine.

2. Residual subsidence

The three basic mechanisms responsible for residual subsidence over room and pillar mines includes:

1. Collapse of roof beds spanning adjacent pillars.
2. Pillar failures.
3. Squeezes or crushes.

i. **Roof collapse *over* remnant pillars**: This is perhaps the most prevalent failure mechanism associated with abandoned room and pillar mines. Depending on certain geometric and geotechnical factors, the caving process may be arrested at some point in the overburden or it may extend upwards to the surface. The surface expression of this process is generally in the form of a localized depression or pit. The height to which the collapse process can take place is a function of –

a. Volume of the original mine opening or room.
b. Bulking factor of the strata material.

c. Location and thickness of overlying competent strata.

Two basic modes of roof failure has been recognized, namely, shear and flexural failure. The former usually initiates diagonal tension cracks near the junction of the mine pillar and the roof, and the latter causes tension cracks near the mid span of the roof. Both result in voids above the mine level. Dependent on the mechanism of failure of the individual roof beds and their tensile and shear strengths, a variety of geometric forms of collapse are possible, ranging from conical through wedge to rectangular. For a given width of mine opening, it can be demonstrated that, for each type of collapse, the height of collapse is a function of the overlying strata. The influence of competent strata in the overburden has been neglected in this analysis (Piggott and Eynon, 1977).

ii. **Pillar failures***:* These phenomena occur due to changes in the environment or surcharged loading and may take place at the time of mining or after considerable delay. They result in trough-like subsidence.

In general, subject to pillar geometry, pillar failure does not ordinarily occur at shallow depths since the size of coal pillars left behind are usually much greater than that required to support the overlying strata or any additional loading from surface development. However, where very small pillars or "stubs" exist within a given mining section, these may fail and cause sufficient loads to be transferred to adjoining pillars by arching, resulting in extended failure. In most instances, pillar failures coincide with some phase of mining, such as pillar robbing on the retreat, abandonment of a particular mining area, or working other seams in close proximity. Another common cause of pillar failure is the action of concentrated foundation loads, from pile foundations or otherwise, being transmitted onto the remnant pillars (Piggot and Eynon, 1977).

iii. **Squeezes or crushes***:* When abandoned pillars punch into either the immediate roof or floor that might have been weakened or altered by the action of water or other weathering processes, squeezes (crushes) may result. Generally, the surface settles as a trough or basin.

The mechanism of failure in this case is not unlike the failure of building foundations as the load carried by the mine pillar is transferred to the floor (or roof). If the bearing capacity of either the roof or floor is exceeded, squeezing may occur. The following factors favor bearing capacity failure:

a. Underclay mine floor.
b. High pillar stresses.
c. Flooded mine condition

3.4 Factors Influencing Duration of Residual Subsidence

The factors in room and pillar mines that govern the duration of residual subsidence have not been quantified as yet. Probably the following parameters play a role:

1. Depth of working*:* Increased depth implies a longer duration for subsidence movements. Any instability caused at the mine level has to propagate through the overburden in order to reach the surface.

2. Mine geometry*:* This may be expressed in terms of the following attributes:

a. Seam thickness.
b. Pillar width-to-height ratio.
c. Extraction ratio.
d. Presence of multiple panels.
e. Presence of multilevel workings.

Increased seam thickness increases the potential for instability of pillars and speeds up the subsidence process. Both the pillar width-to-height ratio and extraction ratio reflect upon the safety factor built into the mine design. Pillar width-to-height ratios greater than 0.1 and extraction ratios of less than 50% have both been claimed to permit no surface subsidence. Although mines designed to these standards have been known to be stable for long periods of time, sometimes more than a hundred years, this is not strictly true. Presence of multiple panels and multilevel workings generally result in a shorter residual subsidence phase since they increase the volume of underground voids.

3. Strength and deformation characteristics of the roof floor, and pillar: Over the long term, these affect the duration of surface subsidence depending on the inter-relationships of these structural members.

4. Types of roof control*:* Roof control practices in a mine influence the relative susceptibility of the roadways to collapse; for example, bolted mines tend to subside faster than those with cribs, steel supports, or other types of bracing.

5. Character of the overburden*:* Significant aspects which profoundly govern the duration of subsidence movements are-

a. Thickness of surficial soil beds.
b. Lithology.
c. Structural geology.

Soil thickness is also important since the fractures propagate through it rapidly. Also granular materials (e.g., sands) offer less bridging capacity than fine-grained soils (i.e., clays).

Although the effect of lithology is poorly understood, weaker rocks (i.e., shale and siltstone) are generally unable to support their own weight and the strata above, and transmit subsidence movements to the surface in a short time span. Competent rocks (e.g., sandstone and limestone) effectively bridge over excavations and delay the residual subsidence period. Besides their relative competency, the thicknesses of these strata govern the duration of subsidence; massive beds inhibit the propagation of subsidence movements longer than thin laminated formations. Also affecting the process are facies changes, lensing, pinch outs, and other lateral variations of geology that may alter the character of the overburden from one place to another. Joints occur even in competent strata, and some slippage along these may be expected with time. Thus even though some investigators suggest that a competent rock layer of thickness greater than 1.75 times the width of the workings will arrest the collapse (Piggott and Eynon, 1977).

Structural geology impacts subsidence in the same manner as lithology, by varying the ability to bridge excavated spans. Generally, surface geologic features (e.g., faults, photo-lineaments, stream valleys), and underground features (e.g., bedding planes, joints, fissures, cleat, folds, or other inhomogeneities) tend to shorten the subsidence period.

6. Presence of old mined-out workings*:* Old workings in the vicinity of an active mine accelerate the rate of residual subsidence, since the surrounding strata are disturbed.

7. In-situ stress field*:* The existence of high horizontal stresses impacts the time for subsidence since the structural integrity of the mine supports is affected.

8. Water*:* The presence of water reduces the strength and stiffness of mine pillars, roof, and floor in flooded mines. Further, softening of the floor (e.g., underclay) encourages pillar punching, resulting in instability and subsidence. Flow of water through fissures causes seepage pressures in the rocks, endangering the rock mass stability. The formation of pits in shallow mines is promoted by these factors. Dewatering of flooded mines accelerates coal pillar deterioration by exposing submerged pillars to the damaging effects of air and removing the buoyant support afforded by the water.

Periodic changes of humidity cause the slow deterioration of pillars, roof, and floor, with similar results.

9. Non-mining factors*:* Those that affect subsidence includes:

a. Mine fires.

b. Surface precipitation.

Although not common, mine fires accelerate the subsidence process due to degradation of abandoned pillars, formation of less rigid burnt out ashes as well as underground voids. It's important to note that in case of Jharia coalfield (JCF), coal fire is one of the major cause of land subsidence *apart* from the mining related subsidence.

CHAPTER 4

LAND SUBSIDENCE :

MEASURING TOOLS AND TECHNIQUES

4.1 Space borne techniques

4.1.1 InSAR

Several methods are available to monitor land subsidence phenomenon. The conventional approaches use repetitive survey with leveling or GPS observations. Spaceborne Synthetic Aperture Radar Interferometry (InSAR) has revolutionized the field of crustal deformation research since its first geophysical application in 1993 (Massonnet, *et al* .,1993). During the last 15 years, InSAR has been used to study a wide range of surface displacements related to active faults, volcanoes, land subsidence, landslides, and glaciers, at a spatial resolution of less than 100 m and cm-level to sub-cm level precision (Zebker *et al*., 1986, 1992; Gabriel *et al* 1989;Goldstein *et al.,* 1993,1995; Rosen *et al*., 1996: Galloway *et al*., 1998; Massonnet *et al*., 1993,1997,1998;Carnec *et al*., 1995; Strozzi. *et al* 2001; Amelung *et al*., 1999,2000; Franceschetti et al 1999; Ferretti et al.,1999.2000,2001,2005;Rosen *et al*., 2000;Usai 2001; Colesanti *et al*., 1999,2001; Hansen *et al*., 2001,2002,2005; Fruneau and Sarti, 2000; Berardino *et al*., 2002; Crosetto. *et al*., 2002,2003; Lanari *et al*., 2004; Chatterjee *et al*., 2006, Raucoules *et al.,* 2007; Hooper *et al*., 2007 & 2008;). The temporal resolution is ranging from 1-day to ~1-month or more. Due to the viewing geometry of the radar satellite, InSAR is particularly sensitive to vertical deformation. Several limitations to the InSAR method exist, especially decorrelation of the scatterers due to vegetation or other surface change processes, incoherence caused by large satellite orbit separations between the two image acquisitions used to make an interferogram, and noise from signal delays in the Earth's atmosphere.

SAR systems illuminate the Earth with a beam of coherent microwave radiation, retaining both amplitude and phase information in the radar echo during data acquisition and subsequent processing. This radiation can be described by three properties:

- Wavelength - the distance between peaks on the wave.
- Amplitude - the displacement of the wave at the peak.
- Phase - describes the shift (in degrees or radians) of the wave from some other wave.

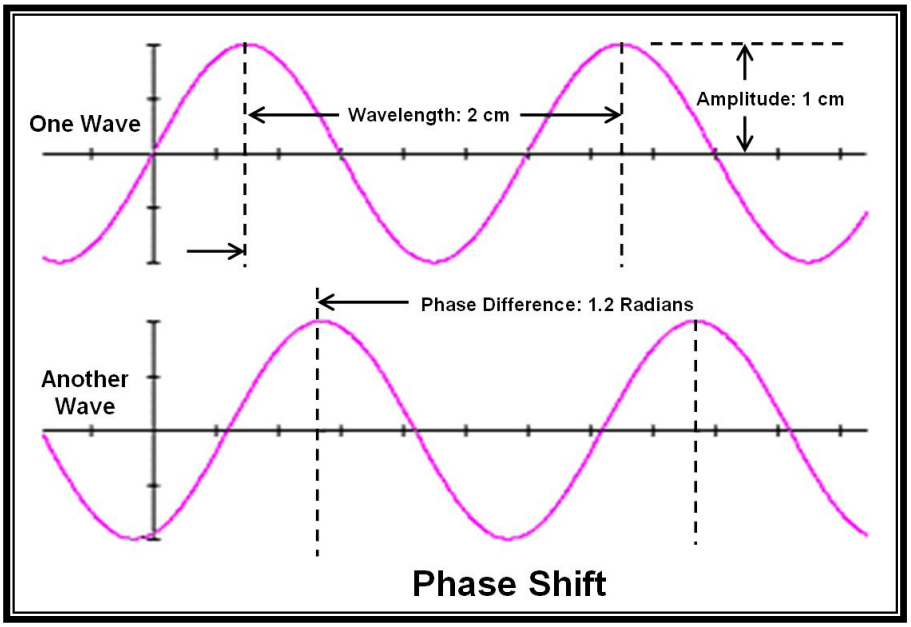

Fig. 4.1.1: Phase shift in SAR Interferometry

SAR interferometry (InSAR) exploits this coherence, using the phase measurements to infer differential range and range change in two or more complex-valued SAR images of the same surface. The resulting difference of phases is a new kind of image, called an interferogram.

For a second SAR image for interferometric measurement, it must be acquired from a slightly different sensor position. The difference between the acquisitions of the first and second images determines the type of interferometric results. Some of the most common forms are:

- Across-track (range) – used primarily for topographical information, this type utilizes a difference in across-track position.
- Along-track (azimuth) – used primarily for ocean currents information and moving object detection, this type utilizes a difference in the along-track position, which can be achieved by a small difference in acquisition time, on the order of microseconds to seconds.
- Differential Interferometry (DInSAR) – this method utilizes a difference in time, on the order of days to years, and is used primarily to observe glacier or lava flows, if the time difference is within days. If the time difference is measured in days to years, it can be a very useful method for studying subsidence, seismic events, volcanic activity, or crustal displacement.

In order to distinguish *cross-track* from *along-track interferometry* is often referred to antenna arrangements built for motion measurements. Cross-track SAR interferometers come in two flavors: *Single-pass* interferometers record the required two SAR images simultaneously by using a

transmit/receive antenna and a secondary receive antenna mounted some distance away. *Repeat-pass* interferometers, on the other hand, use images taken at different times, e.g. separated by days or months. The height to phase sensitivity of a repeat-pass across-track SAR interferometer is

$$\frac{\partial \Delta\phi}{\partial h} = \frac{4\pi B_{\perp}}{\lambda R \sin\theta} \tag{4.1.1}$$

From that it would be desirable to operate at large baselines ($B^{\perp}$). It can be shown, however, that with increasing baseline the two complex SAR images forming the interferogram tend to decorrelate, requiring the so-called spectral shift filtering. Once the spectral shift exceeds the SAR system bandwidth *W,* the interferogram is completely decorrelated and useless for terrain reconstruction. The maximum allowable baseline is often referred to as the *critical baseline*:

$$B_{\perp,crit} = \frac{\lambda W R \tan(\theta - \alpha)}{c} \tag{4.1.2}$$

where α is the component of the local terrain slope in the range direction and *c* is the velocity of light.

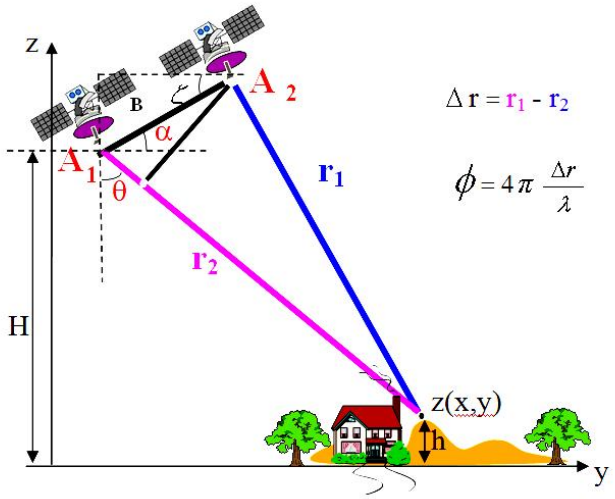

Fig. 4.1.2: Geometry of InSAR

where:

B	: Baseline between two SAR antennas
α	: Inclination angle of baseline
θ	: Incident angle of radar
r_1& r_2	: The length of slant range
H	: The height of satellite 1 from surface of the earth
h	: The elevation value of target point

The difference of r_1 and r_2 (Δr) can be measured from the phase difference ($\Delta\phi$) between the two complex SAR images. This is performed by multiplying one image by the complex conjugate of the other image, where an interferogram is formed whose phase is proportional to the range difference to the point. The phase of the interferogram contains fringes that trace the topography like contour lines.

In this case, multiple acquisitions can be made to measure the topography, and to measure the change in topography (differential effects) over time.

InSAR Phase and Interferogram

The input data for generation of interferogram, are two complex SAR images. It contains intensity and phase information as well as orbit data describing positions and flying directions of the sensor. Considering the InSAR configuration, the phase difference (*interferometric phase*) is found as

$$\Delta\phi = \phi_2 - \phi_1 = \phi_{prop,2} - \phi_{prop,1} = \frac{4\pi}{\lambda}(R_2 - R_1) \tag{4.1.3}$$

Where, the scattering phase is assumed to be invariant, i.e. $\phi_{scatt\,1} = \phi_{scatt\,2}$. Obviously, the range parallax $\Delta R = (R_2 - R_1)$ is a measure for the look angle θ which, in turn, depends on the terrain height *h*.

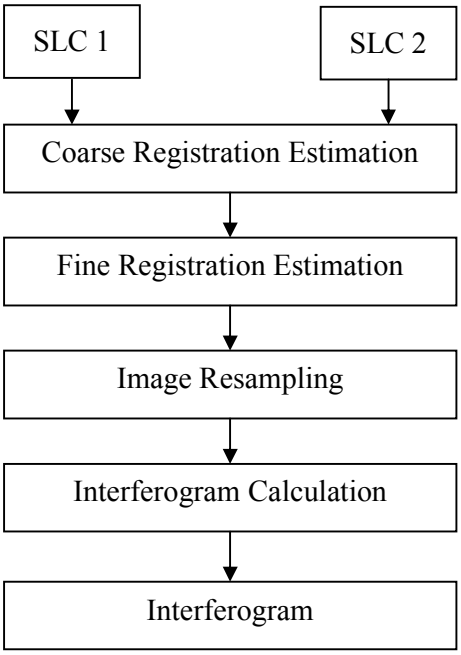

Fig. 4.1.3 Flow diagram for interferogram generation

The diagram shows the main steps involved in the generation of an interferogram. The required inputs are two SLC (complex) images with an appropriate spatial baseline distance between them.

The co-registration parameters between the input data are computed in two steps during the interferogram generation. In the coarse registration estimation, the azimuth offset between the two images is calculated by estimating the maximum of the cross-correlation between the amplitude of the two SLC images.
The subsequent processes includes:

- co-registration of two SAR images on sub-pixel accuracy;
- formation of a rough interferogram with flat-earth phase trend;
- removal of flat-earth phase trend using precise orbit data; and
- filtering of the interferogram.

Following these processes, an enhanced interferogram could be obtained. It is understandable that the uncertainty or errors introduced on different stages of data processing leading to the formation of interferograms affect the quality of resultant interferograms.

Co-registration of SAR Complex Image Pairs

SAR image co-registration is a fundamental and one of the most important step in interferometric SAR processing. Two complex images are used for co-registration, one called *master image* and the other called *slave image*. Assume $Z_1(m,n)$ and $Z_2(m,n)$ represent the master image and the slave image, respectively:

$$Z_1(m,n) = a_1(m,n)\, e^{j\varphi_1(m,n)} \tag{4.1.4a}$$

$$Z_2(m,n) = a_2(m,n)\, e^{j\varphi_2(m,n)} \tag{4.1.4b}$$

where $m=0,1,2,...,M-1$, $n=0,1,2,...,N-1$, the image size is $M \times N$.

The two images are taken of the same scene, but at different times; therefore their orientation could be quite different. Geometrically, they are in different coordinate systems. Therefore, there is a need of an operation to bring them down to an identical coordinate system, i.e., either both to a common ground coordinate system, or one of the two image coordinate systems. The former is termed *rectification*, and the latter is termed *co-registration*. In other words, co-registration is to fit one image to the coordinate systems of the other. In order to carry out this operation, the relationship between these two images needs to be established. Due to the complex nature of the InSAR images, some types of polynomials are normally used as approximate models for the transformation between them. Bicubic function is a commonly used one:

$$U=a_0+a_1x+a_2y+a_3x^2+a_4xy+a_5y^2+a_6x^3+a_7x^2y+a_8xy^2+a_9y^3 \quad (4.1.5a)$$

$$V=b_0+b_1x+b_2y+b_3x^2+b_4xy+b_5y^2+b_6x^3+b_7x^2y+b_8xy^2+b_9y^3 \quad (4.1.5b)$$

where (u,v) is the pixel's coordinate in slave image. (x,y) is the pixel's coordinate in master image.
The interferogram (I) is calculated as the Hermitian product (C1•C2*) of the two complex images C1 and C2. The interferometric phase (ϕ) is expressed as

$$\phi = \tan^{-1}(\text{Image(I)}/\text{Real(I)}) \quad (4.1.6)$$

Where Image(I) and Real(I) are the imaginary and real parts of the calculated interferogram respectively. It should be noted that this phase (ϕ) is only known as modulo 2π , therefore phase unwrapping is necessary to resolve the inherent ambiguity. This is carried out in a subsequent step (Phase unwrapping).

In essence, the interferometric phase is the sums of several contributions, which can be described as below:

$$\phi_{Int} = 4\pi \frac{R_1 - R_2}{\lambda} = \phi_{Topography} + \phi_{Orbits} + \phi_{Movement} + \phi_{Atmosphere} \quad (4.1.7)$$

InSAR Coherence

The interferometric coherence/correlation is a measure of the phase properties of SAR image pairs and indicates displacement and change of the scattering elements within the scene. Coherence can be considered as a direct measure for the similarity of the dielectric properties of the same imaging cell between two SAR acquisitions. It also can be seen as the accuracy in the estimation of the interferometric phase: more accurate phase estimates means less phase interference and change. Coherence decreases with increasing time delay and temporal changes in the targets.
Given two co-registered complex SAR images (S_1 and S_2), one calculates the interferometric coherence (γ) as a ratio between coherent and incoherent summations:

$$\gamma = \frac{\left|\sum s_1(x).s_2(x)^*\right|}{\sqrt{\sum\left|s_1(x)\right|^2.\sum\left|s_2(x)\right|^2}} \quad (4.1.8)$$

The observed coherence - which ranges between 0 and 1 - is a function of systemic spatial decorrelation, the additive noise, and the scene decorrelation that takes place between the two acquisitions.

Actually coherence can be used for determining the quality of the interferometric measurement (i.e. interferometric phase). It must be noted that phase images whose coherence values are lower than

0.25 should not be considered for further processing since those low incoherent pixels shall not provide accurate and reliable phase measurements. The coherence image can also be used to filter the flattened interferogram by using an adaptive filtering technique.

Motion and change in vegetation also affect coherence. Leaf motion will usually cause a total loss of coherence, but this does not imply that areas of vegetation will always appear with zero coherence: radiation will often penetrate the foliage, at least partially, and can be backscattered by the terrain underneath or by the trunk and branches of the trees, which are mechanically much more stable and will therefore contribute to the coherence. In general, deciduous trees will show high coherence during winter when there are no leaves and less coherence in summer due to foliage effects. Similarly, different types of vegetation will show different one-day coherence values, depending on the height of the plant and on the lengths of the leaves: short leaves could be practically transparent to the C-band radiation of ERS or ENVISAT, RADARSAT satellites. Multi-temporal Interferometric analysis of the coherence and amplitude of the backscatter can therefore contribute to the detection and classification of various environmental parameters in general.

The joint use of coherence and the amplitude of the backscatter allows for better image segmentation. While the amplitude of the return depends on the electromagnetic structure of the target, the coherence is mostly related to its mechanical stability.

Actually coherence can be used for determining the quality of the interferometric measurement (i.e. interferometric phase). It must be noted that phase images whose coherence values are lower than 0.25 should not be considered for further processing since those low incoherent pixels shall not provide accurate and reliable phase measurements. The coherence image can also be used to filter the flattened interferogram by using an adaptive filtering technique.

4.1.2 D-InSAR (Differenial Interferometric Synthetic Aparture Radar)

In D-InSAR analysis, the component relevant to the movement or displacement (i.e. movement), is separated from other components, namely from ϕ_{Orbits} and $\phi_{topography}$. $\phi_{atmosphere}$ generally not considered during DInSAR processing but subsequently during post-processing for suppressing or avoiding the component. ϕ_{Orbits} is computed based on the orbit geometry of the data pair and removed at the first step from ϕ_{int}. $\phi_{topography}$ may be obtained from a close temporal interval InSAR data pair (as shown in figure 4.1.2.1) or simulated as synthetic phase image from a good quality DEM of the area and subtracted from ϕ_{int}.

In the following, the principle of the DInSAR technique is briefly summarized. A scheme of the image acquisition is shown in Figure 4.1.2.1, considering a single pixel footprint P:

- The sensors acquire a first SAR image at the time t_o, measuring the phase ϕ_M. The first satellite and the corresponding image are usually referred as the master, *M*.
- Assuming that a land deformation D(t) occurs, which has a given evolution in time, the point *P* moves to *P'*.
- The sensors acquire a second SAR image at the same time t, measuring the phase ϕ_S. The second satellite is usually referred as the slave, S.

The InSAR techniques exploit the phase difference of ϕ_S and ϕ_M, named interferometric phase $\Delta\phi_{Int}$. Assuming that D(t) is naught, i.e. the terrain is stable and P' coincides with P, this phase is related to the distance difference *SP-MP*, which is the key element for the InSAR DEM generation. When the point moves from *P* to *P'* between two image acquisitions, besides the topographic phase component ϕ_{Topo}, $\Delta\phi_{Int}$ includes the terrain movement contribution, ϕ_{Mov}. In the general case $\Delta\phi_{Int}$ includes:

$$\Delta\phi_{Int} = \phi_S - \phi_M = \frac{SP - MP}{\frac{\lambda}{4\pi}} + \frac{SP^1 - SP}{\frac{\lambda}{4\pi}} + \phi_{Atm} + \phi_{Noise} \qquad (4.1.2.1)$$

$$\Delta\phi_{Int} = \phi_{Topo} + \phi_{Mov} + \phi_{Noise} \qquad (4.1.2.2)$$

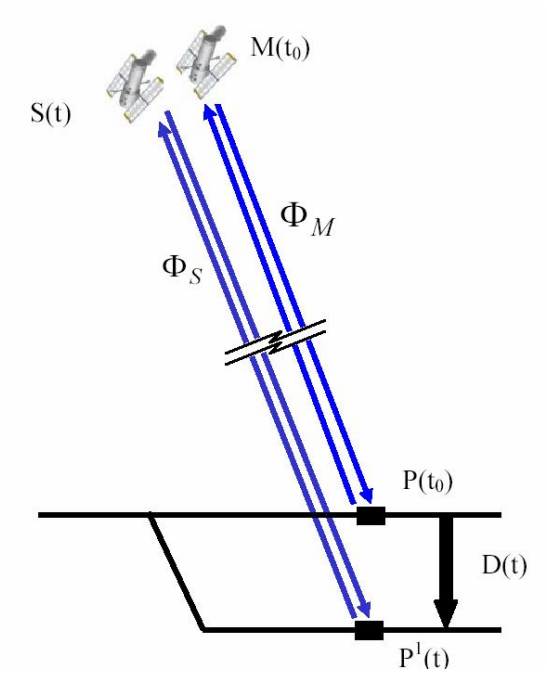

Fig. 4.1.2.1 : Principle of DInSAR for deformation measurement

where ϕ_{Atm} is the atmosphere contribution; ϕ_{Noise} is the phase noise; *SP'* is the slave-to-*P'* distance; and λ is the radar wavelength. As mentioned above, using the topographic component ϕ_{Topo} is possible to generate a DEM of the inverse transformation is used: if a DEM of the imaged scene is available, ϕ_{Topo} can be simulated and subtracted from $\Delta\phi_{Int}$, obtaining the so-called DInSAR phase $\Delta\phi_{D-Int}$:

$$\Delta\phi_{D-Int} = \Delta\phi_{Int} - \phi_{Topo\_Sim} \quad (4.1.2.3)$$

$$\Delta\phi_{D-Int} = \phi_{Mov} + \phi_{Atm} + \phi_{Res\_Topo} + \phi_{Noise} \quad (4.1.2.4)$$

where, ϕ_{Topo_Sim} is the simulated topographic component, and ϕ_{Res_Topo} represents the residual component due to errors in the simulation of ϕ_{Topo}, e. g. errors in the employed DEM. In order to derive information on the terrain movement, ϕ_{Mov} has to be separated from the other phase components. The techniques that use an external DEM in order to derive the topographic phase component use the so-called two-pass D-InSAR configuration. There is another configuration, the three-pass interferometry, which can work without a priori known DEM, but which requires at least three images acquired over the same scene.

4.1.2.1 Precision of DInSAR observation

Topographic sensitivity ($\sigma_{\Phi\ topo}$) $= \frac{\partial\phi}{\partial h}\sigma_h = \frac{4\pi}{\lambda}\frac{b_\perp}{\rho\sin\theta}\sigma_h$

Displacement sensitivity ($\sigma_{\Phi\ disp}$) $= \frac{\partial\phi}{\partial\Delta\rho}\sigma_{\Delta\rho} = \frac{4\pi}{\lambda}\sigma_{\Delta\rho}$

where, $b_\perp$:perpendicular baseline

ρ : slant range distance

λ : SAR wavelength

θ : Look angle

$\sigma_{\Delta\rho}$: phase ambiguity

σ_h : altitude of ambiguity

as b/ ρ <<1; $\frac{\sigma_{\phi_{disp}}}{\sigma_{\Delta\rho}} >> \frac{\sigma_{\phi_{topo}}}{\sigma_h}$

Thus, with DInSAR technique millimeter scale accuracy of surface movement is measurable.

4.2 Differential GPS survey

GPS (Global Positioning System) is a passive, all-weather satellite-based navigation and positioning system, which is designed to provide precise three dimensional position and velocity, as well as time information on a continuous worldwide basis (Wells *et al.,* 1986; Hofmann-Wellenhof *et al.,* 1997; Abidin, 2008). For monitoring land subsidence, in order to monitor the subsidence of even very small magnitude, the ideal positioning accuracy to be achieved is in mm level. In order to achieve that level of accuracy then the GPS static survey method based on phase data should be implemented with stringent measurement and data processing strategies (Leick, 1995; Abidin *et al.,* 2002). Considering the obtainable GPS accuracy and precision which becomes higher and higher, it could be expected that the roles of GPS for monitoring land subsidence would become more and more important in the near future.

The principle of land subsidence monitoring using repeated GPS surveys method is shown in Fig. 4.2.1. With this method, several monuments which are placed on the ground covering the area and its surroundings are accurately positioned using GPS survey relative to a certain reference (stable) point.

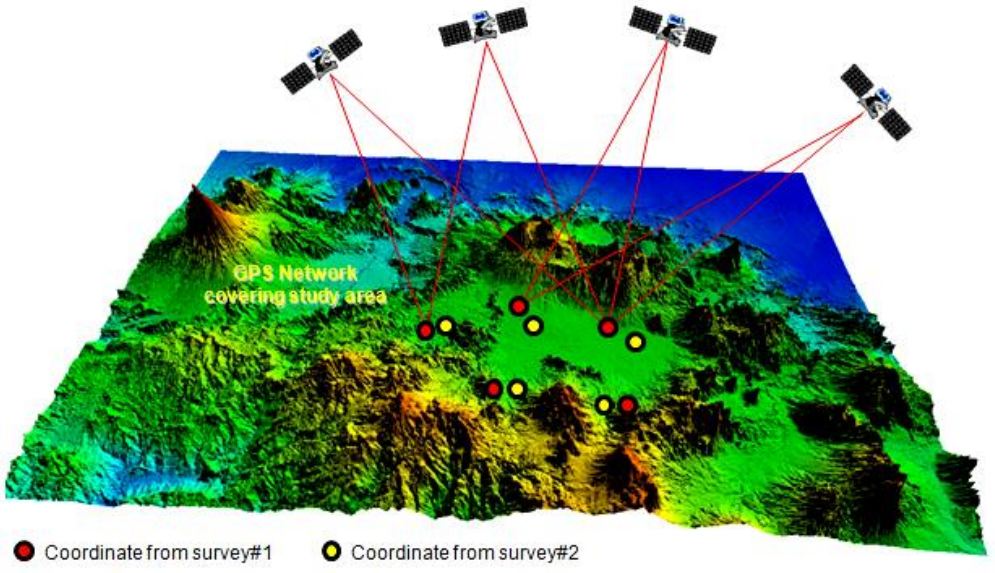

Fig. 4.2.1 **:** Schematic diagram illustrating the principle of land subsidence monitoring by multi date Differential GPS survey

The precise coordinates of the monuments are periodically determined using repeated GPS surveys with certain time interval. By studying the characteristics and rate of changes of the height component of coordinates from survey to survey, the land subsidence characteristics can be analyzed.

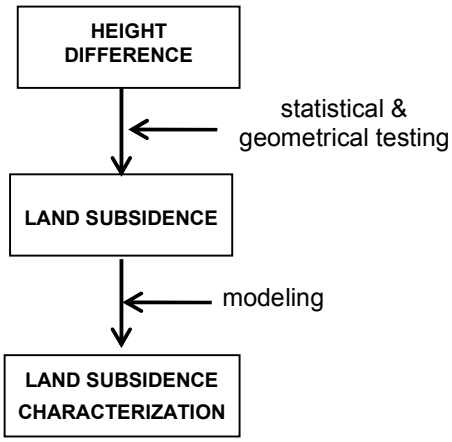

Figure 4.2.2: Flow diagram for land subsidence characterization

4.3 Ground based Monitoring/measurement of subsidence

In order to make subsidence measurements, it is essential to erect permanent survey monuments that will undergo the same vertical or horizontal displacements as the ground, it should be stable and firmly anchored about 5 ft (1.5 m) below the ground surface so as not to be affected by frost or other surface effects.

The choice of measuring instruments that may be used for subsidence measurements depends on a number of parameters (Panek, 1970):

1. Objectives of the investigation.
2. Area to be covered.
3. Topography of the region.
4. Profiles along which monuments are installed.
5. Spacing and number of monuments or observation stations.
6. Total cost that can be tolerated.
7. Duration of the investigation; survey frequency.
8. Labor requirements for surveying and data reduction.

The horizontal distance between monuments depends on the subsidence gradient. Generally, however, a compromise has to be reached between placing the monuments too close, which increases installation and measurement cost, and too far apart, which does not give enough readings to depict the measured variables adequately. The accuracy of the measurements should be such as to detect strains of 10^{-4}, which is about 1/10th the strain-level for structural damage. The method of measurement and the precautions necessary depends on the distance between monuments and may be obtained from any text on surveying.

Vertical displacements may be measured by trigonometric leveling (precision optical or laser), differential leveling, or tilt measurement. When using the theodolite, vertical angles must be measured correct to ½ second of arc. With precise leveling, a micrometer direct reading to about 0.005 ft (1.5 mm) should be employed. An inclinometer with a sensitivity of 10 seconds of arc is generally adequate for subsidence measurements. Second order subsidence surveys with geodetic level and invar scale or equivalent, should close within 0.035 (*M*)1/2 feet, where *M* is the circuit length in miles (Moffitt and Bouchard, 1975), an accuracy of 0.01 ft (3.3 mm) over a 1000-ft (305-m) line. In mountainous or swampy areas, third-order control with a closure of 0.052(*M*) 1 / 2 ft may be used, an accuracy of 0.02 ft (6.5 mm) in 1000 ft (328 m). Tiltmeters for use in long-term (several years) subsidence surveys have been developed (e.g., Jacobsen et al., 1975; Holzhausen,1986).

4.3.1 Optical leveling

Conventionally, heights at mean survey time are derived from observed spatial height differences assuming the height of at least one reference point per survey. Subsidence is computed by differencing heights of the same benchmark at different times. Often raw displacement is finally smoothed and contoured to remove irregularities due to benchmark instabilities. The procedure is easily understood, but insufficiently robust with respect to errors in implied assumptions. Subsidence monitoring seeks to quantify subsidence of the earth surface due to a specific cause, such as groundwater extraction, as a continuous function of time and location. Geodetic subsidence measurements reflect spatial height differences between discrete benchmarks at discrete moments in time. Although geodetic measurements (leveling, Differential GPS, InSAR) represent spatial height differences, subsidence assessment requires temporal differences.

The aim of subsidence monitoring is to measure subsidence of the earth surface, whereas geodetic measurements assess the behavior of benchmarks that are not motionless with respect to the earth's surface. Geodetic measurements capture subsidence at discrete locations and times only, whereas subsidence, as a continuous function of time and place within the confines of the survey area and period, is sought (Houtenbos, 2005).

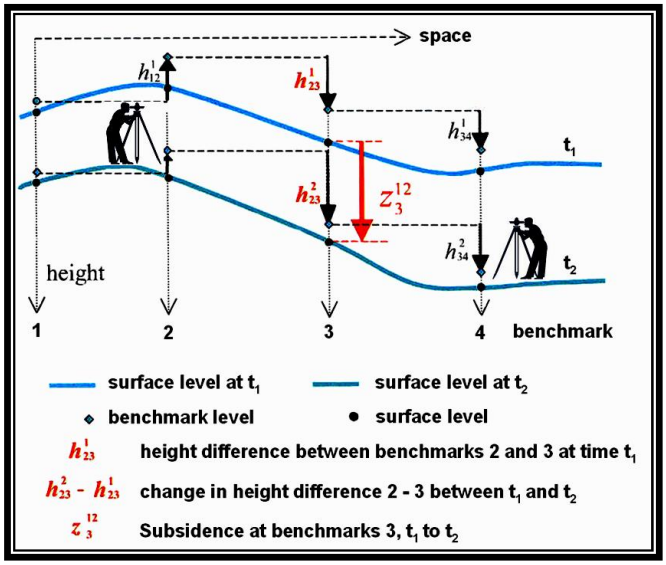

Fig. 4.3.1: Principle of leveling technique for land subsidence measurement (Houtenbos, 2005)

Usually, there will be a special interest in one specific subsidence component, while geodetic measurements reflect undifferentiated aggregate or total subsidence. The data processing challenge is to overcome these limitations of the geodetic measurements with respect to the true nature of the subsidence.

Regardless of the procedure, the differential character of the geodetic measurements makes determination of absolute subsidence impossible. Only relative subsidence (deformation) between locations within the survey area can be resolved.

CHAPTER 5

MATERIALS AND METHODS

5.1 Data used

In this study the following data have been used:

Table 5.1.1 List of the data used in the present study

Type	Date	Quantity	Purpose
Satellite Data (Optical and SAR)			
CARTOSAT-1 stereo data	May 2006	2	High resolstion digital elevatin model generation
Geo rectified LISS-IV MX, CARTO Merge	April 2007	3	Precise localisation of the subsiding areas , mapping of mining features and other enviromental indicators
Geo rectified IRS LISS II PAN merged data	1997	1	
ERS-1,2 tandem pair	April,1996	2	Interferometric digital elevation model generation
ENVISAT ASAR slc data	2003, 2004, 2005 & 2007	19	Differential interferogram generation and subsidence measurement
ENVISAT ASAR alternate polarization data	March & April 2006	2	Delineation of different environmental indicators based on their scattering properties
Topographic Data			
SRTM DEM (90 m)	February, 2000	1	Topographic phase removal in D-InSAR processing,es Comparitive study of the data to evaluate the esesitivity for deliniation of mining features
ASTER DEM (30 m)		1	Comparitive study of the data to evaluate the esesitivity for deliniation of mining features
CARTORSAT-1 DEM (10m)	2006	1	Comparitive study of the data to evaluate the esesitivity for deliniation of mining features
Topographic Map 1:50000 scale	1979	2	Image-georeferencing
Ancillary Data			
GPS Survey	2000, 2001, 2002, 2003 & 2005	≈ 20 points, distributed over the entire area	Validation of D-InSAR based land subsidence
Surface mine plans of the colliery areas of BCCL (1:4000,1:8000 scale)	2006,2007,2008	13	

Differential GPS Survey	2006,2007,2008	Around 20 points (permanent monuments by BCCL) well distributed in the 4 test sites	Land subsidence observation from Differential GPS measurement for the 4 test sites,
	2007,2008	20 GCPs, collected on ground using DGPS (Leica single frequency DGPS receiver)	GCP(Ground Control Point) collection for CARTOSAT-1 DEM generation,
Optical leveling survey	2006,2007,2008	Around 20 points (permanent monuments by BCCL) well distributed in the 4 test sites	Land subsidence observation from Differential GPS measurement for the 4 test sites,

5.1.1 Satellite data

a. Optical satellite data

IRS LISS-IV –CARTO Merge multi-spectral data acquired on April 2007 with spatial resolution 2.5 m has been used for precise localization of subsiding area and thematic map generation namely land use /land cover and various environmental indicators.

b. SAR and InSAR data

Nineteen scenes of ENVISAT ASAR (SLC) have been used for InSAR processing for measuring land subsidence phenomenon of the study area. ENVISAT ASAR images acquired between August 2003 and December 2007 with a temporal interval of 35 days, were used in this study for InSAR processing. Detailed specifications of the SAR data are listed below (Table 5.1.1.1).

Table 5.1.1.1 Detailed spesifications of SAR data

Satellite	Date	Orbit	Incidence angle	Wavelength (cm)
ERS-1	12.04.1996	24799	23°	5.6
ERS-2	13.04.1996	5126	23°	5.6

Sl No.	Satellite	Date	Orbit	Incidence angle	Wavelength (cm)
1	ENVISAT ASAR	30.08.2003	7831	23°	5.6
2	ENVISAT ASAR	04.10.2003	8332		
3	ENVISAT ASAR	08.11.2003	8833		
4	ENVISAT ASAR	13.12.2003	9334		
5	ENVISAT ASAR	17.01.2004	9835		
6	ENVISAT ASAR	01.05.2004	11338		
8	ENVISAT ASAR	05.06.2004	11839		
9	ENVISAT ASAR	03.09.2005	18352		
10	ENVISAT ASAR	17.03.2007	26368		
11	ENVISAT ASAR	25.03.2007	26490		
12	ENVISAT ASAR	21.04.2007	26869		
13	ENVISAT ASAR	26.05.2007	27370		
14	ENVISAT ASAR	30.06.2007	27871		
15	ENVISAT ASAR	04.08.2007	28372		
16	ENVISAT ASAR	08.09.2007	28873		
17	ENVISAT ASAR	13.10.2007	29374		
18	ENVISAT ASAR	17.11.2007	29875		
19	ENVISAT ASAR	22.12.2007	30376		

Sl No	Date	Orbit	Spatial Resolution (m)	Look angle	Polarization
1.	March 2006	26490	30	IS3 (18-26°)	HH,VV
2.	April 2006	26991			HH, HV

5.1.2 Topographic data

a. Topographic map

Topographic maps of the study area on 1:50000 scale (Survey of India toposheet No. 73I1,2,5 &6) published by Survey of India in the year 1979 have been used.

b. DEM (Digital Elevation Model)

SRTM (Shuttle Radar Topographic Mission) DEM with 90m X 90m spatial resolution has been used for topographic phase compensation and differential interferogram generation.

High resolution CARTOSAT -1 DEM with 10 m spatial resolution, along with ASTER with 30 m spatial resolution (source: ASTER GDEM) & SRTM with 90 m spatial resolution is used for comparative study to for evaluation of the data for delineation of various mining features.

5.1.3 Ancillary data

Differential GPS-based measurements

Table 5.1.3.1 : Differential GPS survey details for the four test sites of BCCL for the duration 2006-2008

GPS Surveys	Survey Year	Observation Points
Survey-1	2006	Dobari: Stn. No. DS2, Stn. No.DS04, Stn. No.DS05, Stn. No.DS07, Stn. No.DS09, Stn. No.DS011, Stn. No.DS13, Stn. No.DS15,Stn. No.DS17, Stn. No.DS21 Bassuriya: Stn. No.-EBF01,Stn. No.-EBF03, Stn. No.-EBF04, Stn. No.-EBF05, Stn. No.-EBF06, Stn. No.-EBF07, Stn. No.-EBF08, Stn. No.-EBF09 Jayrampur: : Stn. No.-JRF01, Stn. No.-JRF02, Stn. No.-JRF03, Stn. No.-JRF05, : Stn. No.-JRF12, : Stn. No.-JRF13, : Stn. No.-JRF14, : Stn. No.-JRF15, : Stn. No.-JRF016, : Stn. No.-JRF23 Sudamdih: Stn. No.-17B, Stn. No.-23B, Stn. No.-23C, Stn. No.-26B,Stn. No.-32C, Stn. No.-32D, Stn. No.-36B
Survey-2	2007	Dobari: Stn. No. DS2, Stn. No.DS04, Stn. No.DS05, Stn. No.DS07, Stn. No. DS09, Stn. No.DS11, Stn. No.DS13, Stn. No.DS15, Stn. No. DS17, Stn. No. DS21. Bassuriya: : Stn. No.-EBF01,Stn. No.-EBF03, Stn. No.-EBF04, Stn. No.-EBF05, Stn. No.-EBF06, Stn. No.-EBF07, Stn. No.-EBF08, Stn. No.-EBF09 Jayrampur: Stn. No.-JRF01,Stn. No.-JRF02, Stn. No.-JRF03, Stn. No.-JRF05, Stn. No.-JRF12, Stn. No.-JRF13, Stn. No.-JRF14, Stn. No.-JRF23 Sudamdih: Stn. No.-B2, Stn. No.-CI , Stn. No.-17B ,Stn. No.-23B, Stn. No.-23C, Stn. No.-26B, Stn. No.-32C, Stn. No.-32D, Stn. No.-36B,
Survey-3	2008	Dobari: Stn. No. DS2, Stn. No.DS16, Stn. No. DS05, Stn. No. DS06, Stn. No.DS04 Bassuriya: Stn. No. DS2, Stn. No.DS04, Stn. No.DS05, Stn. No.DS07, Stn. No. DS09 Jayrampur: Stn. No.-JRF01,Stn. No.-JRF12, Stn. No.-JRF13, Stn. No.-JRF14, Stn. No.-JRF15, Stn. No.-JRF23 Sudamdih: Stn. No.-CI , Stn. No. 17B,Stn. No.-23B , Stn. No.-23C, Stn. No.-29B, Stn. No.-36B,

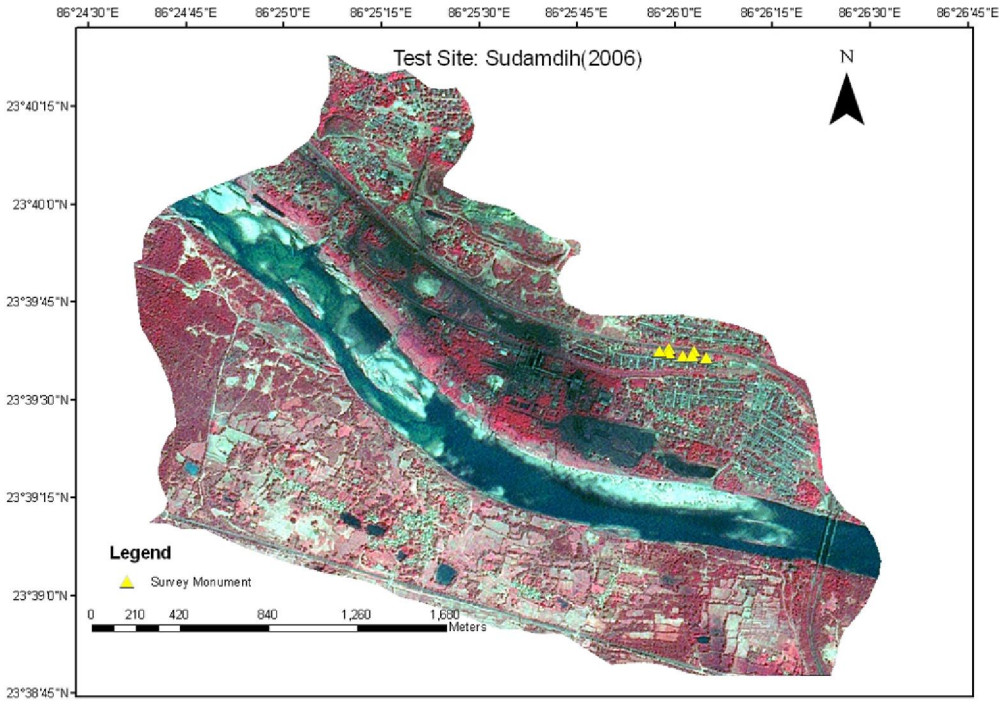

Fig. 5.1.3.1 Survey monument locations of the test site Sudamdih for multi-date DGPS & optical leveling survey, marked on LISS IV CART merge data

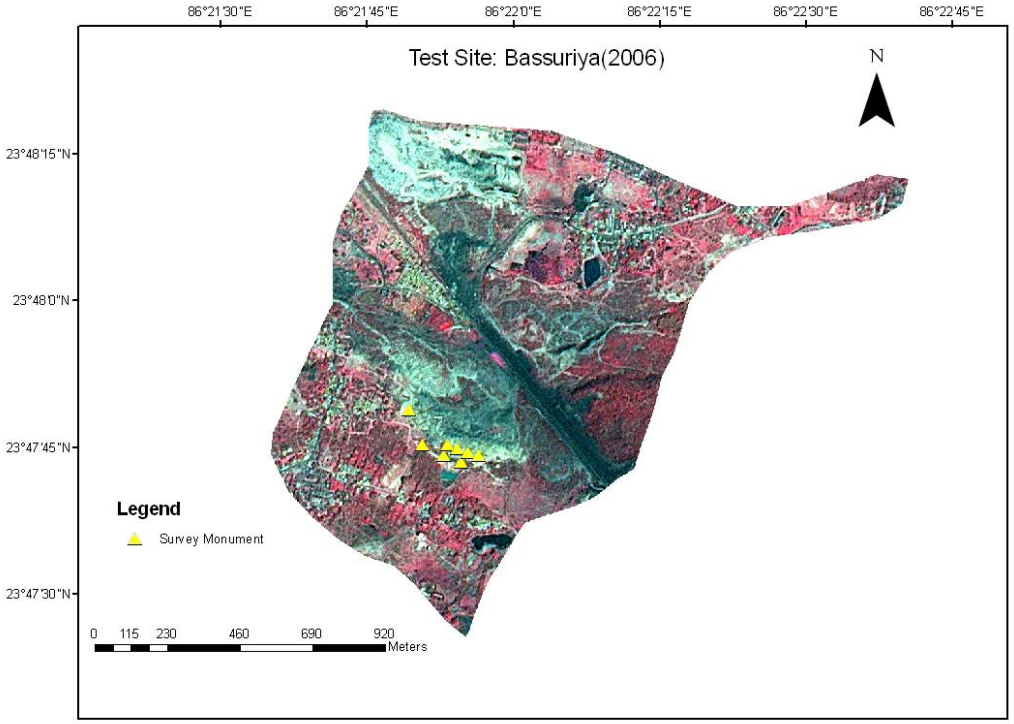

Fig. 5.1.3.2: Survey monument locations of the test site Bassuriya for multi-date DGPS & optical leveling survey, marked On LISS IV CART merge data

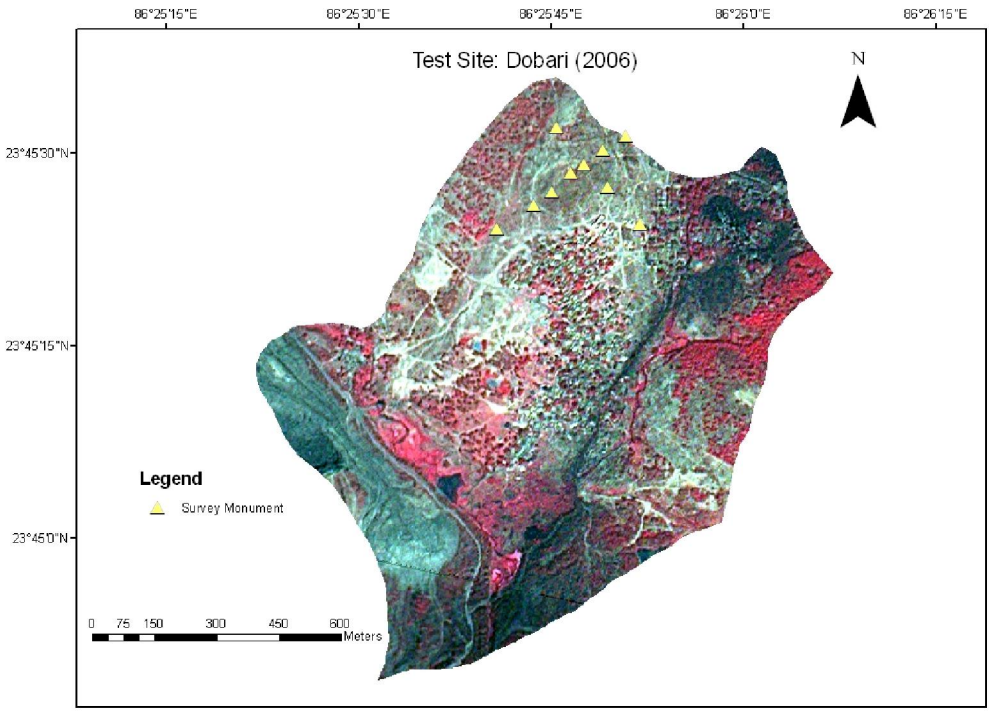

Fig. 5.1.3.3: Survey monument locations of the test site Dobari for multi-date DGPS & optical leveling survey, marked on LISS IV CART merge data

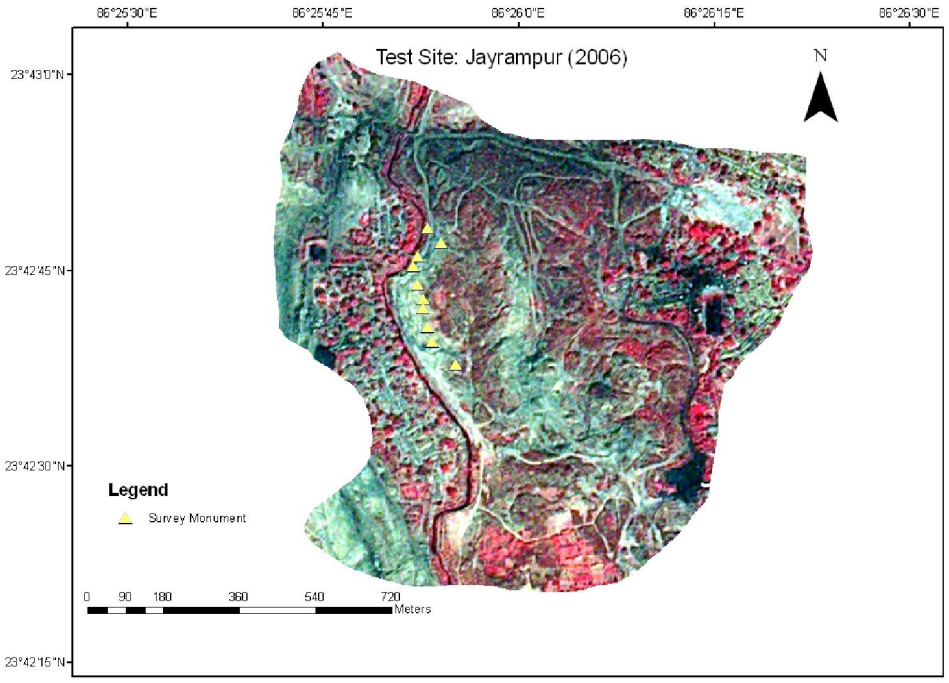

Fig. 5.1.3.4.:Survey monument locations of the test site Jayrampur for multi-date DGPS & optical leveling survey, marked on LISS IV CART merge data

5.2 Methodology

Broadly the following methodologies were adopted in the present study is as follows:

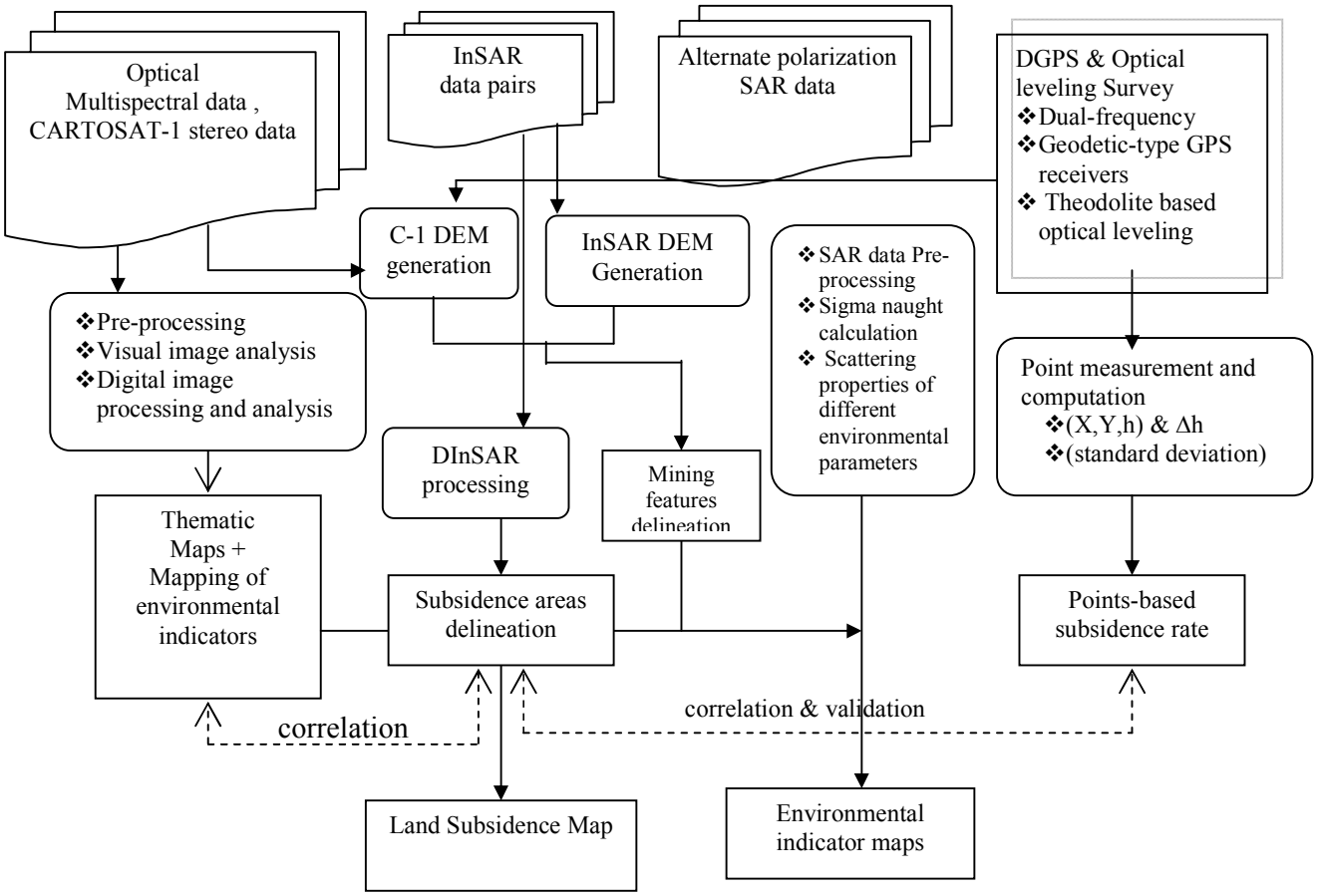

Fig. 5.2.1 Work flow diagram of describing the broad methodology adopted in the present study

5.2.1 D-InSAR data processing

The interferometric phase ($\Delta\phi_{int}$) obtained by combining two complex SAR images can be expressed as the sum of several terms (Hanssen, 2001):

$$\Delta\phi_{int} = \Delta\phi_{flat} + \Delta\phi_{topo} + \Delta\phi_{mov} + \Delta\phi_{atmos} + \Delta\phi_{noise} \quad (5.2.1)$$

where $\Delta\phi_{flat}$ is the flat-earth component related to range distance differences in ease of flat topography, $\Delta\phi_{topo}$ is the topographic phase, $\Delta\phi_{mov}$ is the phase contribution due to ground displacement occurring between the two SAR image acquisitions, measured along LOS, $\Delta\phi_{atmos}$ is the phase component due to atmospheric disturbances or artifacts, and, finally, $\Delta\phi_{noise}$ includes the remaining noise sources. The first two terms in equation 5.2.1 can be expressed analytically. $\Delta\phi_{flat}$

can be simulated from the satellite geometry, and $\Delta\phi_{topo}$ can be extracted from an external DEM and satellite geometry.

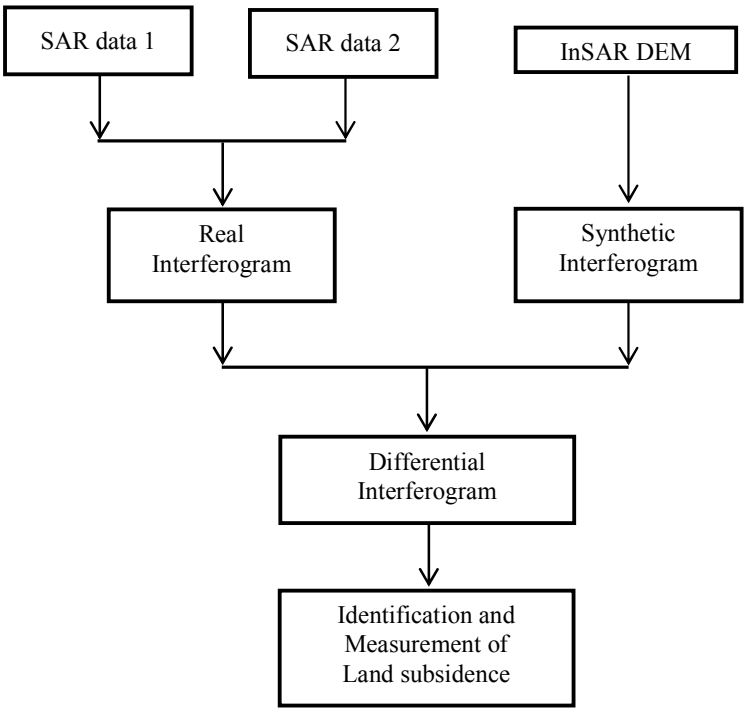

Fig. 5.2.1.1 Flow diagram describing differential InSAR data processing for land subsidence measurement

5.2.2 Analysis of interferograms

The phase differences are measured in the repeating interval from zero to 2π, where every 2π cycle is equivalent to a Line-of-Sight (LOS) change equal to one-half the radar wavelength, which is about 28 mm (2.8 cm) for SAR data collected by ENVISAT ASAR (C-band) sensors. The phase-difference data are unwrapped to create an unwrapped interferogram that represents a continuous surface of absolute displacement values.

In this work, each fringe (phase cycle) in the differential interferogram is representing by "rainbow" color scheme as shown below.

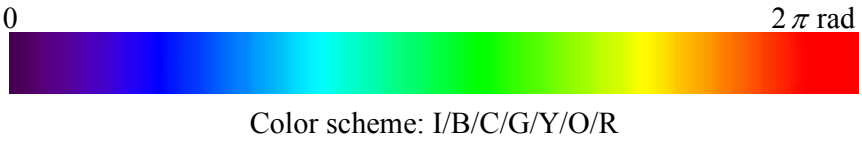

Fig. 5.2.2.1: Color scheme for one cycle of Interferometric fringe

Multi-color interferograms depict displacement with a repeating color sequence. The order of colors indicates whether deformation is subsidence or uplift, as shown in the color-scale bar. Displacement should be estimated only for those areas with well-defined fringes. The estimated displacement is relative to the surrounding areas and is not necessarily the total amount of displacement.

SARscape v. 3.2 of SARMAP, Switzerland was used for both InSAR and DInSAR data processing for land subsidence delineation and generation of InSAR based DEM.

5.2.3 Differential GPS-based measurement and analysis

In this method, several monuments which are placed on the ground covering the area and its surroundings, are accurately positioned using GPS survey relative to a certain reference (stable) point. The precise coordinates of the monuments are periodically determined using repeated GPS surveys with certain time interval. By studying the characteristics and rate of changes of the height component of the coordinates from survey to survey, the land subsidence characteristics can be derived.

Differential GPS survey was carried out using dual-frequency geodetic-type Trimble dual frequency GPS receivers in a campaign mode, for each of the four test sites. The permanent survey monuments constructed by the BCCL were used as the reference (stable) point with known coordinates. For Differential GPS survey, the length of each session was kept as 1 hour. The data were collected at an interval of 10 seconds, and elevation mask was set at 15^{o}.

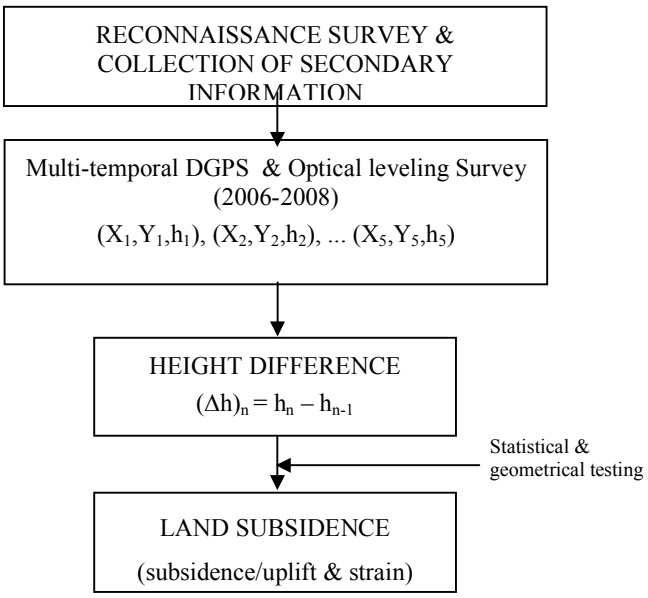

Fig. 5.2.3.1 Flow diagram showing the principle of point based land subsidence measurement using GPS technique

DGPS data Processing were carried out by the survey team of Survey of India for subsidence study. Pre-planning and DGPS data post processing were using Trimble Geomatic Office (TGO) software. The final coordinates were estimated using the ionospheric free linear combination signal after fixing the integer ambiguities of L1 and L2 signals.

Ground control Point collcetion using Differential GPS for High resolution Digital Elvation model generation.

For deliniation of various mining features (e.g. opencast quaries, abandoned mine, burden dumps, mine benches, etc.), an attepmpt has been made to generate a high resolution digital elevation model by photogrammetric technique using CARTOSAT-1 2.5m spatial resolution stereo data and InSAR based digital elevation model from ERS1-2 tandem data and then to evaluate the result with availale SRTM & ASTER digital elevation model to deliniate aforesaid surficial features more distinctively for environmental monitoring purpose.

In this process, well distributed and accurate ground control points (GCP) were collected using single frequency Leica Differential GPS instrument in campaign mode for a duration of 1 hour for each.

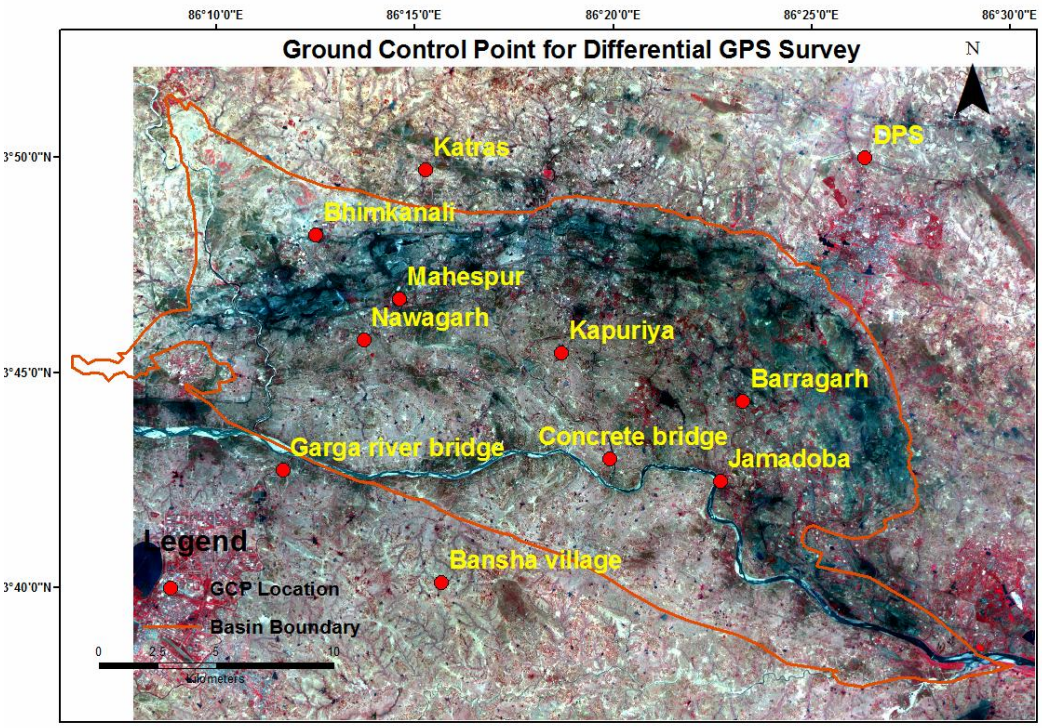

Fig.5.2.3.2 GCP locations using Differenntial GPS for Photogrammatric DEM generation plotted on IRS LISS IV CARTO mareged data of Jharia basin

As the quality of the measured GCP's severely affected by the ionospheric effecs (after about 1200 hrs IST), in terms of DOP (Dilution of Precision), preplanning of survey were carried out using Trimble

Geomatics Office software suite before collcetion of the data. Post processing were carried out using Leica SkiPro v.3.0 software.

(a)

(b)

(c)

(d)

Fig.5.2.3.3: GCP location using DGPS survey: (a) non-metallic 'Y' road junction at Azadnagar near cinema hall; (b) Saharjuri concrete road crossing; (c) road crossing near Garga river bridge; (d) ; non metal tri-road junction at Kalapathar village

5.2.4 Optical leveling-based measurement

Optical leveling was carried out by the experienced survey team of Central Institute of Fuel & Mining Research, Dhanbad using Theodolite survey instrument for the same monuments constructed by the BCCL in four test sites in a periodic interval from 2006-2008.

(a) (b)

Fig: 5.2.4: (a) CMFRI's levelling team at East Bassuriya test site;(b) BCCL's survey monument for subsidence monitoring at Dobari test site with SOI's DGPS team & project supervisor

5.2.5 Surfacial mining features characterisation from DEM:

Cartosat-1 stereo pairs over Jharia coal field along with the corresponding Rational Polynomial Functions (RPC) were used to generate DEM for the areas. For any particular area, RPCs relate object space to image space and vice versa. The accuracy of the coordinates depends on the RPCs used. The Root Mean Square Errors (RMSE) in planimetry and elevation values at all the checkpoints (10) have been computed. The checkpoints were established through differential GPS survey of the study area. The flow diagram for generation of digital elevation model from CARTOSAT-1 stereo data, using photogrammetric technique is shown in the Fig. 5.2.5.1

Leica Photogrammetric Suite v. 9.0 was used to process and generate Digital Elevation Model (DEM) from CARTOSAT-1 stereo data with RPC files.

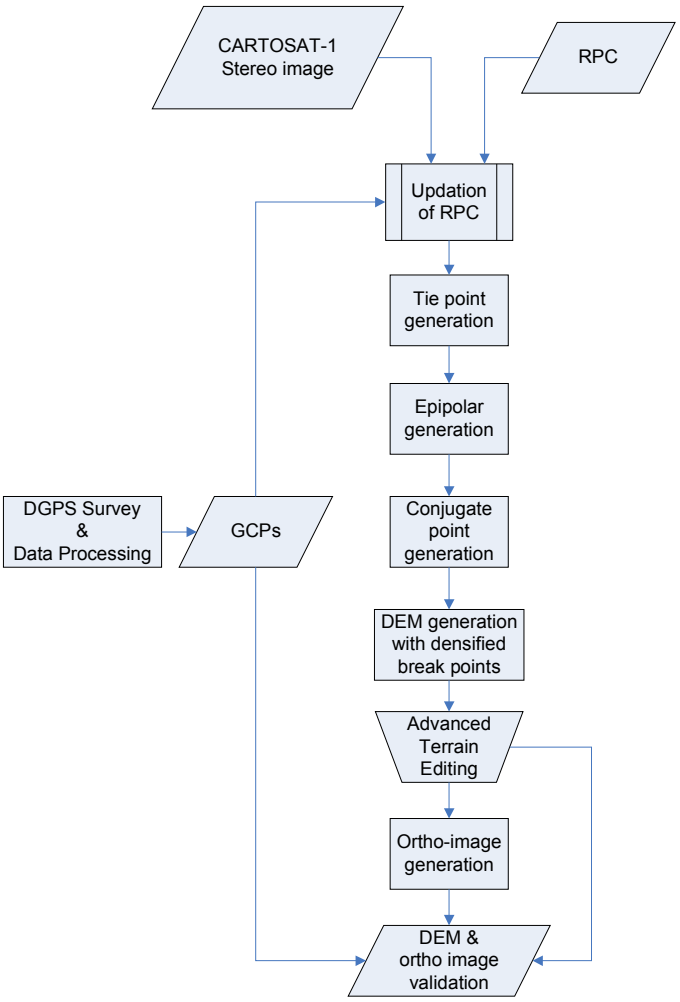

Fig. 5.2.5.1: Schematic representation of DEM generation with CARTOSAT-1 stereo data with RPC and GCPs (Ahmed 2007)

Interferometric DEM generation with ERS-1&2 tandem pair data

The quality assessment of a space-borne InSAR DEM is not straight forward. Usually, the vertical standard deviation is provided. Its value can, however, vary significantly, depending mainly on the normal baseline ($B_{\perp}$) of the interferograms involved, on local decorrelation phenomena, For areas with high relief topographic features reasonable figures range from 5–10 to 15–20 m (excluding pixels affected by geometric distortion where phase information can hardly be exploited). Whenever topography is gentle the precision can be finer. Due to the side looking geometry and availability of ascending and descending mode of pass, InSAR Dem is more sensitive for terrain characterization.

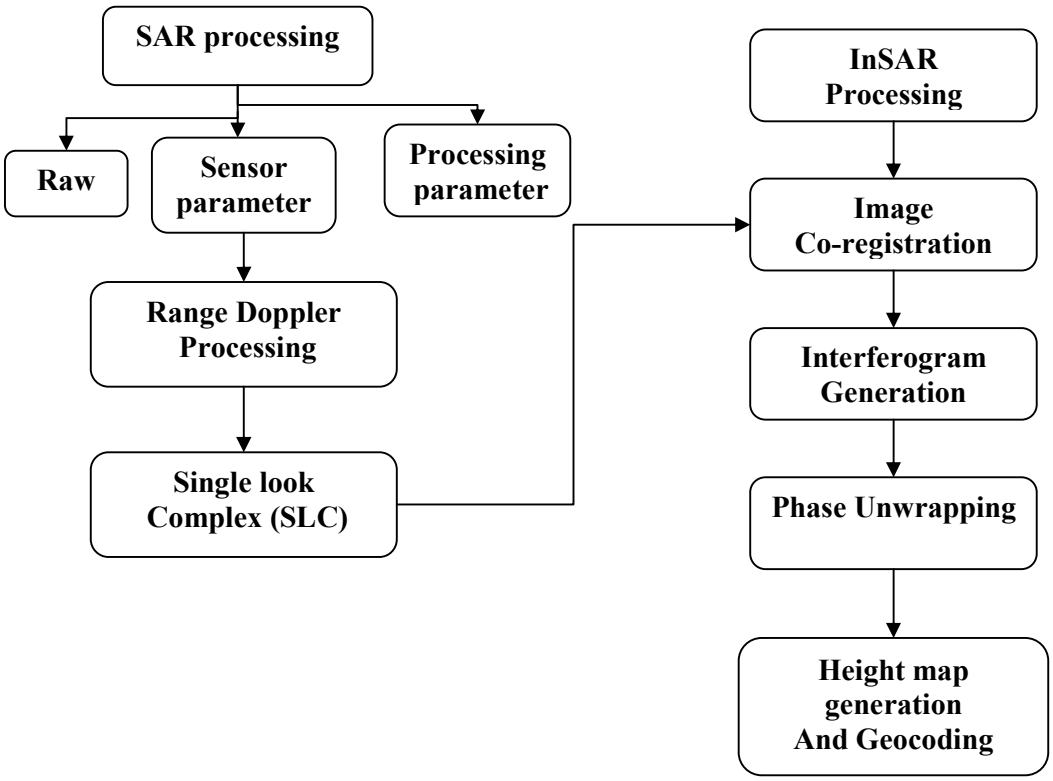

Fig:5.2.6.1: Flow diagram for Interferometric Digital Elevation Model generation

Terrain characterization & delineation of mining related features from DEM

Digital Elevation Models (DEMs) are increasingly used for visual and mathematical analysis of topography, landscapes and landforms, as well as modeling of surface processes.

DEM offers the most common method for extracting vital topographic information and even enables the modeling of flow across topography, a controlling factor in distributed models of landform processes. To accomplish this, the DEM must represent the terrain as accurately as possible, since the accuracy of the DEM determines the reliability of the geo-morphometric analysis.

In this section an attempt has been taken to evaluate various DEM & its derived parameters (e.g. slope aspect, contour , surface, hillshade etc.) their sensitivity to delineate the surface mining related terrain characteristics.

5.2.6 Delineation of the terrain response in multi- polarization SAR data for environmental indicators based on their scattering properties

Two sets of ENVISAT ASAR alternate polarization (HH/VV and HH/HV) data with a temporal difference of 35-days were analysed to derive σ° images in HH-, VV-, and HV-polarizations. DN images were radiometrically calibrated using the gain-offset parameters and distributed incidence angle extracted from the satellite ephemeris as described below:

$$\sigma^{\circ} = \frac{\left(A^2\right)}{K}.Sin\left(\alpha_D\right)$$

$$\sigma^{\circ}\left(dB\right) = 10.\log\left(\frac{\left(A^2\right)}{K}\right) + 10.\log.\left(Sin\left(\alpha_D\right)\right)$$

Where,

$<A^2>$ = average pixel intensity = $(DN+Offset)^2$

K = absolute calibration constant (or expanded gain scaling table value)

σ° = distributed target backscattering coefficient or sigma nought

σ°(dB) = distributed target sigma nought in logarithmic scale

α_D = distributed target incidence angle

PCI Geomatica (v. 10.0) software tools were used to calibrate and correct the data for generating σ°(dB) images. Subsequently, σ^{o} (dB)-values were retrieved at a regular grid interval corresponding to the environmental indicators in the study area.

CHAPTER 6

RESULTS AND DISCUSSION

6.1 Differential InSAR-based land subsidence detection

As discussed in chapter 5, the interferometric phase difference depends on the geometric baseline (perpendicular baseline, temporal as well as seasonal variation and coherence information.

Out of nineteen (19) ENVISAT ASAR single look complex scenes with minimum 35 days temporal interval were pre-processed and data pair are selected based on the perpendicular baseline ($B^{\perp}$) for further InSAR processing.

It is observed (Fig. 6.1.1) that the interferometric data pairs with high temporal interval shows high temporal decorrelation in terms of coherence loss and results in noisy interferograms, even if the geometric baseline criteria is getting satisfied. The amplitude, coherence and differential interferograms of the selected interferometric data pairs are illustrated from Fig. 6.1.2 to 6.1. 21

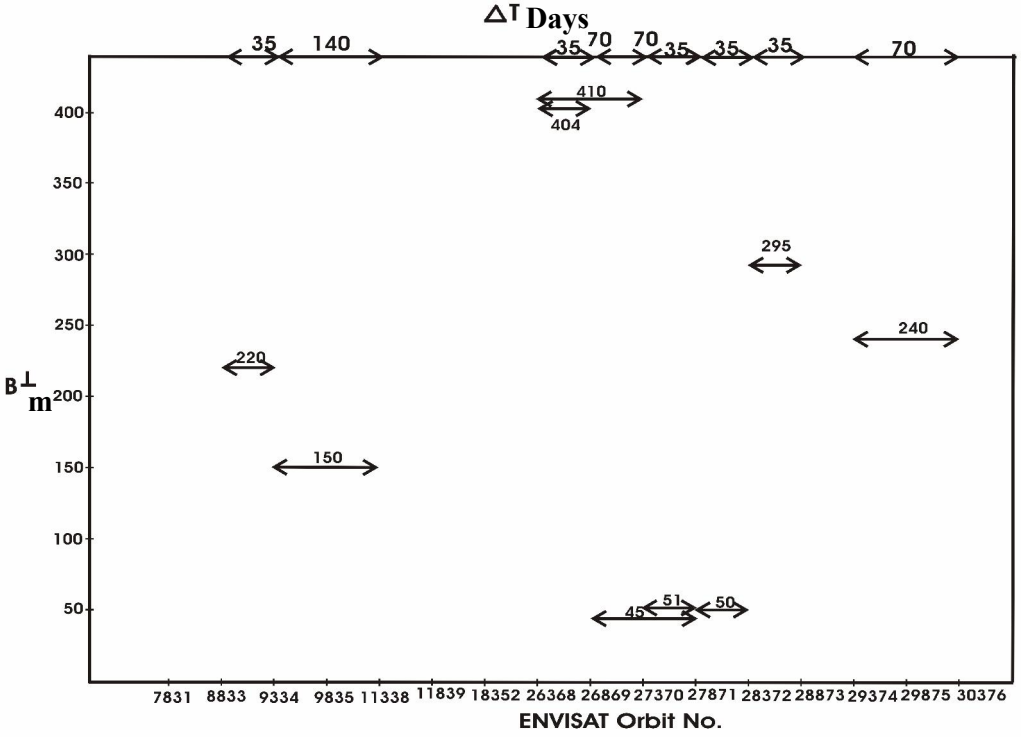

Fig. 6.1.1:Perpendicular baseline and temporal baseline relationship between the ENVISAT ASAR interferometric data pair.

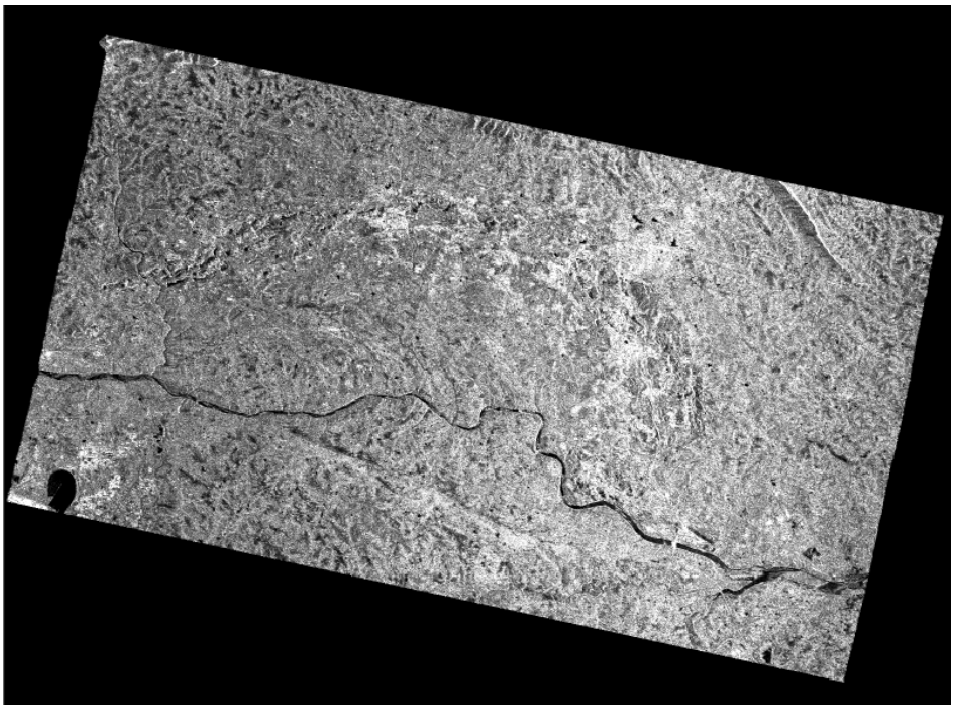

Fig.6.1.2 Amplitude image of ENVISAT ASAR data (08.11.2003) of Jharia coalfield (JCF)

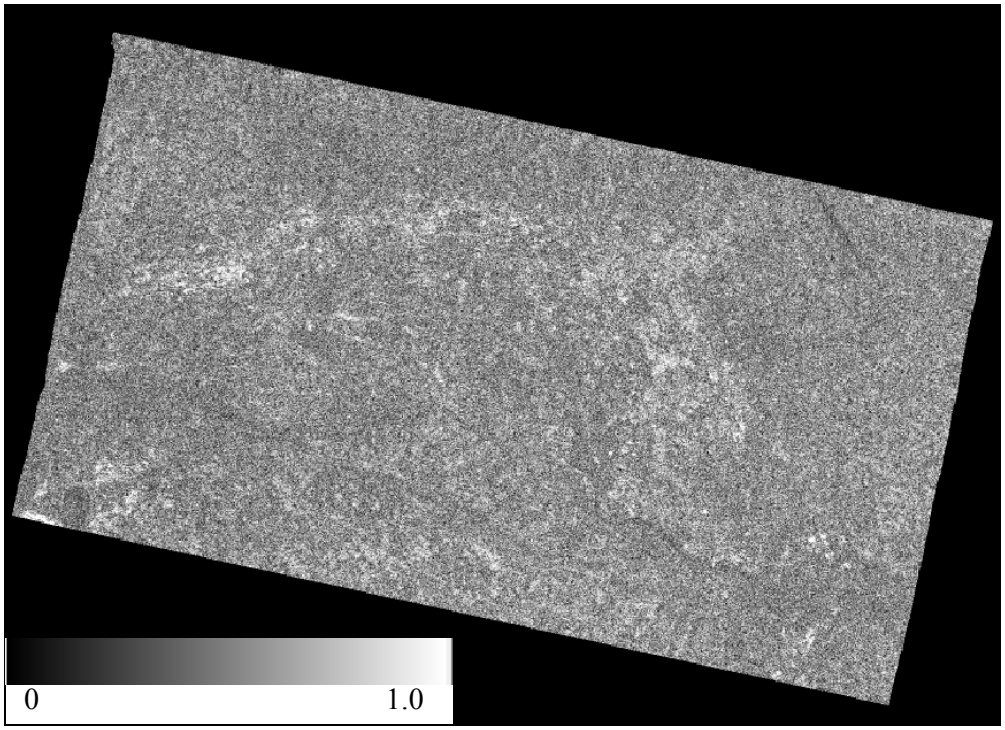

Fig.6.1.3: Coherence image of ENVISAT ASAR data pair (08.11.2003 & 13.12.2003) for Jharia coalfield (JCF)

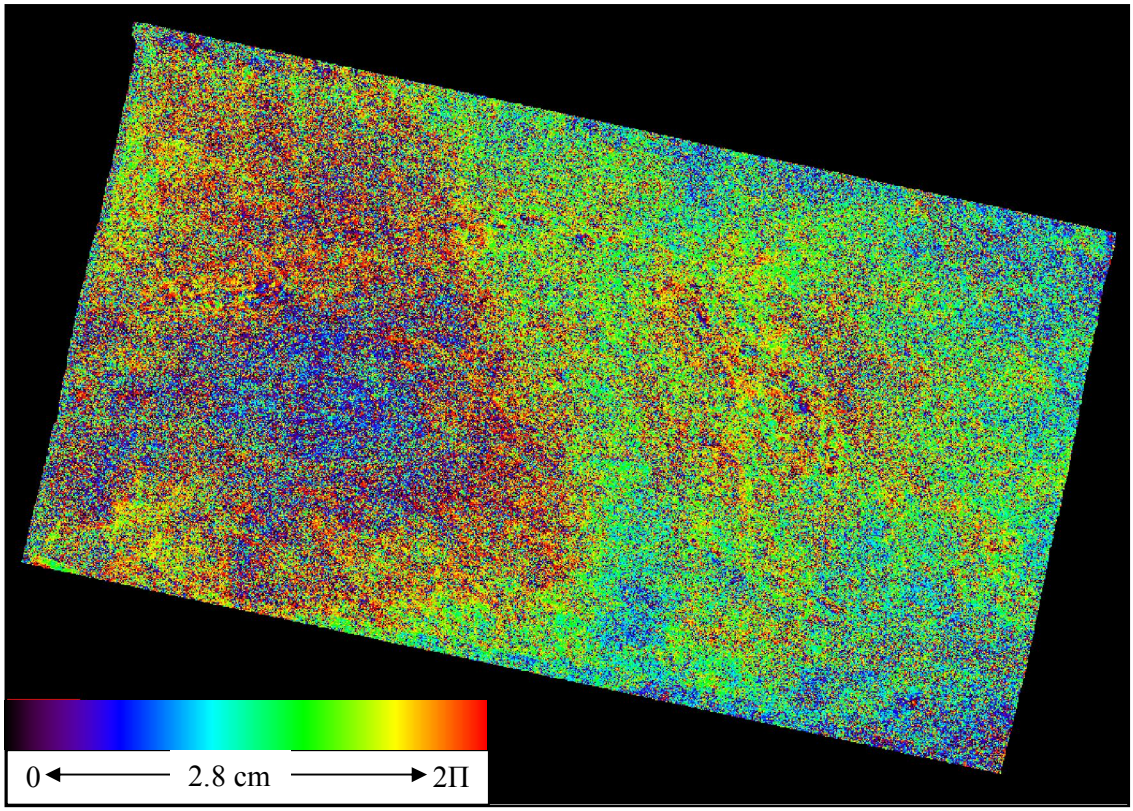

Fig. 6.1.4:Differential Interferogram of ENVISAT ASAR data pair (08.11.2003 & 13.12.2003) of Jharia coalfield (JCF)

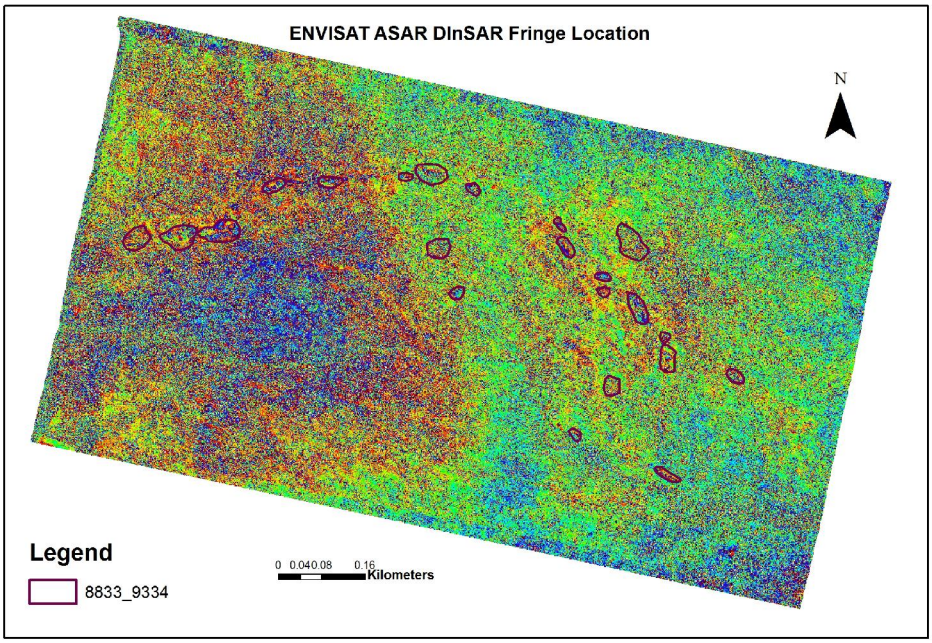

Fig.6.1.5 : Fringe area delineated on Differential interferogram of ENVISAT data pair (08.11.2003 & 13.12.2003) for Jharia coalfield (JCF)

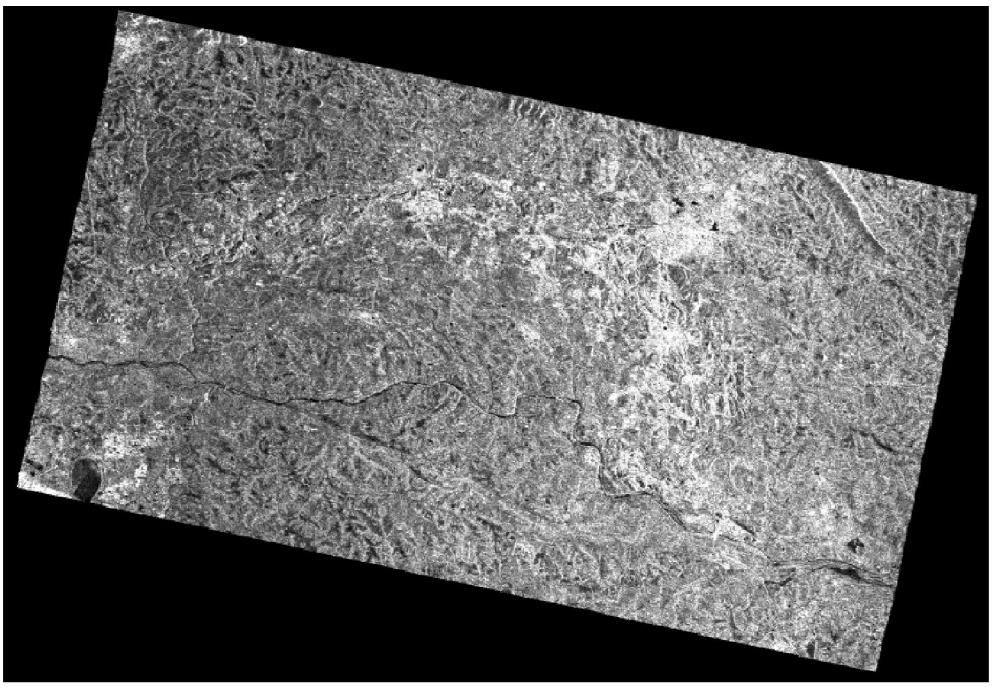

Fig.6.1.6: Amplitude image of ENVISAT ASAR data (17.01.2004) of Jharia coalfield (JCF)

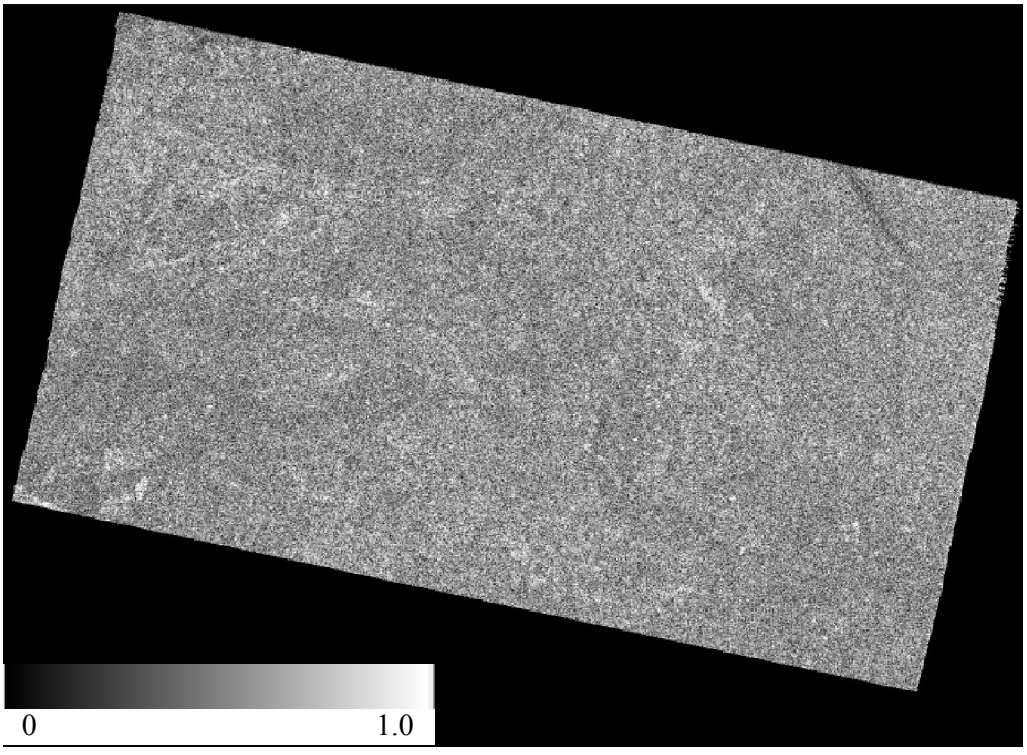

Fig.6.1.7: Coherence image of ENVISAT ASAR data pair (17.01.2004 & 0 1.05.2004) for Jharia coalfield (JCF)

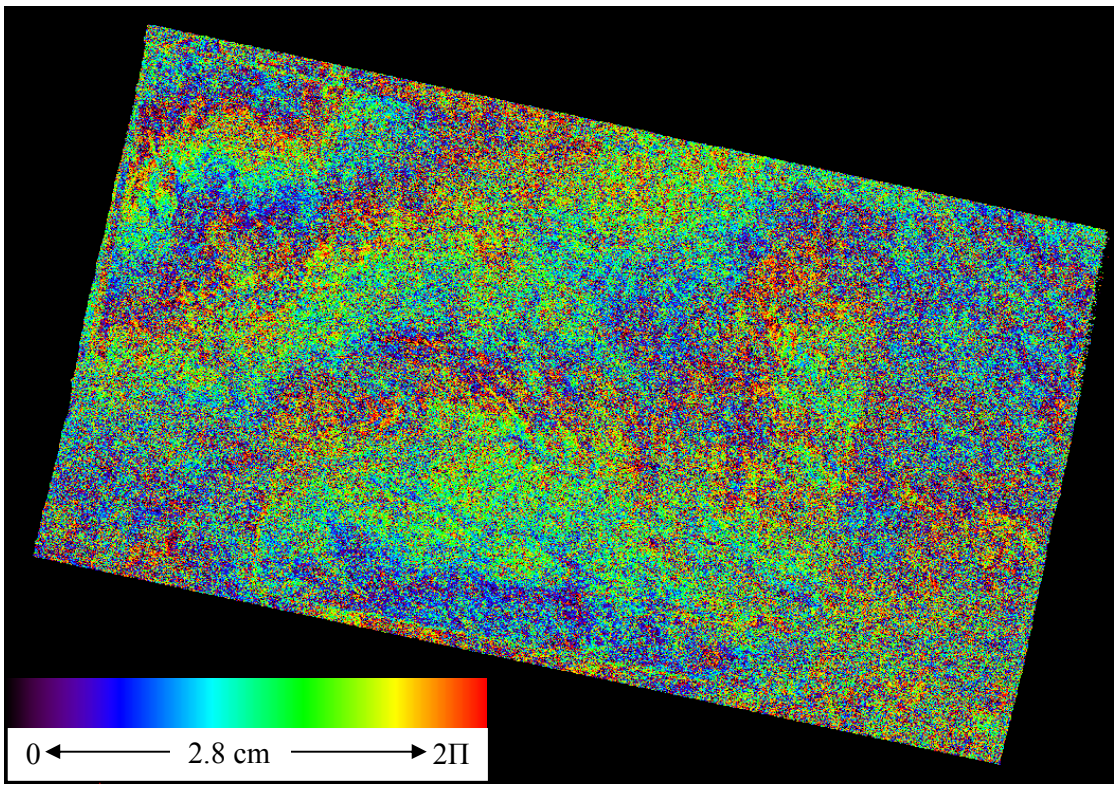

Fig. 6.1.8:Differential Interferogram of ENVISAT ASAR data pair (17.01.2004 & 01.05.2004) for Jharia coalfield (JCF)

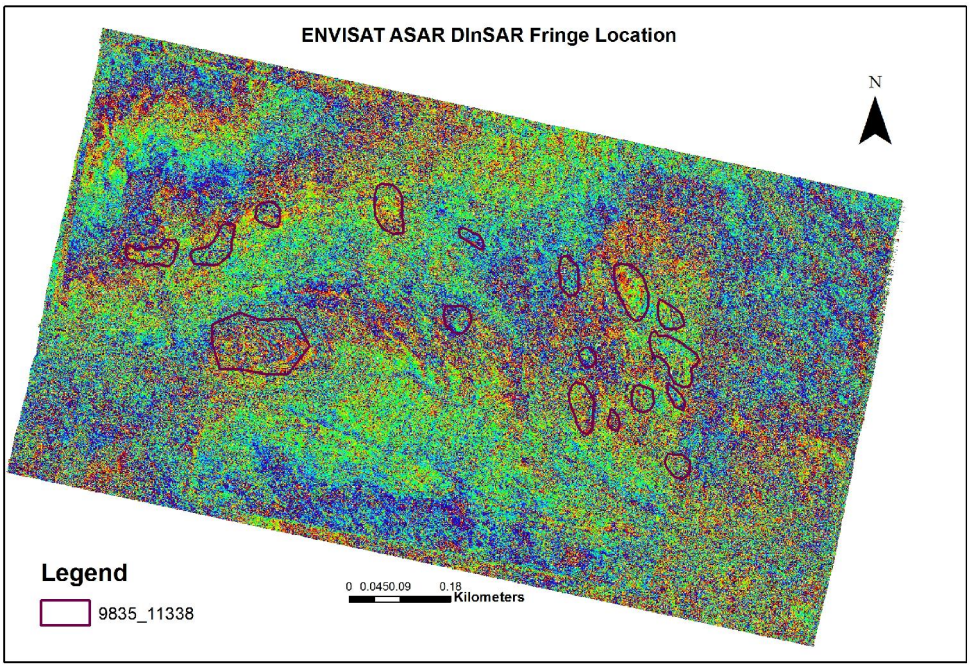

Fig. 6.1.9: Fringe area delineated on Differential interferogram of ENVISAT data pair (17.01.2004 & 01.05.2004) for Jharia coalfield (JCF);

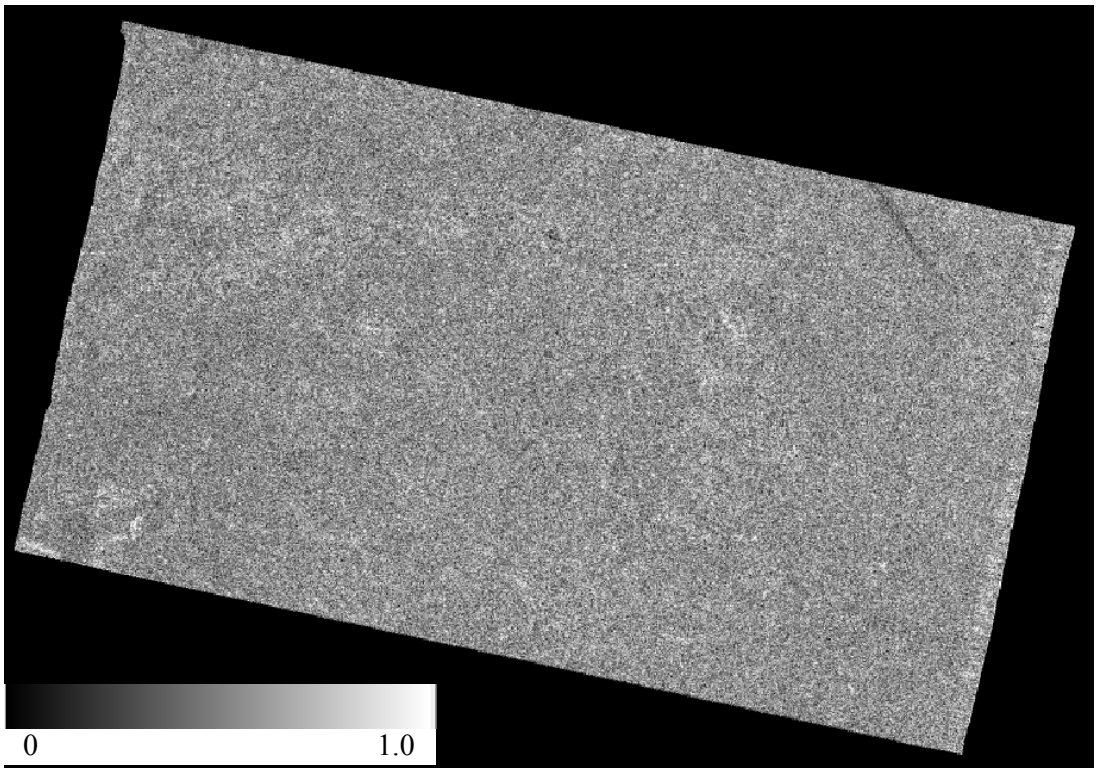

Fig.6.1.10: Coherence image of ENVISAT ASAR data pair (13.12.2003 & 01.05.2004) for Jharia coalfield (JCF)

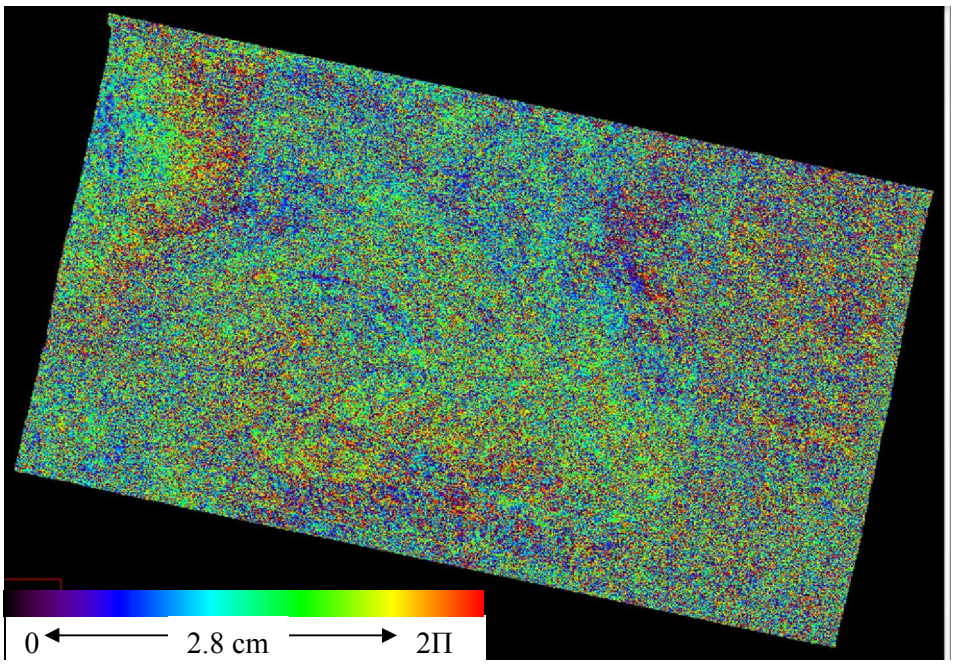

Fig.6.1.11:Differential Interferogram of ENVISAT ASAR data pair (13.12.2003 & 01.05.2004) for Jharia coalfield (JCF)

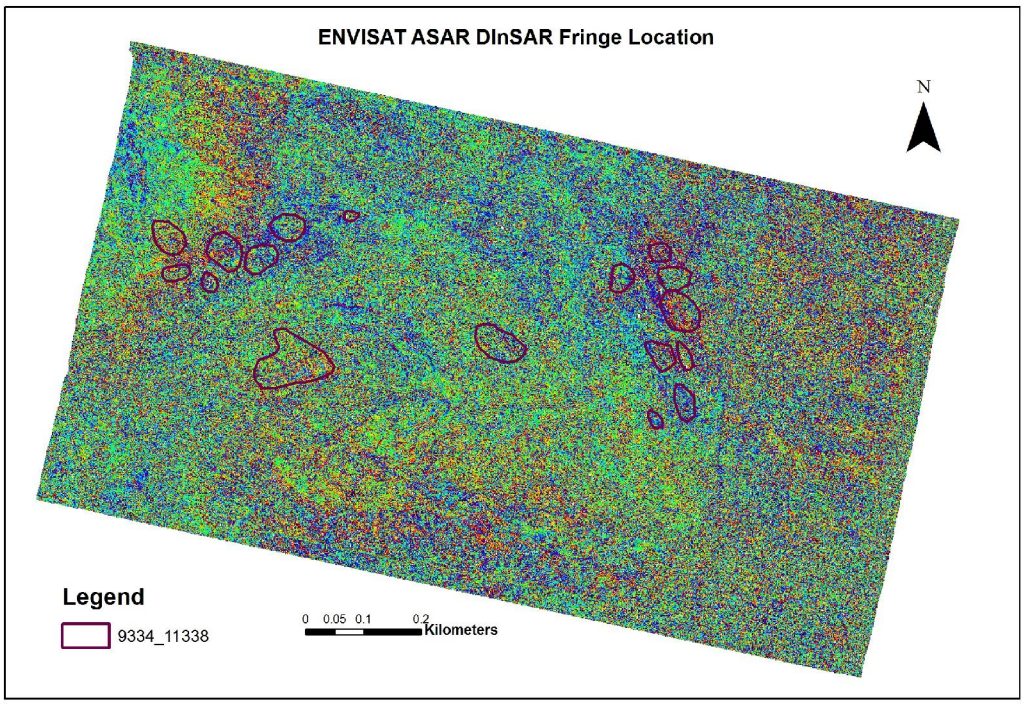

Fig. 6.1.12: : Fringe area delineated on Differential interferogram of ENVISAT data pair (13.12.2003 & 01.05.2004) for Jharia coalfield (JCF);

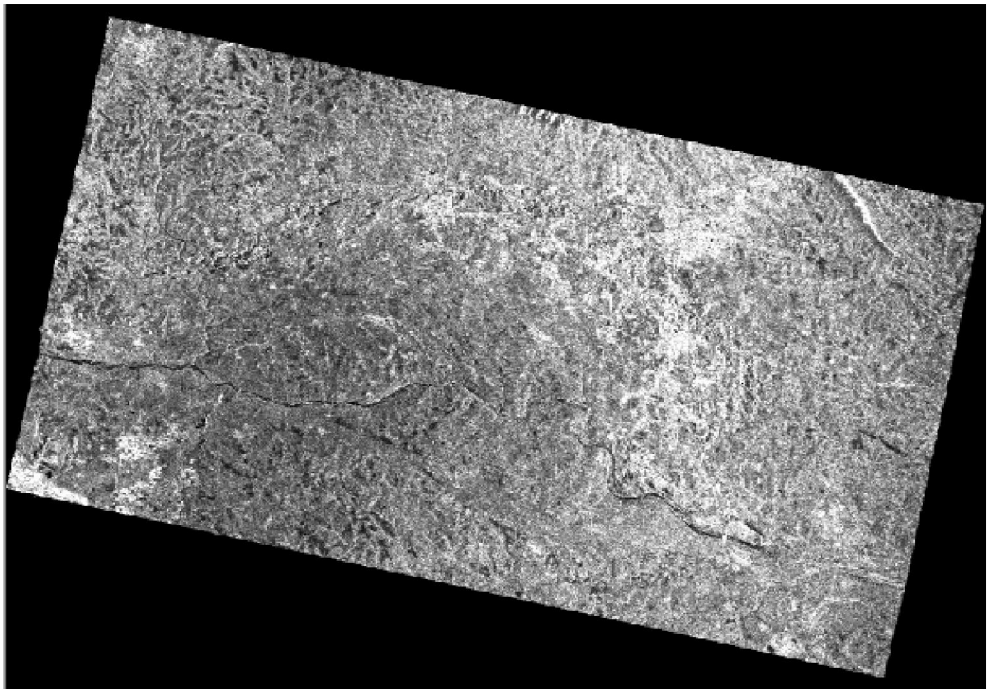

;

Fig.6.1.13: Amplitude image of ENVISAT ASAR data (17.03.2007) of Jharia coalfield (JCF)

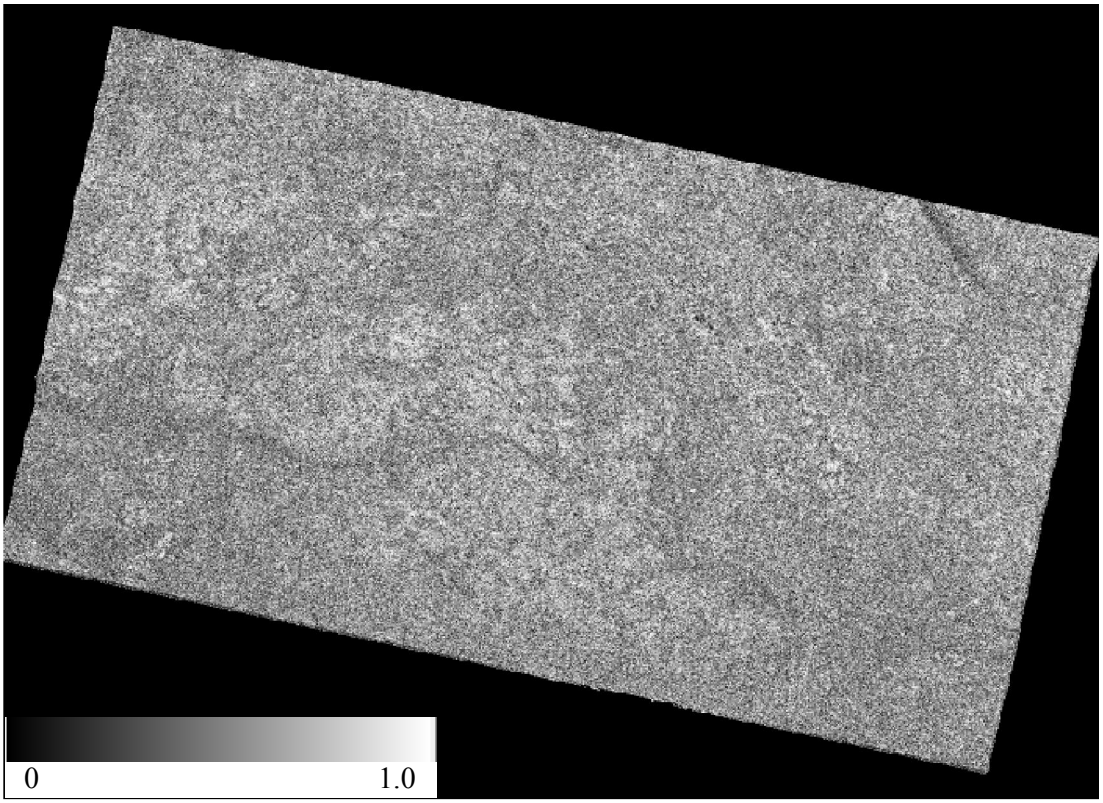

Fig.6.1.14: Coherence image of ENVISAT ASAR data pair (17.03.2007& 21.04.2007) for Jharia coalfield (JCF)

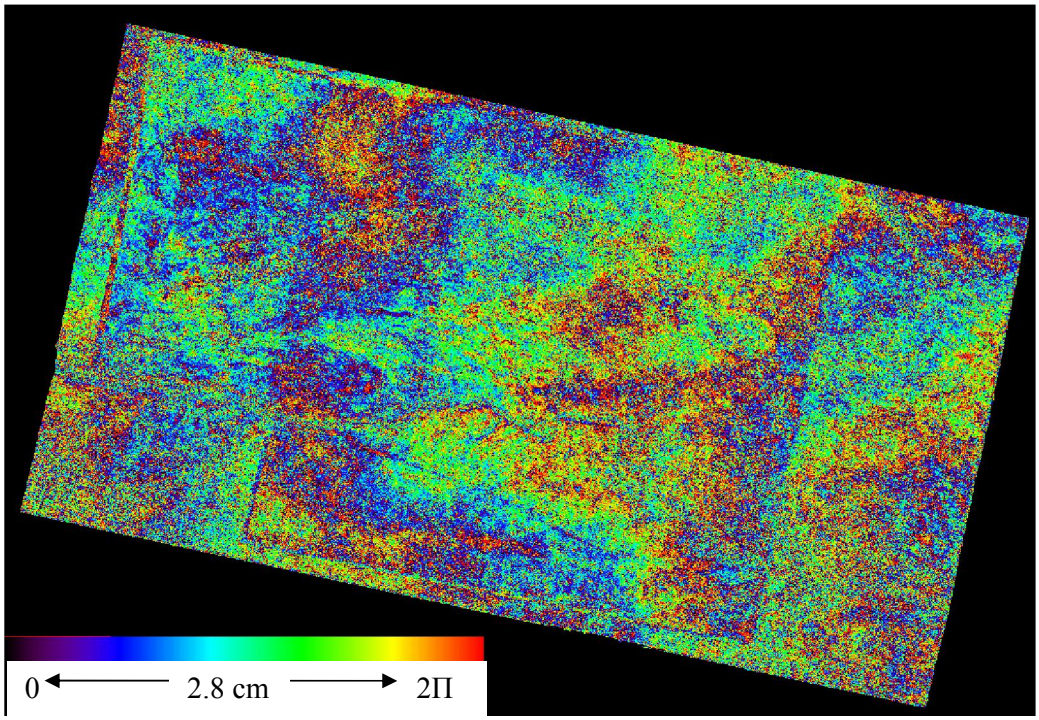

Fig.6.1.15:Differential Interferogram of ENVISAT ASAR data pair (17.03.2007& 21.04.2007) for Jharia coalfield (JCF)

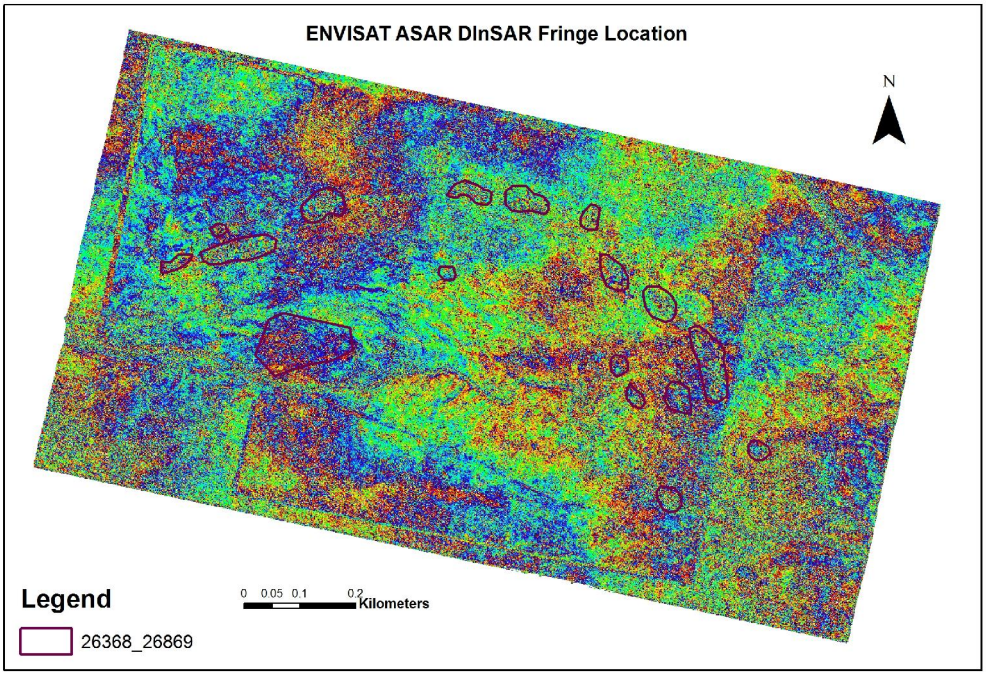

Fig. 6.1.16 : Fringe area delineated on Differential interferogram of ENVISAT data pair (17.03.2007& 21.04.2007) for Jharia coalfield (JCF);

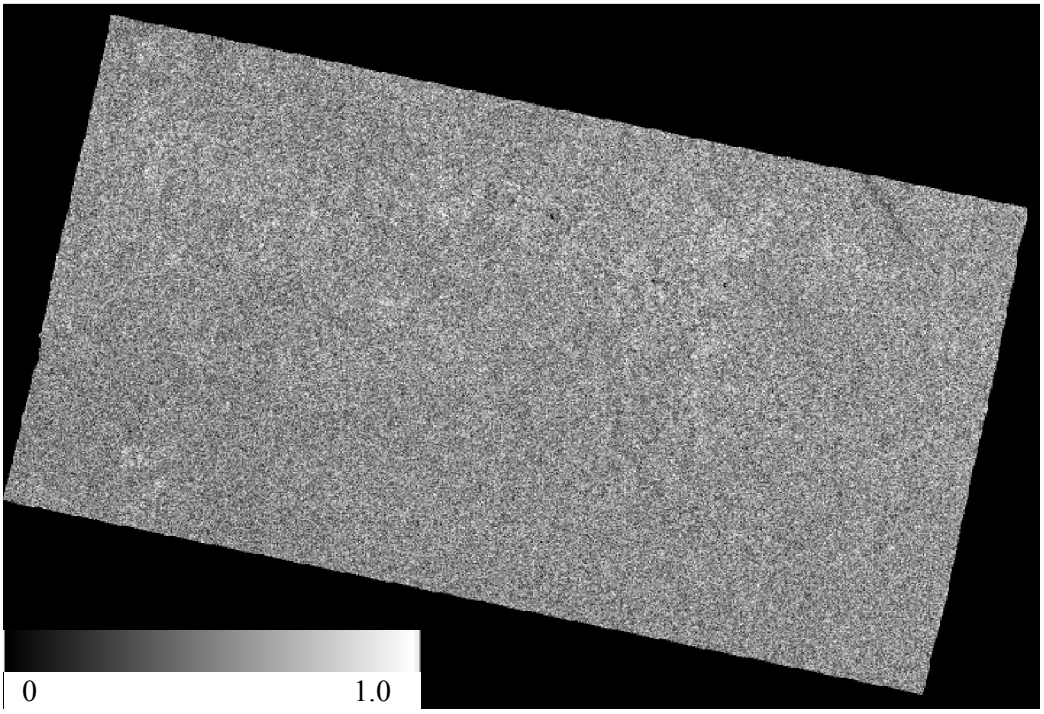

Fig.6.1.17: Coherence image of ENVISAT ASAR data pair (17.03.2007& 26.05.2007) for Jharia coalfield (JCF)

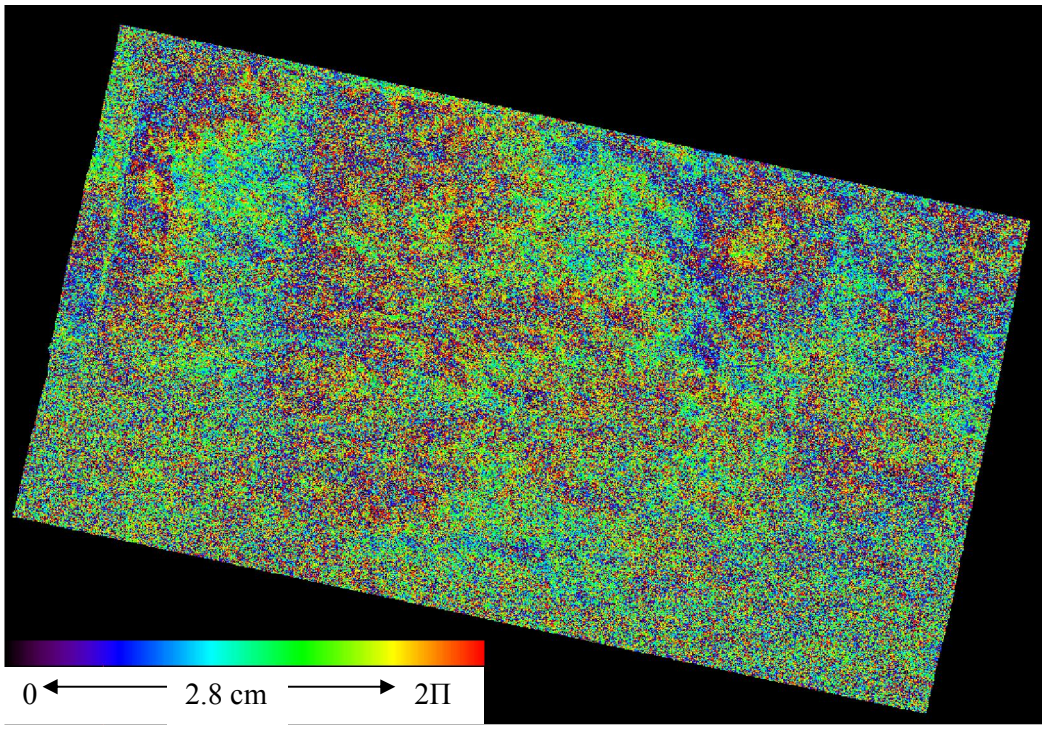

Fig.6.1.17:Differential Interferogram of ENVISAT ASAR data pair (17.03.2007& 26.05.2007) for Jharia coalfield (JCF)

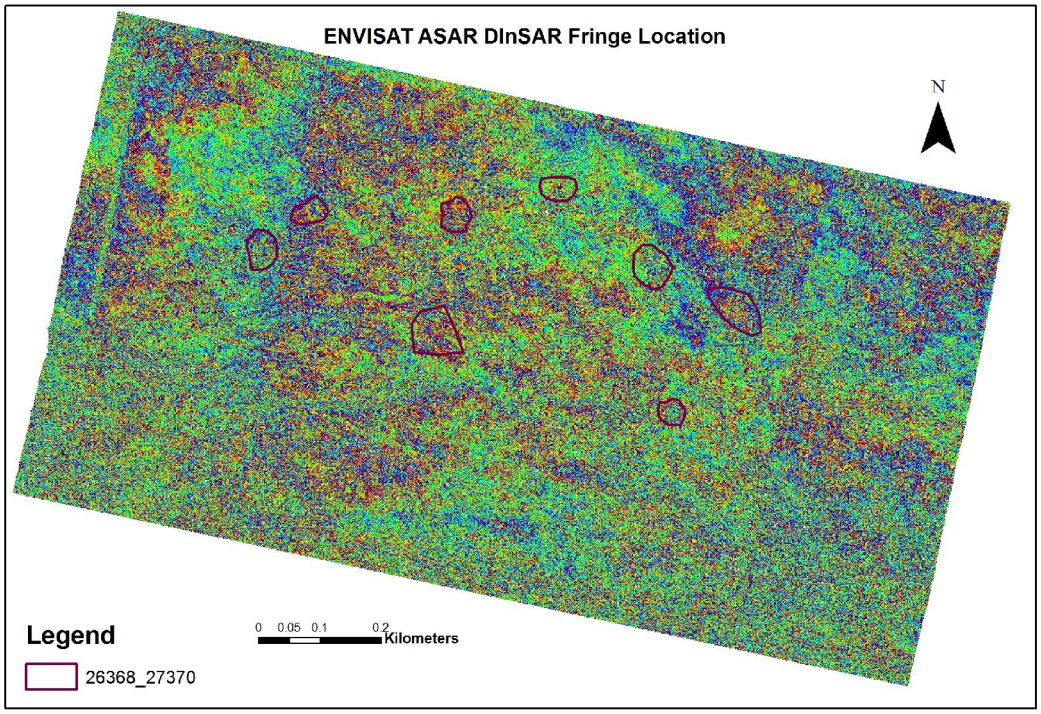

Fig.6.1.19 : Fringe area delineated on Differential interferogram of ENVISAT data pair (17.03.2007& 26.05.2007) for Jharia coalfield (JCF).

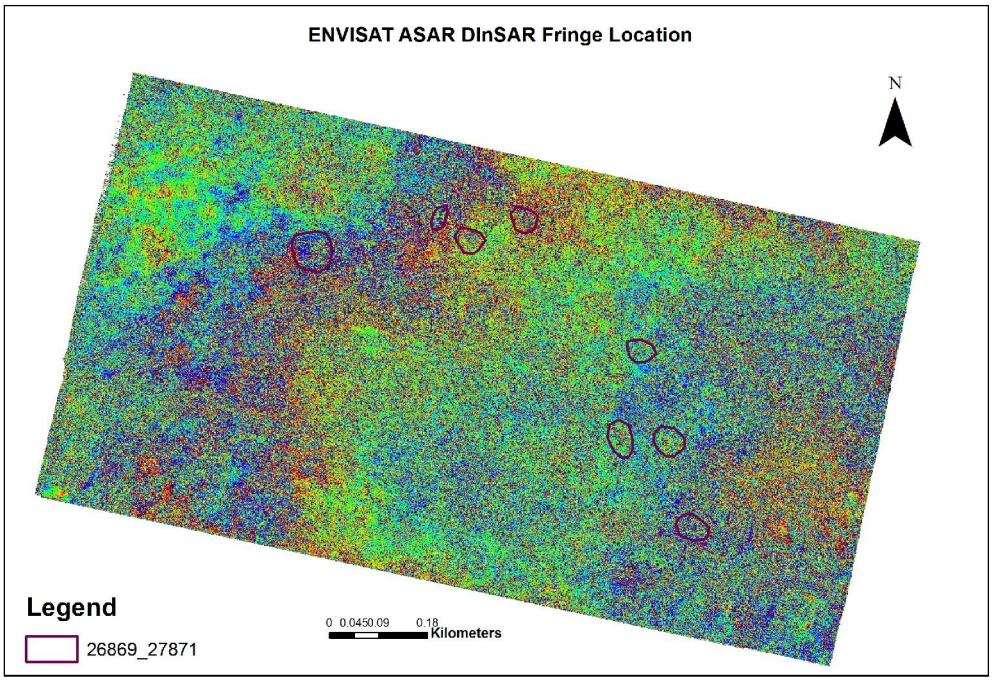

Fig.6.1.20 : Fringe area delineated on Differential interferogram of ENVISAT data pair (21.04.2007& 26.05.2007) for Jharia coalfield (JCF).

;

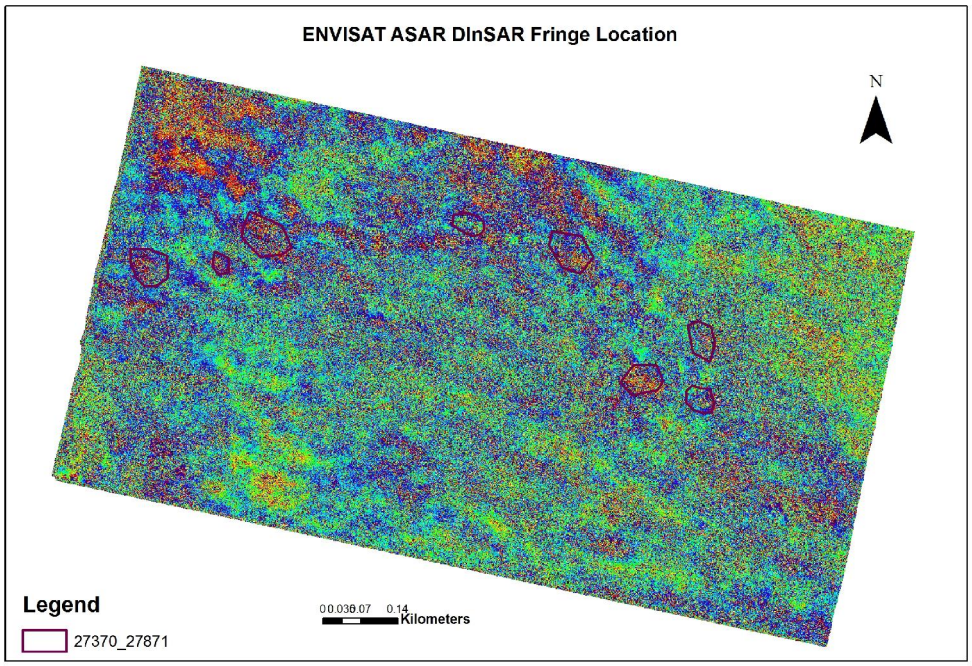

Fig.6.1.21 : Fringe area delineated on Differential interferogram of ENVISAT data pair (26.05.2007& 30.06.2007) for Jharia coalfield (JCF).

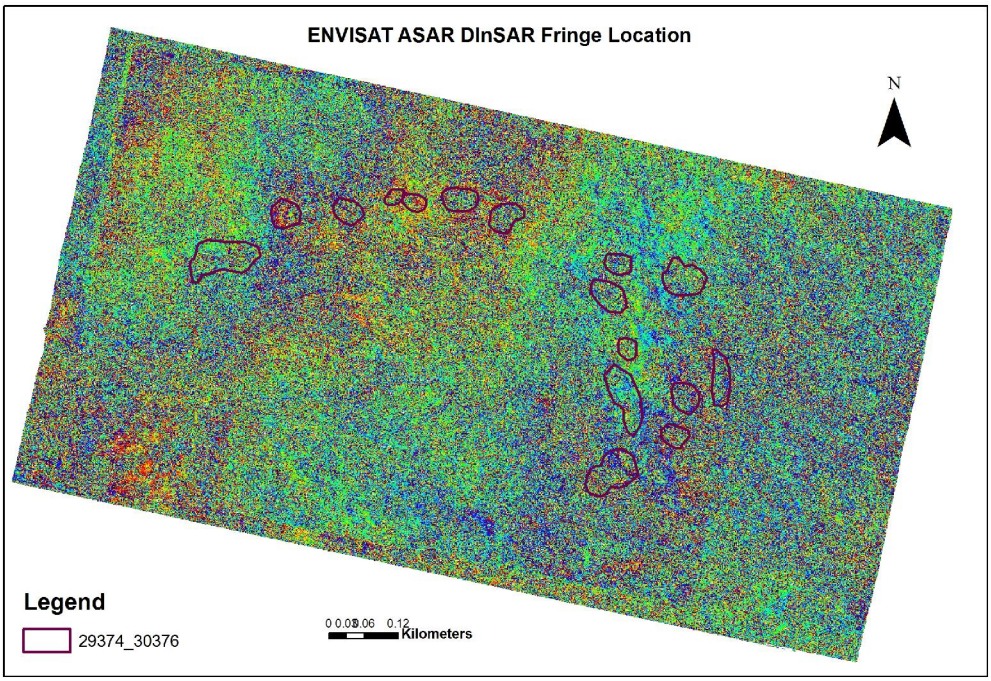

Fig.6.1.22 : Fringe area delineated on Differential interferogram of ENVISAT data pair (13.10.2007 & 22.012.2007) for Jharia coalfield (JCF).

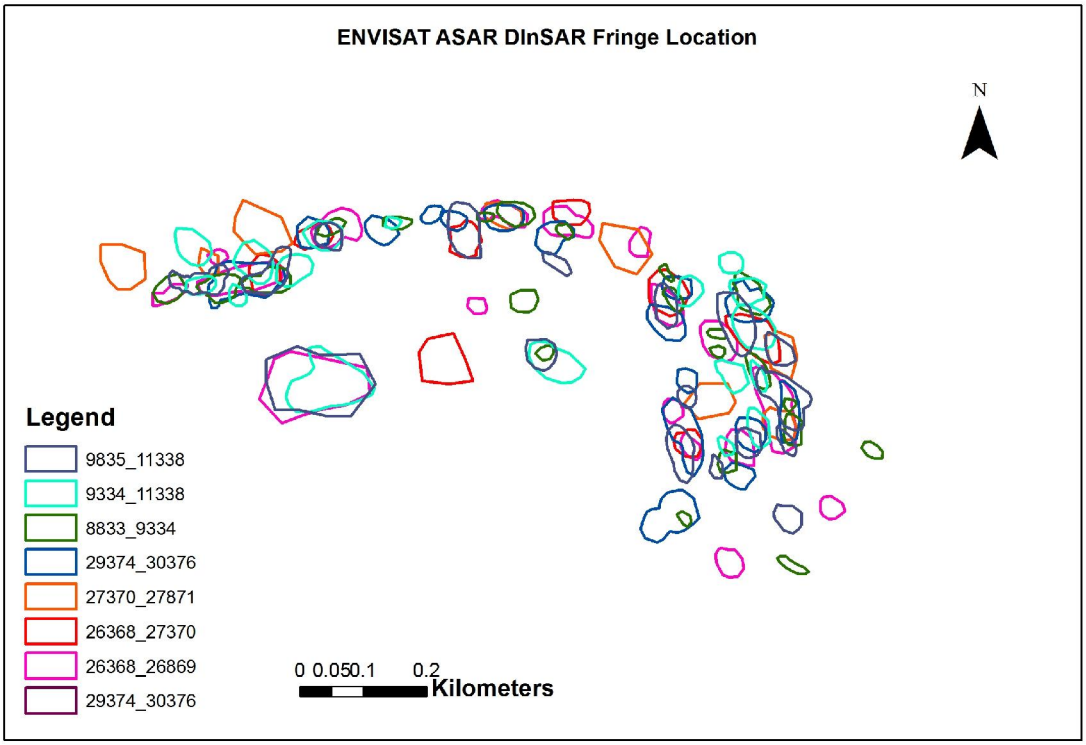

Fig.

Fig.6.1.23 :Fringe location for ENVISAT' ASAR DInSAR data pairs for period 2003-2007

It has been observed that the coherence and differential interferograms of high temporal and or seasonal variation of master and slaves results in distinct loss of the coherence as well as in the interferograms. The observation are tabulated in Table 6.1.1.

Table: 6.1.1: Interferometric fringe characteristics

Sl no.	Master orbit_date	Slave orbit_date	$B_{\perp}$ (m)	ΔT (days)	Seasonal variation	Fringe characteristics	Remarks
1	8833 08.11.2003	9334 13.12.2003	220	35	winter	Circular to elliptical fringes, topographic fringes are also present	High coherence, deformation fringes are prominent and differentiable from the topography. Small temporal variation terrain dynamicity other than subsidence can be compensated
2	9334 13.12.2003	11338 01.05.2004	150	140	winter-summer	Circular to elliptical fringes, topographic fringes are also present	High coherence, deformation fringes are prominent and differentiable from the topography. Small temporal variation terrain dynamicity other than subsidence can be compensated
3	9835 17.01.2004	11338 01.05.2004			Winter-summer	Shape of the deformation fringes are gradational, in some cases not detectable	low coherence, high temporal variation results in high terrain dynamicity and their response in the phase image, strong seasonal variability may also be the cause of coherence loss and noisy interferogram
4	26368 17.03.2007	26869 21.04.2007	404	35	summer	Circular to elliptical fringes, topographic fringes are also present	High coherence, deformation fringes are prominent and differentiable from the topography. Small temporal variation terrain dynamicity other than subsidence can be compensated
5	26368 17.03.2007	27370 26.05.2007	410	70	summer	Shape of the deformation fringes are gradational, in some cases not detectable	Very low coherence, high temporal variation results in high terrain dynamicity and their response in the phase image
6	26869 21.04.2007	27871 30.06.2007	45	70	Summer-rain	Shape of the deformation fringes are gradational, in some cases not detectable	low coherence, high temporal variation results in high terrain dynamicity and their response in the phase image, strong seasonal variability may also be the cause (?).
7	27370 26.05.2007	27871 30.06.2007	51	35	summer-rain	Shape of the deformation fringes are gradational, in some cases not detectable	Very low coherence, strong seasonal variability may also be the cause of coherence loss and noisy interferogram

8	27871 30.06.2007	28372 04.08.2007	50	35	rain	Shape of the deformation fringes are gradational, in some cases not detectable	Very low coherence, strong seasonal variability may also be the cause of coherence loss and noisy interferogram .
9	28372 04.08.2007	28873 08.09.2007	295	35	rain	Shape of the deformation fringes are gradational, in some cases not detectable	Very low coherence, strong seasonal variability may also be the cause of coherence loss and noisy interferogram
10	29374 13.10.2007	30376 22.12.2007	240	70	Autumn-winter	Shape of the deformation fringes are gradational, in some cases not detectable	Very low coherence, high temporal variation results in high terrain dynamicity and their response in the phase image, strong seasonal variability may also be the cause of coherence loss and noisy interferogram

From change detection point of view, due to extensive mining activities and also due to rapid urbanization, Jharia coalfield is very dynamic. From Differential Interferometric observation, the surfacial changes that was delineated from 2003 to 2007, 5 year survey, includes subsidence due to mining or fire or both, reclamation of the abandoned mines, generation of overburden dump and coal dump and their removal and also the urbanization. Fringes generated due to atmospheric phase screen (APS) and uncompensated topographic fringes are also included in the result. Thus to evaluate the surfacial changes that are only due to mining and or coal fire related subsidence, an extensive field traverse was carried out for the delineated areas. And the areas affected by subsidence due to mining and or fire are chosen for the present study (Fig. 6.1.24).

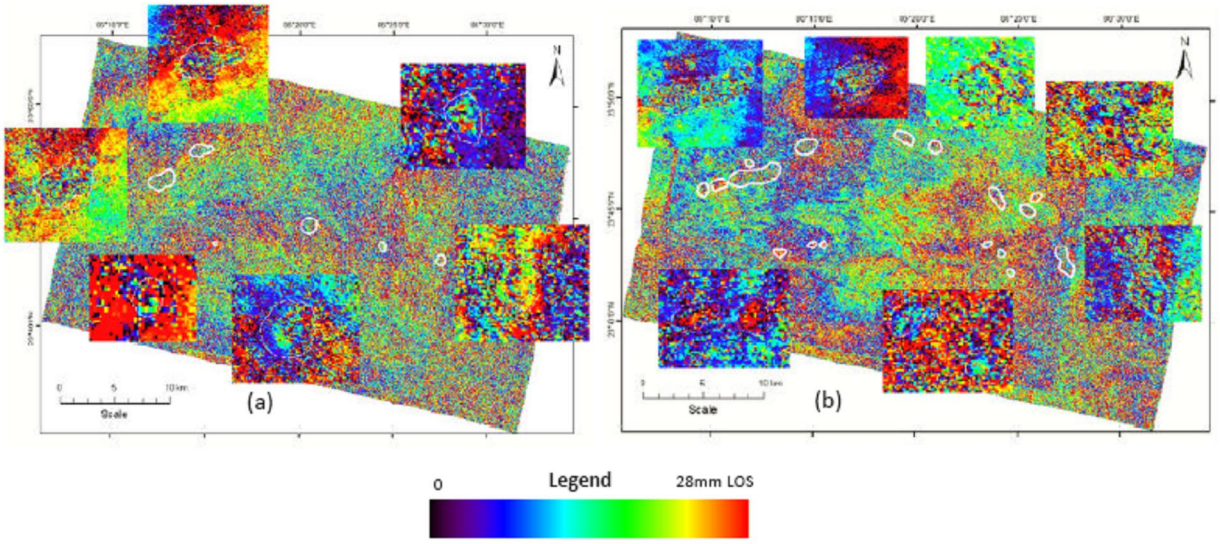

Fig. 6.1.24 : Land subsidence fringes as observed in the differential interferograms processed from the ENVISAT data pairs of 2004 (a) and 2007 (b).

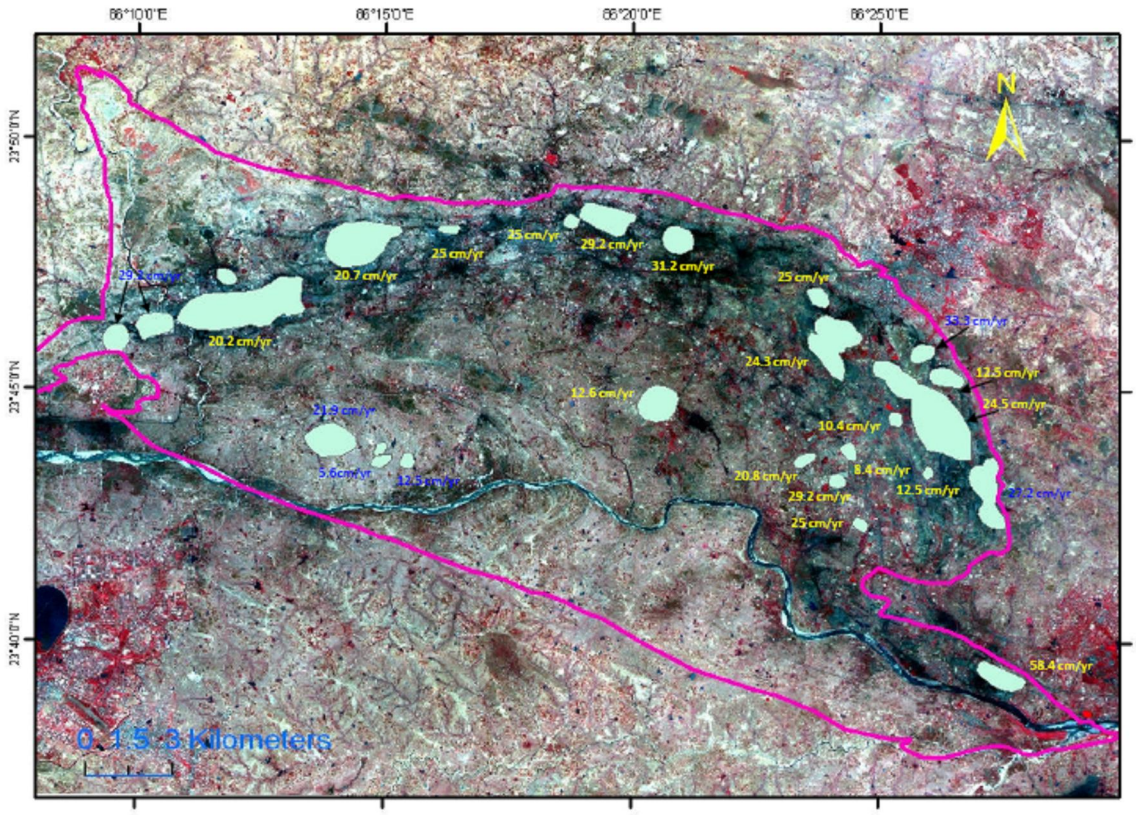

Fig. 6.1.25: Subsidence-affected areas during the period of 2003-2007 (draped on PAN-sharpened IRS LISS-IV FCC432) integrated from the differential interferograms of the observation period 2003-2007

6.2 Differential GPS & Optical leveling based land subsidence detection

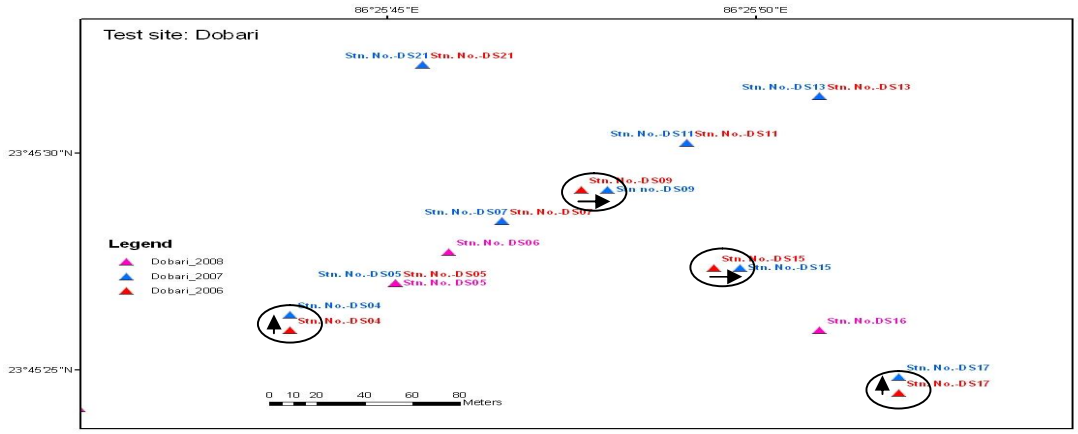

Fig. 6.2.1: Lateral displacement (strain) for 2006-2008 observation period at Dobari test Site (black arrow marks the direction of displacement)

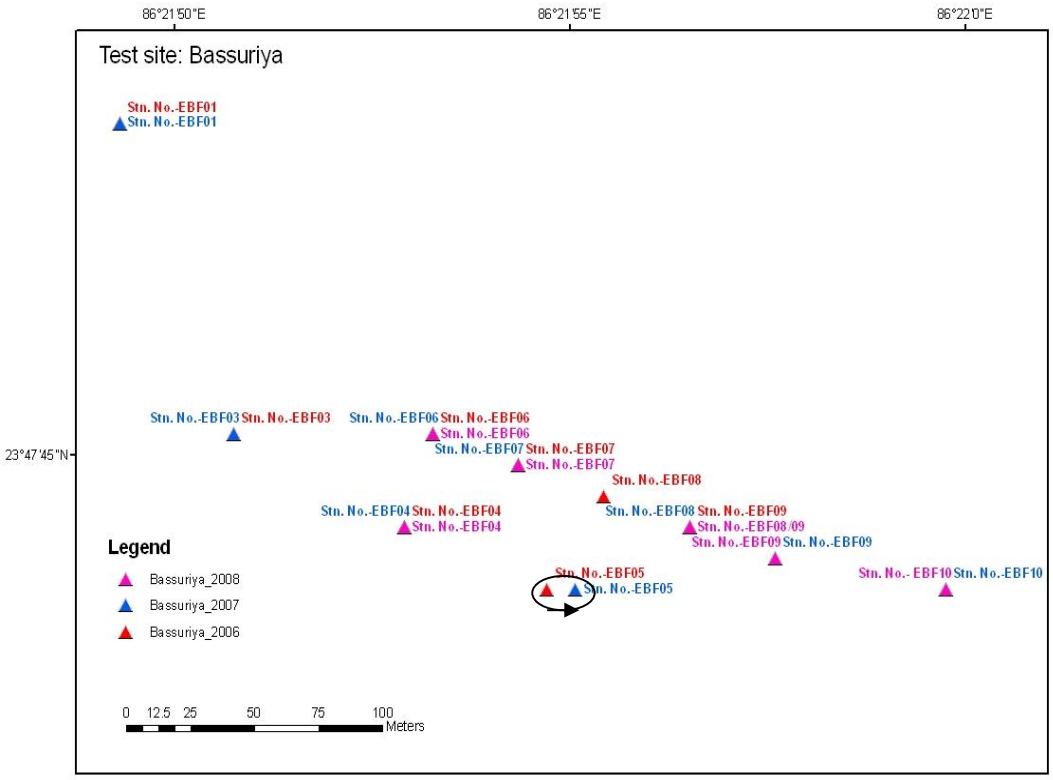

Fig. 6.2.2: Lateral displacement (strain) for 2006-2008 observation period at Bassuriya test Site (black arrow marks the direction of displacement)

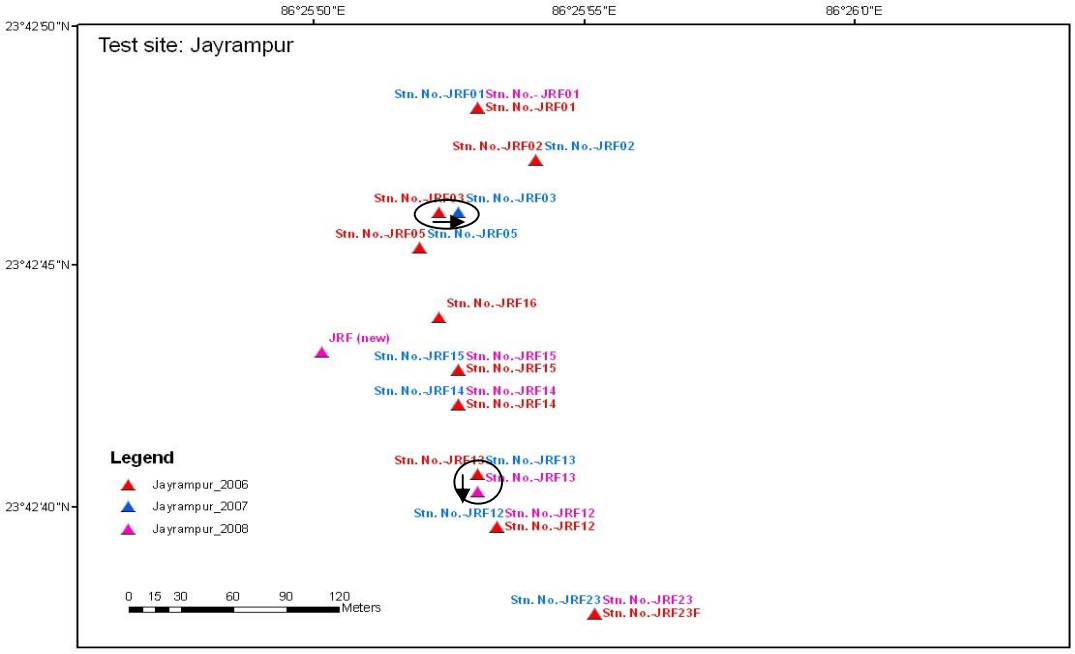

Fig. 6.2.3: Lateral displacement (strain) for 2006-2008 observation period at Jayrampur test Site (black arrow marks the direction of displacement)

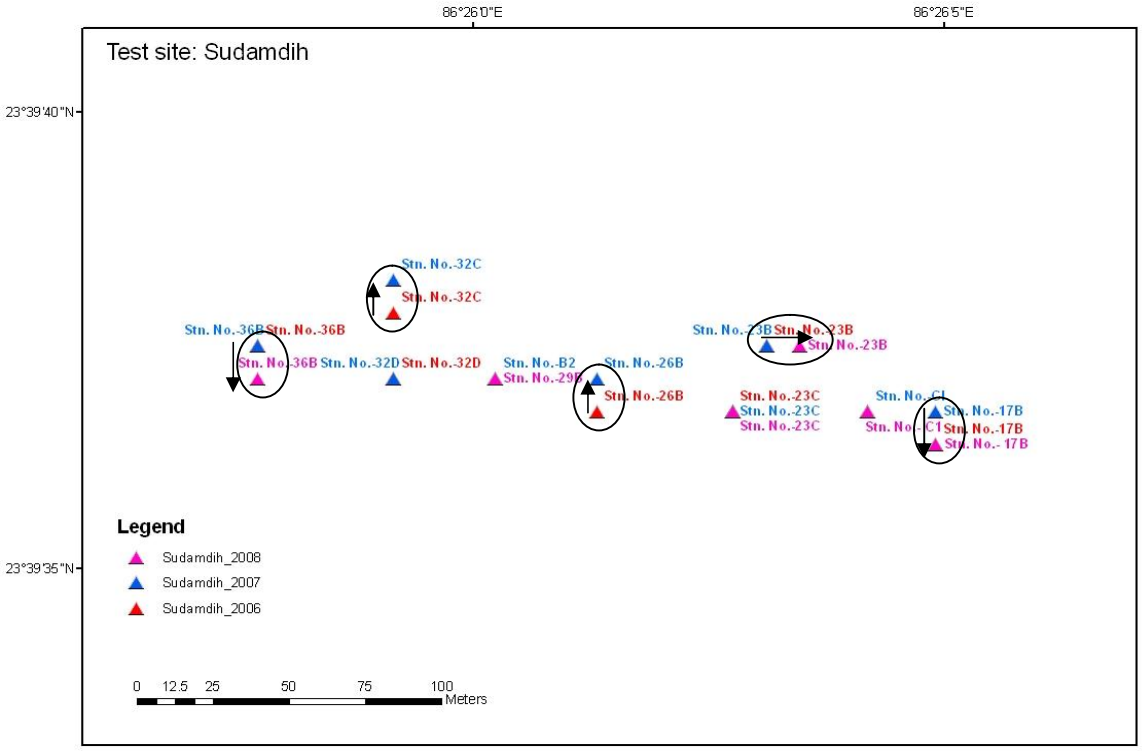

Fig. 6.2.4: Lateral displacement (strain) for 2006-2008 observation period at Sudamdih test Site (black arrow marks the direction of displacement)

6.3 Characterization of surface mining features from Digital Elevation Model

Available ASTER,SRTM DEM were evaluated with the processed ERS1-2 InSAR DEM and photogrammetric CARTOSAT-1 DEM (Fig. 6.3.1- 6.3.4) along with their surface derivatives (e.g. slope hillshade, contour etc.)

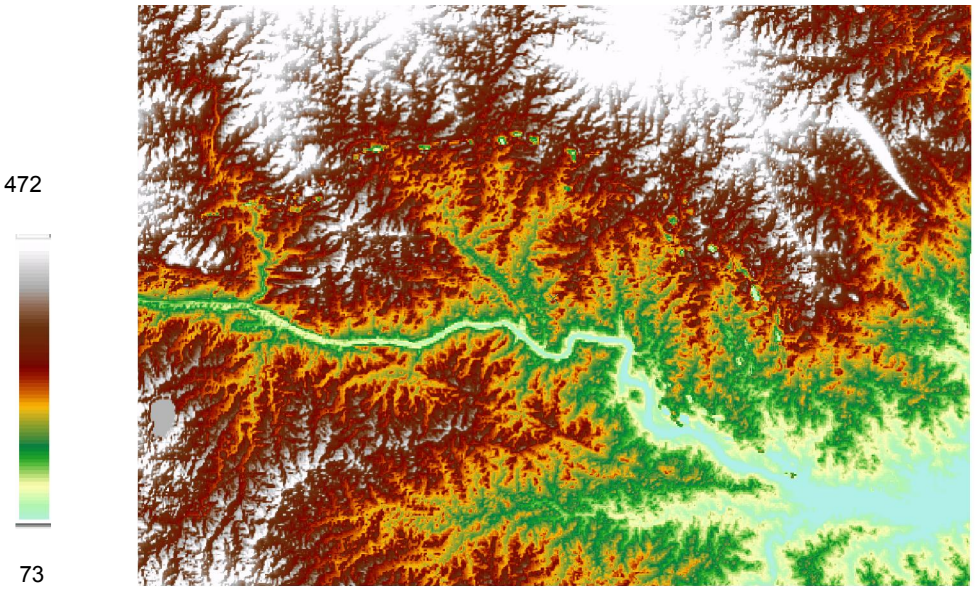

Fig.6.3.1: 90 m SRTM Digital Elevation Model of Jharia coal field (JCF)

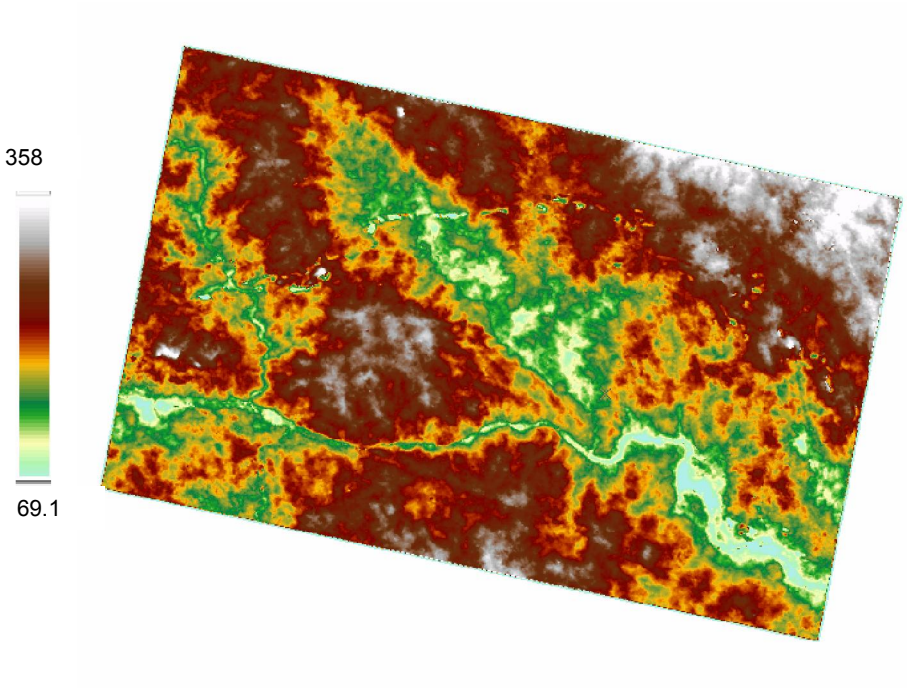

Fig.6.3.2: 20 m ERS-1.2 InSAR based Digital Elevation Model of Jharia coal field (JCF)

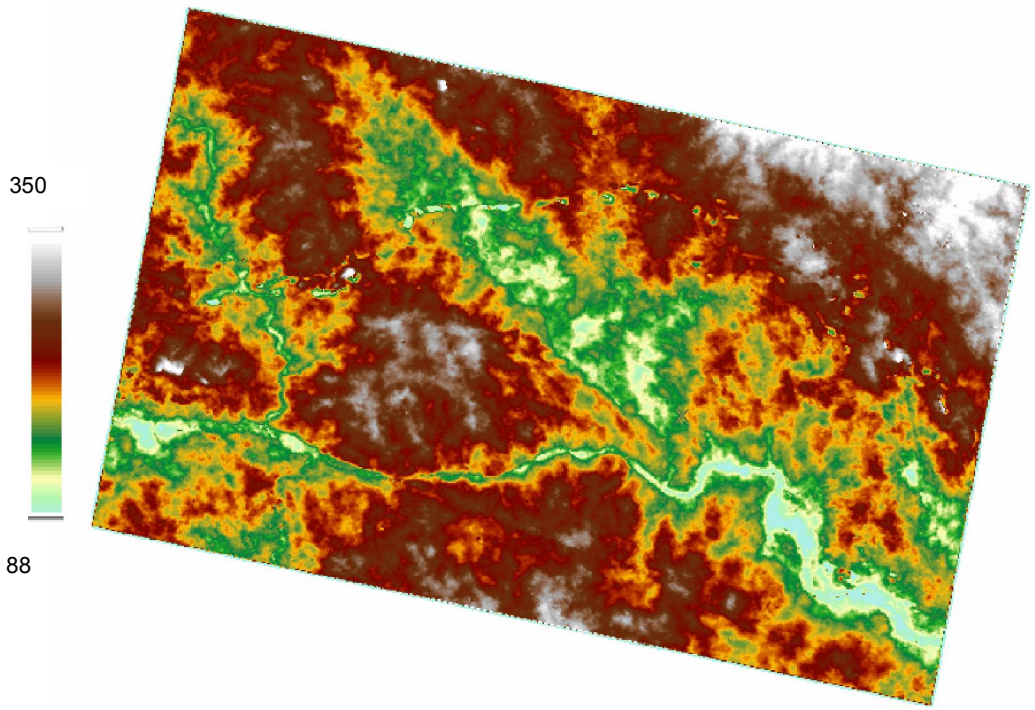

Fig.6.3.3: 30 m ASTER Digital Elevation Model of Jharia coal field (JCF)

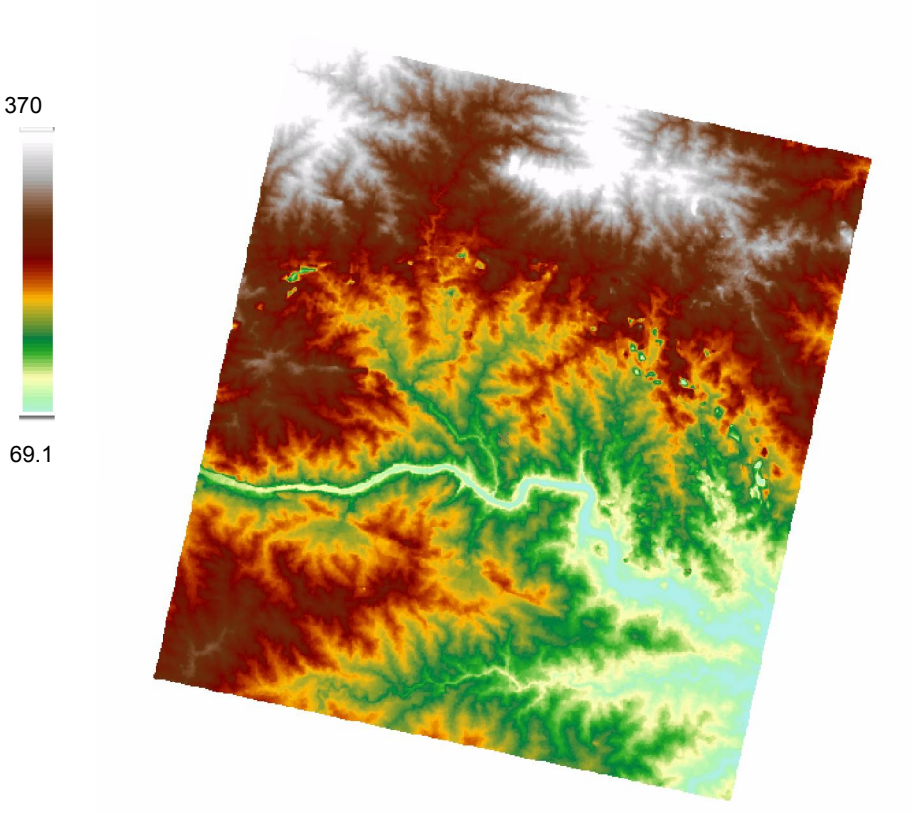

Fig..6.3.4: 10 m CARTOSAT-1 Digital Elevation Model of Jharia coal field (JCF)

The variation in the elevation corresponds to the sensitivity of the DEM to measure the terrain parameters.

It has been observed that even if the coarser spatial resolution (90m) SRTM is able to delineate the open cast quarry boundary better than the ASTER DEM. CARTOSAT -1 photogrammetric DEM with a very high spatial resolution can detect the variation in the terrain undulation resulting the detection of small coal dumps are easily delineable from the data. The shape of the contours are a good indicator of the terrain parameters. In Fig. 6.3.4.5, 20 m interval contours map for all the four DEM used (e.g. CARTOSAT-1, ERS-1& 2 InSAR based, ASTER & SRTM DEM) for south eastern part of Jharia basin has been shown.

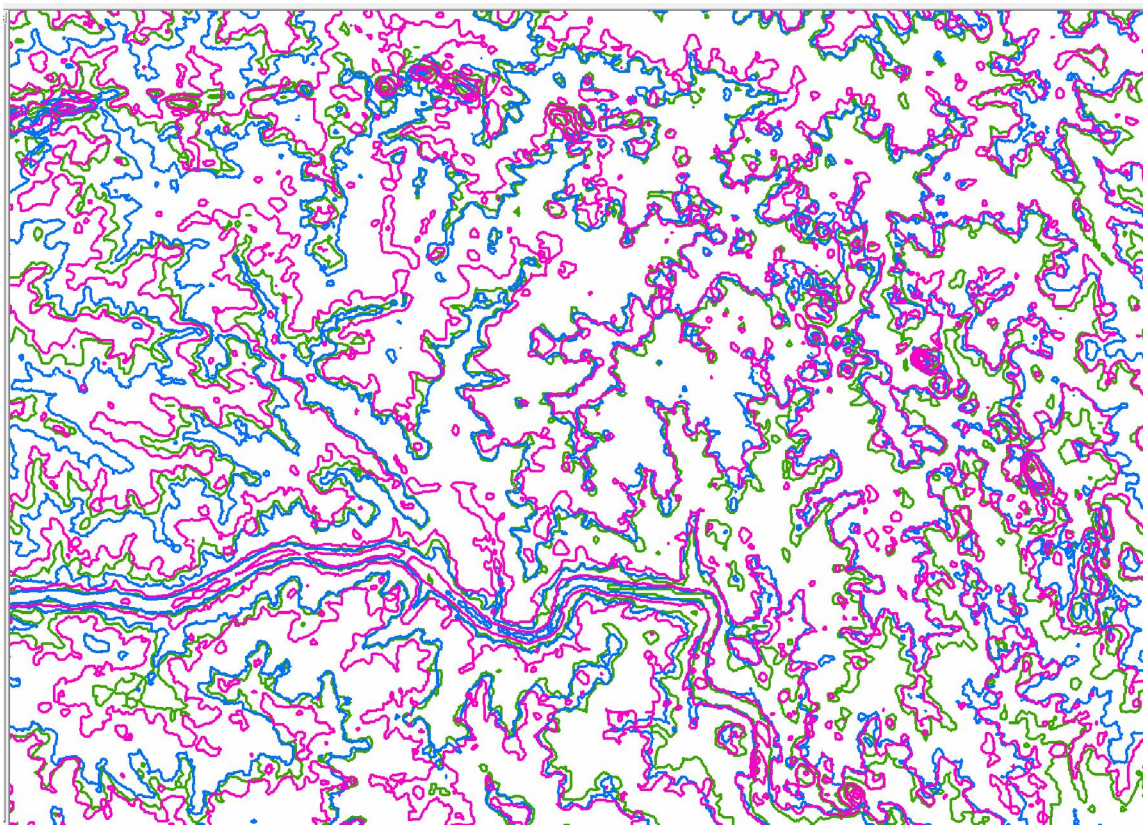

Fig.6.3.5: 20 m interval Contour map of SE Jharia basin, where SRTM contour is marked by green, InSAR contours marked by red, ASTER contour marked by pink and CARTOSAT-1 contour is marked by blue

The shape and pattern of contour is also an important parameter to measure the terrain characteristics and undulation. In Fig. 6.3.5 it has been observed the general pattern of the contours remains more or less similar for SRTM,ASTER and InSAR based DEM. CARTOSAT-1 generated contours shows a sharps discontinuity is many mining areas as well as in non mining areas due to its high spatial resolution to pick up local undulations.

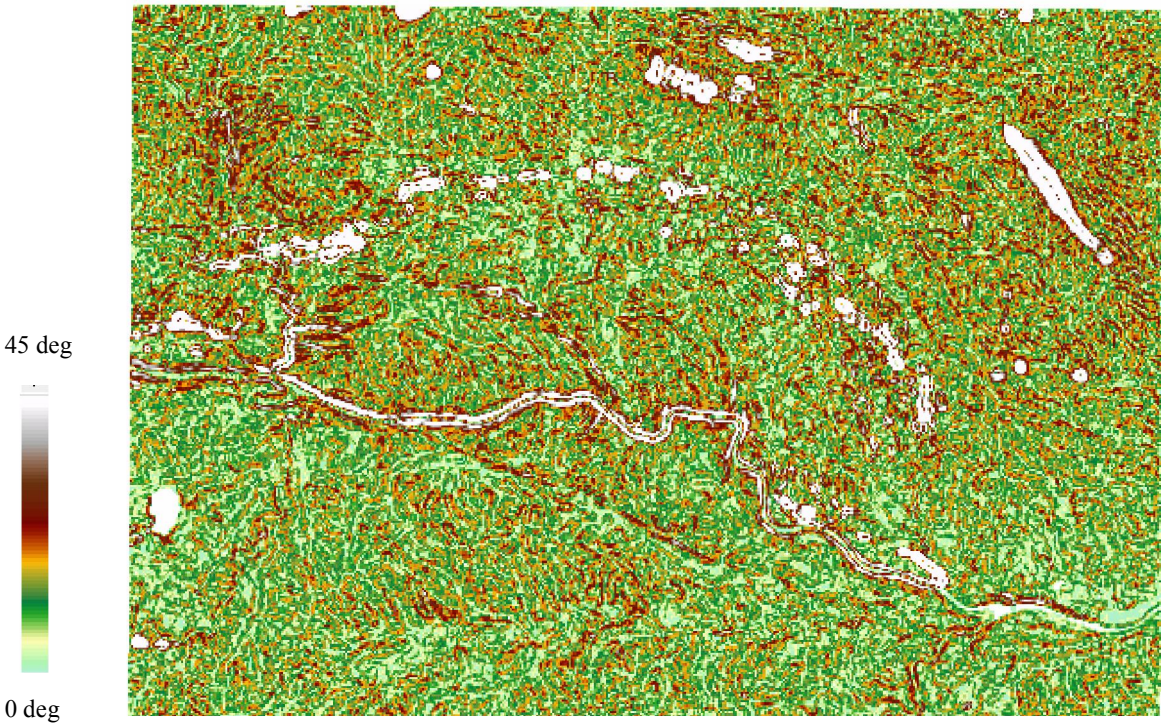

Fig. 6.3.6: Slope map derived from SRTM DEM for Jharia coalfield(JCF)

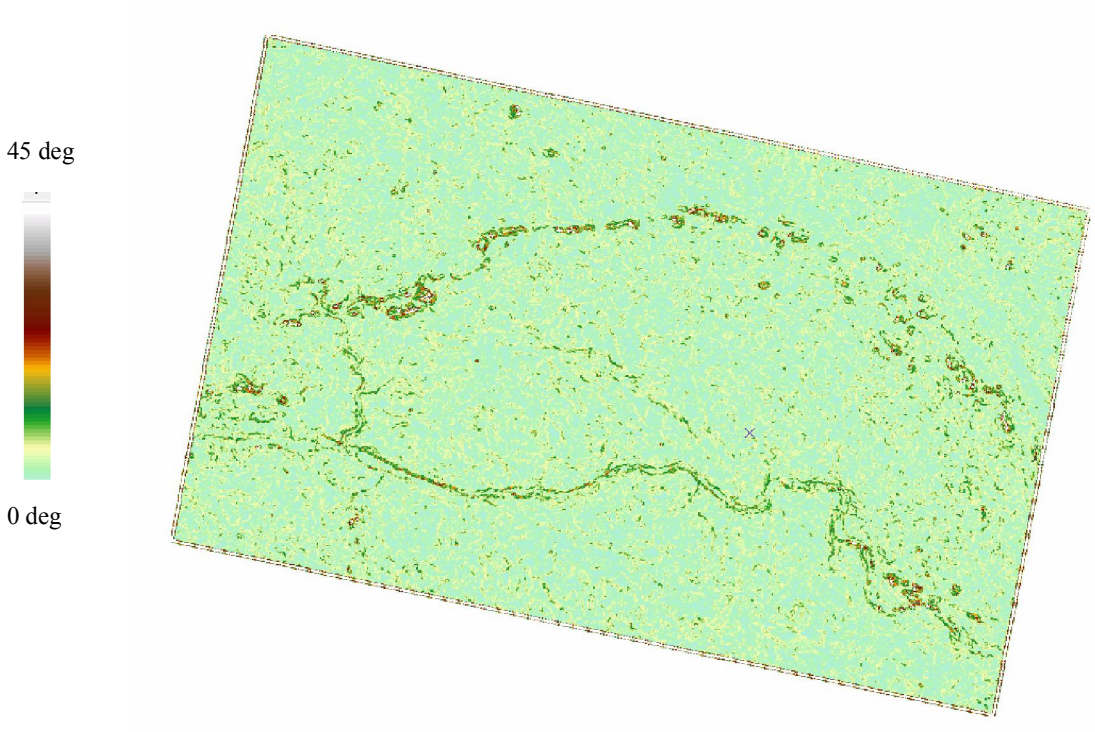

Fig. 6.3.7: Slope map derived from ERS-1,2 InSAR DEM for Jharia coalfield(JCF)

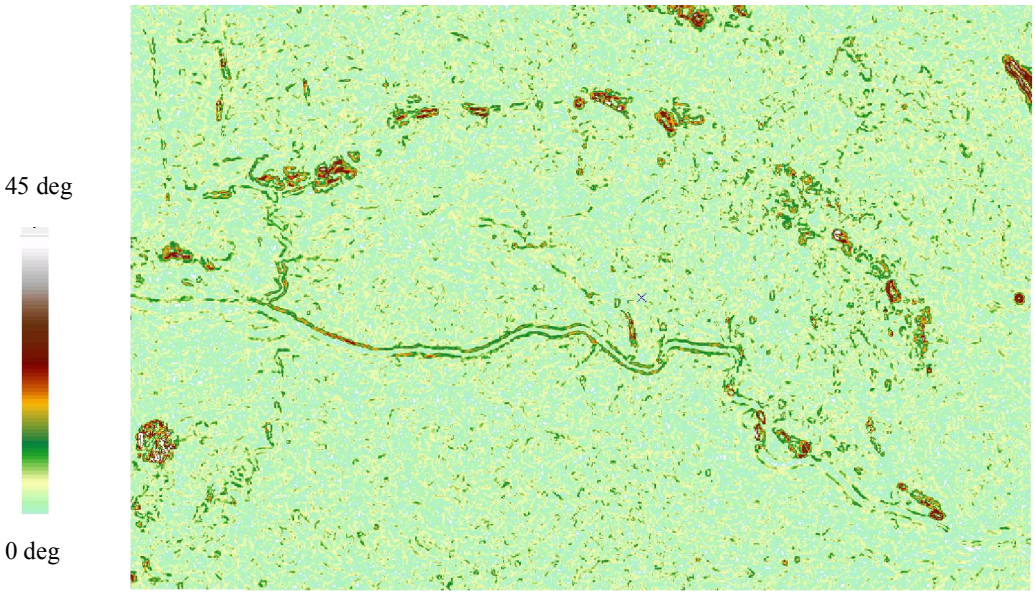

Fig. 6.3.8: Slope map derived from ASTER DEM for Jharia coalfield(JCF)

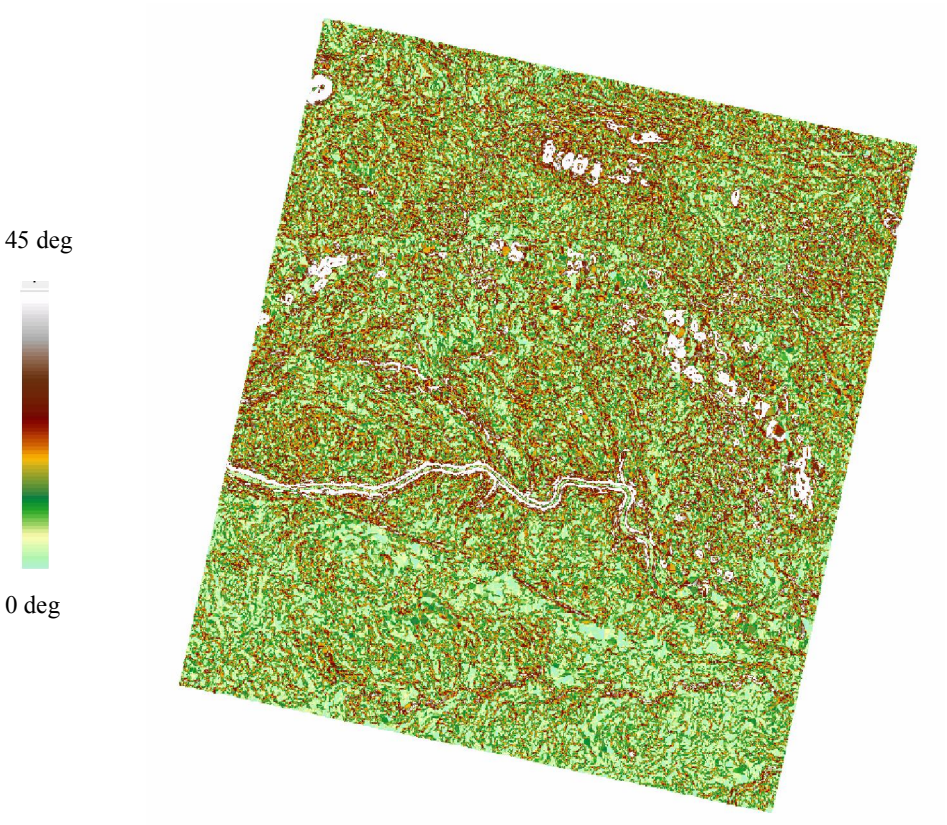

Fig. 6.3.9: Slope map derived from CARTOSAT-1 DEM for Jharia coalfield(JCF)

Comparative study of the slope maps (fig.6.3.6-6.3.9) derived from the four DEM reveals that SRTM, CARTOSAT detect the terrain undulation and slope better than the other two due to its higher sensitivity (SRTM) towards the terrain characteristics and high spatial resolution (CARTOSAT-1) to detect gradual undulation in the terrain.

Thus, to detect and identify the gradual as well as small terrain features (OBD, Coal dump, fallow lands) CARTOSAT-1 DEM shows significant positive result compared to others. Even if the SRTM and ERS-1,2 InSAR based DEM works on the same principle, but the former shows a better response for delineation of the terrain features. It may be due to the fact that for the present study only descending mode Tandem pair was utilized which has significantly highlighted certain terrain features along its line of sight but fails to detect the features present on the back slope. On the other hand, SRTM DEM is a combination of both ascending and descending mode data and processed and merged to generate the DEM which results in a complete picture about the terrain in the area.

6.4 Environmental indicators delineation from Alternate polarized SAR data based on their scattering properties

Two sets of ENVISAT ASAR alternate polarization (HH/VV and HH/HV) data with a minimum possible temporal difference of 35-days were procured for generating σ° images in HH-, VV-, and HV-polarizations (Fig. 6.4.1).

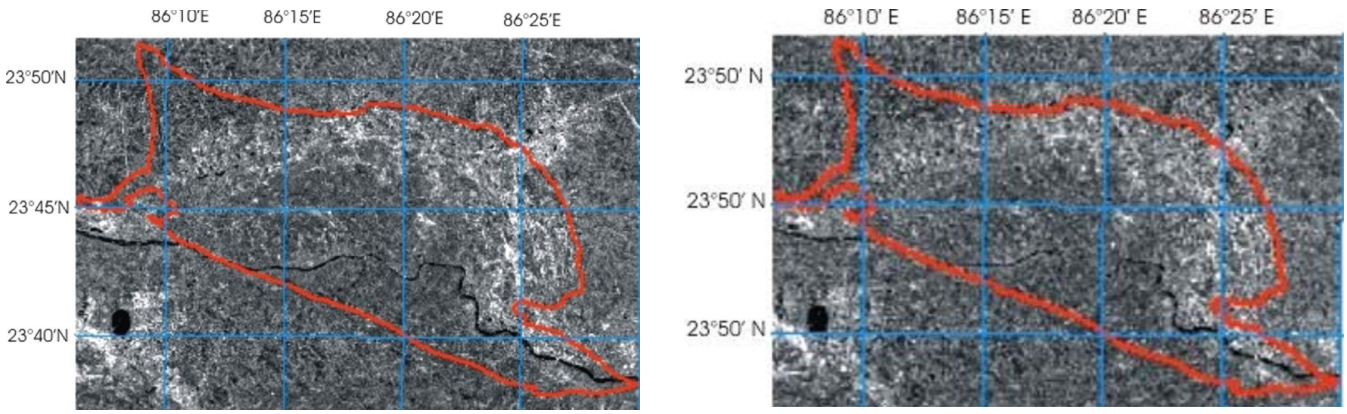

Fig. 6.4.1a,b: Backscatter image of Jharia basin in HH- and VV- polarizations respectively. Red boundary marks the aerial extent of the Jharia Coal Basin

The backscattering coefficient (σº) from space-borne ENVISAT ASAR C-band multi-polarization data, for each of the environmental parameters in the coalfield were retrieved and their mean and standard deviation values were calculated to characterize the mining related environmental indicators and other land-use/land-cover classes, (Table 6.4.1).

Table 6.4.1 Mean and standard deviation of backscattering coefficients of the environmental parameters in ENVISAT ASAR C-band multi-polarization (HH-, VV-, and HV-polarizations) of Jharia Coalfield.

Environmental Parameters	HH- Polarization		VV Polarization		HV Polarization	
	Mean σ° (dB)	Standard Deviation	Mean σ° (dB)	Standard Deviation	Mean σ° (dB)	Standard Deviation
Functional Opencast Mine	-2.37	0.892	-2.37	0.74	-8.67	1.41
Overburden/Coal Dump	-3.25	3.49	-3.36	3.34	-11.56	1.86
Abandoned /Closed Opencast Mine	-18.46	3.74	-17.04	7.38	-24.65	3.48
Coal Washery	-1.82	4.37	-2.59	5.39	-13.55	4.18
Settlement	3.24	1.68	0.88	1.41	-6.09	0.38
Barren Land	-5.33	0.67	-4.96	1.35	-11.20	0.94
Fallow land	-6.84	3.49	-6.87	1.65	-12.56	2.71
Vegetation	-2.08	3.12	-1.97	2.85	-7.78	1.89
Agriculture Land	-5.76	0.61	-5.14	0.75	-11.62	0.98
Water Body	-21.87	2.57	-21.38	2.13	-27.47	2.33

It is observed that in co-polarization (HH- and VV-polarizations) and cross polarization (HV-polarization) data, the variation pattern of mean backscattering coefficients are more or less similar but with a difference in backscattering level of about 5-7dB between co- (greater) and cross-polarization (lesser) responses.

In co-polarizations (HH- and VV-), the mean backscattering response is high in case of settlements followed by vegetation, functional opencast mines, overburden/coal dumps and coal washery; moderate in case of barren land, agricultural land and fallow land; and low in case of water body and abandoned/closed opencast mines. The overall backscattering response of the environmental parameters in HH- and VV-polarizations is closely similar. However, in some of the environmental parameters namely, settlements and vegetation, HH-polarization response is higher than that in VV polarization indicating dominantly a *Fresnel*-type surface scattering mechanism. On the other hand, in case of overburden/coal dumps, abandoned/closed opencast mines and coal washeries, HH-polarization response is lower than that in VV-polarization which indicates dominantly a *Bragg*-type surface scattering mechanism. For the remaining environmental parameters namely, functional opencast mines, barren land, fallow land, agricultural land and water bodies (irregular outline), HH- and VV-polarization responses are similar which suggests that both the scattering mechanisms are operating equally for these environmental parameters.

The relative differences in HH- and VV-polarization responses describes the variation in surface scattering strength due to the differences in the relative proportion of *Fresnel* vs. *Bragg* scatterers in the environmental parameters. This is primarily governed by the parameters namely, surface geometry (or terrain ruggedness), surface roughness, and wetness (dielectric property) of the surface materials. A sufficiently high HH-polarization response compared to that in VV-polarization in case of

settlements can be considered to be caused due to strong surface scattering from dihedral *Fresnel* scatterers.

In cross polarization (HV-), the mean backscattering response is high in case of settlements, vegetation and functional opencast mines; moderate in case of agricultural land, barren land and functional opencast mines followed by fallow land and coal washeries; and low in case of water body and abandoned/closed opencast mines. The backscattering strength in cross-polarization (HV-) is due to two main scattering processes: volume scattering as a function of dielectric inhomogeneity and multiple (surface-) scattering as a result of strong variation in surface geometry or terrain ruggedness.

A line diagram showing the variation of mean backscattering coefficients of the environmental parameters describes the relative separability of the environmental parameters in space borne C-band multi-polarizations data(Fig. 6.4.2)

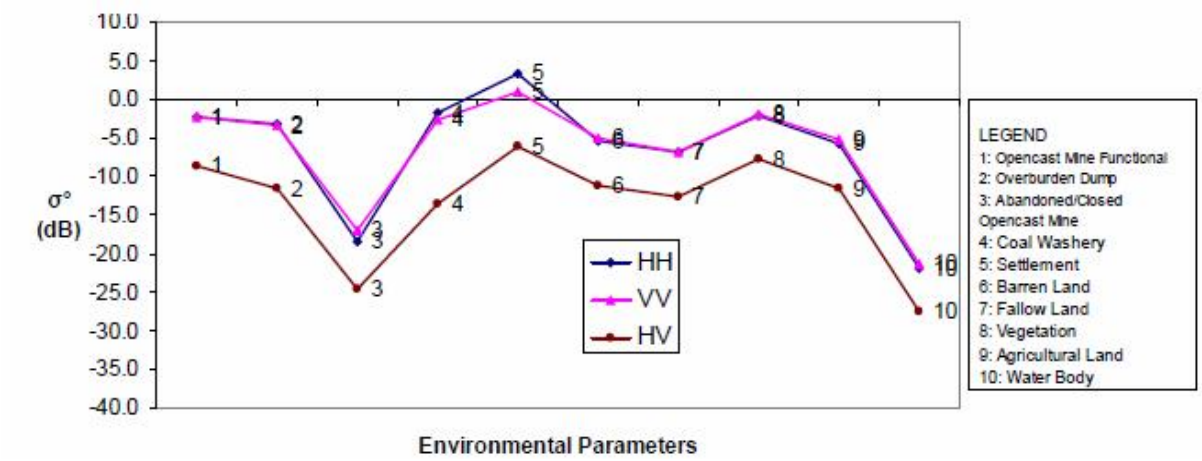

Fig. 6.4.2: Line diagram showing the variation of mean backscattering coefficient of the environmental parameters in ENVISAT ASAR C-band HH-, VV- and HV-polarization data of Jharia Coalfield

The randomness of the scattering process (entropy) in different polarizations (HH-, VV- and HV-) has been studied comparing the standard deviation values of backscattering coefficient for different environmental parameters. The exercise has been performed only in case of ENVISAT ASAR C-band multi-polarization data (Table 6.41, Fig. 6.4.3). It is observed that in case of HH polarization (with dominantly *Fresnel* scattering), the scattering process is largely uniform in case of functional opencast mines, barren land, agricultural land, settlements; and moderate to less uniform in case of overburden/coal dumps, abandoned/closed opencast mines, coal washeries, fallow land, vegetation and water bodies (irregular outline). In case of VV polarization (with dominantly *Bragg* scattering), the scattering process is largely uniform in case of functional opencast mines, settlements, barren land, agricultural land and fallow land; moderately uniform in case of vegetation, overburden/coal dumps and water bodies (irregular outline), and less uniform in case of abandoned/closed opencast mines and coal washeries.

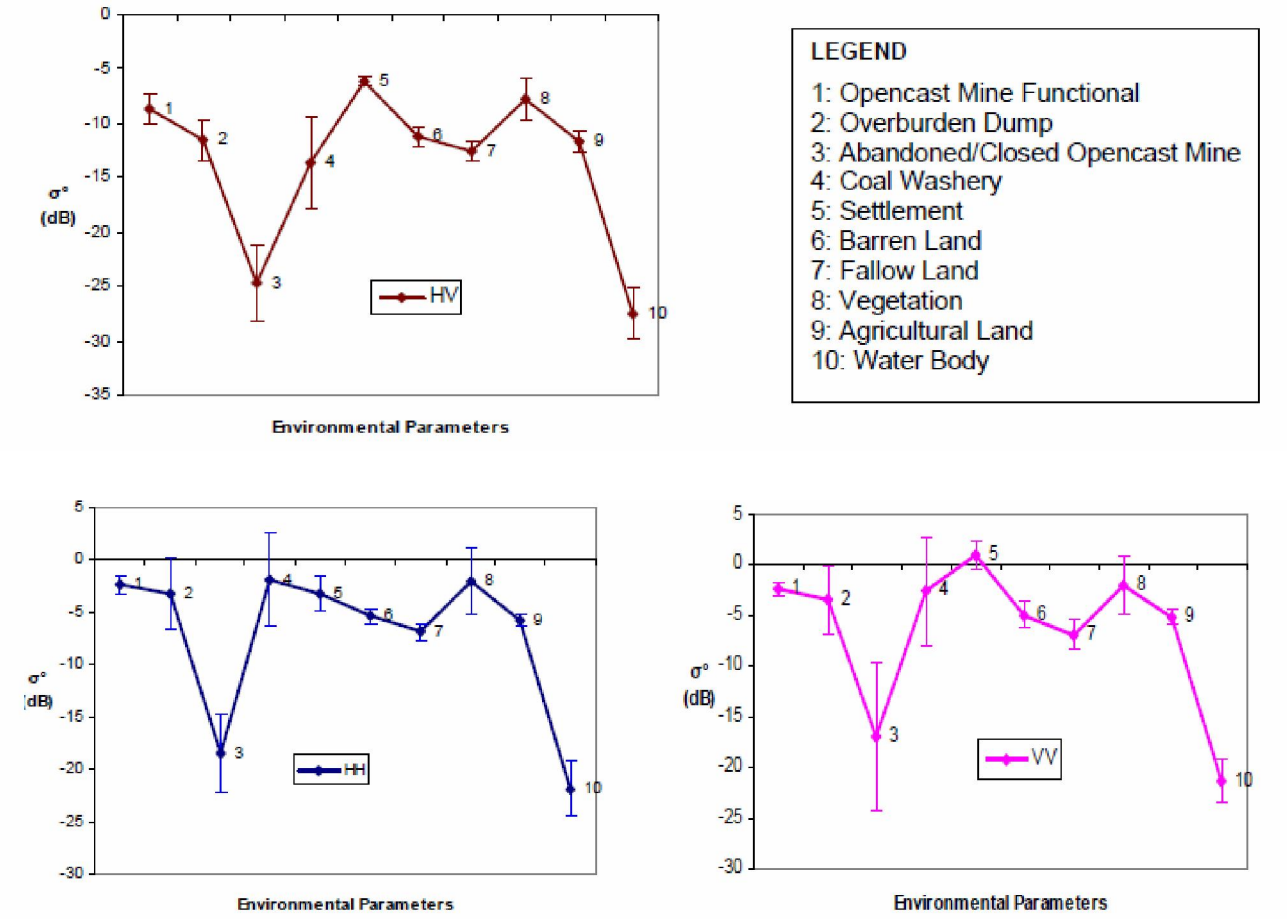

Fig.6.4.3: Mean backscattering coefficient with standard deviation as error bar for different environmental parameters in HH-, VV- and HV-Polarizations of ENVISAT ASAR data

In case of HV-polarization (with dominantly volume scattering), the scattering process is largely uniform in case of settlements, barren land, agricultural land, functional opencast mines, overburden/coal dumps and vegetation, and moderate to less uniform in case of abandoned/closed opencast mines, coal washeries, fallow land and water body (irregular outline).

CHAPTER 7

CONCLUSION

From environmental impact point of view, land subsidence in Jharia coal field has been a major concern throughout the decades. As discussed extensively about the effect of active and residual subsidence due to coal mining in chapter 3, Un-planned underground mining, depillaring of the old/abandoned underground mines and also the subsurface coal fire are the main causes of land subsidence in Jharia coal field.

In the present work, an attempt has been made to detect and delineate the land subsidence of Jharia coal field using an integrated space and ground based approach. Space borne DInSAR technique was utilized over the period of five years (from 2003 to 2007) to detect the ground movement/ subsidence over the Jharia coal field. DInSAR technique provides a spatially continuous perspective of the ground deformation over a time series, as compared to the Ground based techniques like Geodetic GPS and optical leveling provides the same but only along the point of observations. Thus in the present study, DInSAR technique for entire Jharia coal field and ground based GPS and Optical leveling survey were carried out for four selected study area known to be subsiding due to underground mining, depillaring of the abandoned working and coal fire for detection and validation of the techniques and results respectively.

Due to extensive mining processes, rapid urbanization and also the surfacial feature development along with the coal mines (e.g. coal dump over burden dumps), makes the Jharia coalfield highly dynamic, which has caused hindrance to the land subsidence rate measurement using DInSAR technique for the said time series due to high temporal and spatial decorrelation. Topographic compensation is one of the key parameter for land subsidence measurement using DInSAR technique. Land subsidence phenomena in a typical coal mining area occurs generally in localized patches, resulted in smaller deformation fringes. Thus, if high resolution digital elevation model is not available for the topographic compensation, the deformation fringes generated by the DInSAR technique will always contain some topographic fringes along with the deformation, resulting ambiguity in the interpretation. Even though Space borne DInSAR technique has been found highly efficient in detecting the land subsidence phenomena in the Jharia coalfield. The GPS and optical leveling measurements of the four study areas reveals nonlinear movement/displacements and the non-linearity is mainly due to the subsidence caused due to coal fire and or residual subsidence due to underground mining /depillaring of old underground workings.

As the land subsidence in Jharia coal field has a major impact on the environment as well as the people living there, continuous monitoring of the land subsidence is very necessary using both space and ground based techniques. A highly coherent L-band SAR DInSAR, Permanent Scatterer technique can be useful for monitoring land subsidence phenomena in Jharia coal field due to its dynamicity of the terrain over time by urbanization and also mining impact.

An attempt has also being made to utilize Digital elevation model to delineate the mining related landform feature in Jharia coalfield. It has been observed the Photogrammetric digital elevation model from high resolution CARTOSAT-1 stereo data can be able to detect the small coal dump or overburden dump features due to its higher spatial resolution. On the other hand the InSAR based digital elevation model (SRTM, ERS-tandem pair) has the capability of detecting abandoned and also opencast mine boundary and shapes due its terrain sensitivity parameters.

Using space borne multi-polarized SAR data the various environmental factors were mapped. Based on the backscatter coefficient of the different environmental factors in VV,HH,HV polarization the scattering properties were identified. Settlements and vegetation show fresnel type surface scattering, over burden dumps, coal dumps, abandoned mines, open cast mines and other mining related land features shows braggs type of surface scattering. The scattering process in some of the environmental parameters namely, functional opencast mines, settlements, barren land and agricultural and, is largely uniform in both co- and cross-polarizations (HH-, VV- and HV-) independent of the scattering mechanism. In other environmental parameters, the randomness in the scattering process varies as a function of the polarization and therefore the scattering mechanism.

List of Figures

List of Tables

REFERENCES

Ahmed. N., Mahtab. A., Agrawal. R., Jayaprasad. P.,Pathan. S. K., Ajai., Singh. D.K., Singh. A. K., (2007). Extraction and validation of cartosat-1 DEM. Photonirvachak Journal of the Indian Society of Remote Sensing, Vol. 35, No. 2,pp121-127.

Amelung, F., Galloway. D.L.,. Bell. J.W., Zebker. H.A., and Laczniak. R.J., (1999). Sensing the ups and downs of Las Vegas: InSAR reveals structural control of land subsidence and aquifer system deformation. *Geology*, 27(6), 483-486.

Amelung, F., Jonson. S., Zebker. H.A., and Segall. P., (2000). Widespread uplift and 'trapdoor' faulting on Gal_pagos volcanoes observed with radar interferometry. *Nature*, 407, 993-996.

Abidin. H.Z., Jones. A. , Kahar. J., (2002). Survei Dengan GPS. P.T. Pradnya Paramita, Jakarta. ISBN 979-408-380-1. Second Edition. 280 pp.

Abidin, H. Z., R. Djaja, D. Darmawan, S. Hadi, A. Akbar, H. Rajiyowiryono, Y. Sudibyo, I. Meilano,M. A. Kusuma, J. Kahar, C. Subarya (2001). "Land Subsidence of Jakarta (Indonesia) and its Geodetic-Based Monitoring System." Natural Hazards. Journal of the International Society of the Prevention and Mitigation of Natural Hazards, Vol. 23, No. 2/3, March, pp. 365 - 387

Abidin, H.Z., H. Andreas, M. Gamal, M. Hendrasto, O.K. Suganda, Surono (2004). " The Use of GPS Surveys Method for Natural Hazard Mitigation in Indonesia". Proceedings of the Monitoring, Prediction and Mitigation of Disasters by Satellite Remote Sensing, Awaji, Jepang, 19-21 Januari, pp. 95-112

Ashutosh, A., (2002). Two mine mishaps in state, one person dead. Times of India, September 21, 2002. Bennett, Coleman & Co. Ltd., Bombay. Retrieved May 22, 2003 from http:// timesofindia.indiatimes.com/ cms.dll/ html/ uncomp/articleshow?art_id = 22807569.

Arefi. H., d'Angelo. P., Mayer. H., Reinartz. P.,(2011). Iterative approach for efficient digital terrain model production from CARTOSAT-1 stereo images. Journal of Applied Remote Sensing 5 (1), 053527.

Barsi, J.A., Schott, J.R., Palluconi, F.D., Helder, D.L., Hook, S.J., Markham, B.L., Chander, G., O'Donnell, E.M., (2003). Landsat TM and ETM+ thermal band calibration. Canadian Journal of Remote Sensing 29 (2), 141–153

Barapanda. P., Singh. S. K. and Pal. B.K., (2001). Utilization of coal mining wastes: An Overview, National Seminar on Environmental Issues and Waste Management in Mining and Allied Industries, Regional Engg College, Rourkela, Orissa, India.pp. 177 182.

Becker B (1997) Sustainability assessment: a review of values, concepts, and methodological approaches. Consultative Group on International Agricultural Research, The World Bank, Washington, DC, USA, p 70.

Bharat Coking Coal, (2003.) Brief history of BCCL. Dhanbad, Bharat Coking Coal Ltd. Retrieved August 20, 2003 from http://bccl.nic.in/About-us.htm

Bhattacharya, A., Reddy, C.S.S., (1992). Airborne scanner survey and data analysis for underground and surface coal mine fire detection in Jharia Coalfield, Bihar. Report from the Geosciences Division Applications Group, National Remote Sensing Agency Hyderabad, (India), Report No. NRSA-AG-GD-TR-2/92

BCCL Annul Report (2008)

Brauner. G.,(1973). Subsidence due to Underground mining: Part II. Ground movement and mining damages .53 pp. Washington DC: Bureau of Mines, Department of the Interior, US government Printing office.

Berardino. P., Fornaro. G., Lanari, R., (2002). A new algorithm for surface deformation monitoring based on small baseline differential SAR interferograms. IEEE Transactions on Geoscience and Remote Sensing 40 (11), pp. 2375–2383.

Carnec. C., King. C., and Massonet. D., (1995) Measurement of land subsidence by means of differential SAR Interferometry. In FBJ Barends, FJJ Brouwer, and FH Schoder (Eds), Land subsidence:139-148, Rotterdam, AA Balkema Publishers.

Cartosat-1 Data User's Handbook, (2006). <http://bhuvan.nrsc.gov.in/bhuvan/PDF/ cartosat1.pdf>

Chandra. D., & Chakraborty. N.C., (1989). Coalification trends in Indian coals. International Journal of Coal geology.13, pp. 413-435.

Chandra. D., (1992) Jharia Coalfield. Geological Society of India, Bangalore.

Chandra. D., Sinha. A., (1988). An analytical review of fatal accidents in Indian coal mines. Trans. Min. Geol. Metall. Inst. India,85,2,pp.71-89.

Chattejee. R.S., Benedicte. F., Rudant. J.P., Roy. P.S ., Pierre-Louis. F., Lakhera. R.C.,.Dadhwal. V.K., and Ranajit. S., (2006). Subsidence of Kolkata (Calcutta) City, India during the 1990s as obserbed from space by Differential Synthetic Aperture Radar Interferometry (D-InSAR) technique. *Remote Sensing of Environment* 102: 176-185

Chatterjee. R.S., Banerjee. D., Roy. J. and Bhattacharya. A.K., (1994). Landsat TM data processing techniques for identifying and delineating environmental impacts of coal mining, *ITC Journal*, 1994-2: pp.155-162.

Colesanti, C., Ferretti. A., Prati. C., Rocca. F., (2001). Comparing GPS, optical levelling and Permanent Scatterers. Proceedings of the IEEE International Geoscience and Remote Sensing Symposium (IGARSS 2001), Sydney, 9–13 July, 2001, vol. 6, pp. 2622–2624.

Costantini. M., and Rosen. P., (1999). A generalized phase unwrapping approach for sparse data. *Proc. Int. Geosci. Remote Sensing Symp.*, Hamburg, Germany, June 28-July 2 1999, pp. 267-269.

Crosetto. M., Arnaud. A., Duro. J., Biescas. E., and Agudo. M.,(2003) Deformation monitoring using remotely sensed radar interferometric data. Proceedings, 11th FIG Symposium on Deformation Measurements, Santorini, Greece.

Crosetto. M., Tscherning. C.C. , Crippa. B., and. Castillo. M., (2002). Subsidence Monitoring using SAR interferometry: reduction of the atmospheric effects using stochastic filtering. *Geophys. Research Letters*, Vol. 29(9), pp.26-29.

Franceschetti. G., Lanari. R.,(1999). (*Eds*)Synthetic Aperture Radar Processing. CRC Press, New York.

Fox. C.S., (1930), The Jharia Coalfield, *Memoir Geological Survey of India*, 56: 159p.

Ferretti. A., Prati. C., Rocca. F., (1999a). Multi baseline InSAR DEM reconstruction: the wavelet approach. IEEE Transactions on Geoscience and Remote Sensing 37 (2), 705–715.

Ferretti. A., Prati. C., Rocca. F., (1999b). Permanent scatterers in SAR interferometry. Proceedings of the IEEE International Geoscience and Remote Sensing Symposium (IGARSS 1999), Hamburg (Germany), 28 June– 2 July 1999, vol. 3, pp. 1528–1530.

Ferretti. A., Prati. C., Rocca. F.,(2000a). Nonlinear subsidence rate estimation using Permanent Scatterers in Differential SAR Interferometry. IEEE Transactions on Geoscience and Remote Sensing 38 (5), 2202–2212.

Ferretti. A., Ferrucci. F., Prati. C., Rocca. F., (2000b). SAR Analysis of Building Collapse by means of the Permanent Scatterers Technique. Proceedings of IEEE International Geoscience and Remote Sensing Symposium (IGARSS 2000), Honolulu (USA), vol. 7, pp. 3219–3221.

Ferretti. A., Prati. C., Rocca. F., (2001a). Permanent Scatterers in SAR Interferometry. IEEE Transactions on Geoscience and Remote Sensing 39 (1),pp. 8–20.

Ferretti. A., Prati. C., Rocca. F., (2001b). Multi baseline phase unwrapping for InSAR topography estimation. Il Nuovo Cimento 124 (1), 159–176.

Ferretti. A., Perissin. D., Prati. C., Rocca. F., (2005). On the physical nature of SAR Permanent Scatterers. Proceedings of the 2005 URSI Commission F Symposium on Microwave Remote Sensing of the Earth, Oceans, Ice, and Atmosphere, Ispra (Italy), 20–21 April 2005.

Feretti. A., Cespa. S., Novali. F., Perissin. D.,, Rocca. F., Pratti. C., (2006) PSInSAR: Using satellite radar data to measure surface deformation remotely. 3rd IAG/12th FIG Symposium. Baden, May 22-24.

Fruneau. B., and Sarti. F., (2000) Detection of ground subsidence in the city of Paris using radar interferometry: Isolation from atmospheric artefacts using correlation. *Geophys. Res. Lett.*, **27**, p3981–3984

Gabriel. A.K., Goldstein. R.M., and Zebker. H.A., (1989). Mapping small elevation changes over large areas: differential radar interferometry. *J. of Geophys. Research*, 94(B7),pp. 9183-9191.

Galloway. D.L., Hudnut. K. W., Ingebritsen. S. E., Phillips. S. P., Peltzer. G., Rogez. F., and Rosen. P.A., (1998).Detection of aquifer system compaction and land subsidence using interferometric synthetic aperture radar, Antelope Valley, Mojave Desert, California. Water Resources Research, Vol. 34, No. 10, P 2573–2585

Ghosh. R. and Ghosh. D.N., (1990), Landuse map of Jharia Coalfield, Eastern India, aided by remote sensing, *Photonirvachak, Journal of the Indian Society of Remote Sensing* 18(1&2):23-27.

Ghosh. S.K., & Mukhopadhyay. (1985) Tectonic history of the Jharia basin-an intracratonic Gondwana basin in eastern India. Quart. J. Geol. Min. Metall. Soc. India. 57,1,pp 33-58.

Ghosh. R.,(1987a). Land use and land protectionin mining areas- A case study of the Jharia coalfield. J. Geol. Soc. India, 29,2,pp 250-255.

Ghosh. R.(1987b). Geological considerations for urban development in Jharia coalfield, Eastern India, Role of Geology in urban development, Geological Society of Hong Kong, Bull. No.3. 87-96.

Ghosh. R., (1988), Environmental impact of coal mining in Jharia Coalfield, Eastern India – its past, present and future, *Trans. Min. Geol. Metall. Inst. India* 85(2):90-98. *Memoir Geoloigical Survey of India*, 1964 84(2).

Ghosh R., (2002). Land use in mining areas of India. Envis Monograph No.9 by CME, ISSN: 0972 4656.

Goldstein. R.M., H. Englehardt, B. Kamb and R.M. Frolich (1993). Satellite radar interferometry for monitoring ice sheet motion: application to an Antarctic ice stream. *Science*, 262, 1525-1530.

Goldstein. R.M., (1995) Atmospheric limitations to repeat-track radar interferometry, *Geophys. Res. Lett.*, *22*(18), 2517–2520,.

Hanssen. R.F., (2001) *eds.* Radar Interferometry: data interpretation and error analysis, Kluwer Academic Publishers, The Netherlands.

Hansen. R.F., (2005): Satellite radar interferometry for deformation monitoring: a priori assessment of feasibility and accuracy. – International Journal of Applied Earth Observation and Geo-information, 6,253–260.

Hansen. R.F., & Ferretti. A., (2002): Deformation Monitoring by Satellite Interferometry. – GIM International, 16/9, 52–57.

Hooper, A., (2008). A multi-temporal InSAR method incorporating both persistent scatterer and small baseline approaches. Geophysical Research Letters 35,.

Hooper. A., Segall. P., Zebker. H., (2007). Persistent scatterer InSAR for crustal deformation analysis, with application to Volcan Alcedo, Galapagos. Journal of Geophysical Research 112.

Hofmann-Wellenhof. B., Lichtenegger. H., and Collins. J., (1997) Global Positioning System, Theory and Practice, Fourth Revised Edition, Springer Verlag, Wien

Houtenbos. A.P.E.M., Micheline. W.A.H., and Frans. B.J.B., (2005) Subsidence from geodetic measurements in the Ravenna area. *Proceedings of the Seventh International Symposium on Land Subsidence*, Shanghai, PR China, October 23-28.

Jacobsen. W.E., Bhutani. J.S., and Elliot. J.C., 1975, "Subsidence Monitoring in Conjunction With Underground Mine Flushing Operations," Report by MITRE Corporation for US Bureau of Mines, Contract No. S0144073, Oct. PB 250818, 155 pp.

Jacobsen, K., (2004). DEM generation from satellite data. In: Goossens, R. (Ed.): Remote Sensing in Transition. In: Proceedings 23rd EARSeL symposium 2003, Ghent, Belgium, pp. 513–525.

Lanari. R., Mora. O., Manunta. M., Mallorqui. J.J., Berardino. P., Sansosti. E., (2004). A small baseline approach for investigating deformations on full resolution Differential SAR Interferograms. IEEE Transactions on Geoscience and Remote Sensing 42, 1377–1386.

Lee. H.Y., Kim. T., Park. W., Lee. H.K., (2003). Extraction of digital elevation models from satellite stereo images through stereo matching based on epipolarity and scene geometry. Image and Vision Computing 21 (9), 789–796.

Leick. A., (1995) GPS Satellite Surveying, John Wiley & Sons, Second Edition, New York, ISBN 0-471-30626-6, 560 pp.

Leica Photogrammetric Suite user Handbook.

Li. Z., Zhu. Q., Gold. C.,(2005). Digital Terrain Modeling: Principles and Methodology. CRC.

Mansor. S.B., Cracknell. A.P., Shilin. B.V., Gornyi. V.I., (1994). Monitoring of underground coal fires using thermal infrared data. International Journal of Remote Sensing 15 (8), 1675–1685.

Morgan. T.A., (1973) "Coal Mine Roof Problems," *Proceedings Bureau of Mines Technology Transfer Seminar,* Lexington, KY.

Massonnet. D., and Feigl. K.L., (1998) Radar interferometry and its applications to changes in the earth's surface. *Reviews of Geophysics*, 36(4), 441-500.

Massonnet. D., Rossi. M., Carmona. C., Adragna. F., Peltzer. G., Feigl. K., Rabaute. T., (1993). The displacement field of the Landers earthquake mapped by Radar Interferometry. Nature 364, 138–142.

Massonnet. D., Briole. P., Arnaud. A., (1995). Deflation of Mount Etna monitored by Spaceborne Radar Interferometry. Nature 375, 567–570.

Massonnet. D., Vadon. H., Rossi. M., (1996). Reduction of the need for phase unwrapping in Radar Interferometry. IEEE Transactions on Geoscience and Remote Sensing 34, 489–497.

Massonnet. D., T. Holzer. and Vadon. H. , (1997) Land subsidence caused by the East Mesa geothermal field, California, observed using SAR interferometry, *Geophys. Res. Lett*., *24*(8), 901–904,.

Michalski. S. R. (2004). The Jharia mine fire control technical assistance project: an analysis. International Journal of Coal Geology, Volume 59, Issues 1–2, 12 July 2004, Pages 83-90.

Michalski, S.R., Gray, R.E., (2001). Ash disposal—mine fires—environment: an Indian dilemma. Journal of the International Association for Engineering Geology and the Environment 60 (1),23– 29.

Moffitt, F.H., and Bouchard, H., (1975). *Surveying,* 6th ed., Intext Education Publishers, New York.

Mukhopadhyay. A.,(1981) Structural evolusion of the Jharia coal basin, Eastern INdia. Ph.D. thesis, Jadavpur University, Calcutta. p.90.

Muralikrishnan. S., Pillai. A., Narender. B., Reddy. S., Venkataraman. V.R., Dadhwal. V.K.,(2012). Validation of Indian national DEM from Cartosat-1 data. Journal of the Indian Society of Remote Sensing 40 (1), 1–13.

Nandakumar. R., Chamy. M.P.T., Kopparthi. S.S.S., Paswan. G., Prakash. S., Singh. S., (2008). Synthesis of investigations under ISPRS-ISRO Cartosat-1 scientific assessment programme primarily for DSM generation. International Archives of the Photogrammetry, Remote Sensing and Spatial Information Science 37 (Part B1), 1279–1286.

Navalgund. R.R., Jayaraman. V., Roy. P.S., (2007). remote sensing applications: An overview. Current Science 93 (12), 1747–1766.

Panek. L.A., (1970), "Method and Equipment for Measuring Subsidence," *Proceedings, 3rd Symposium on Salt,* Vol. 2, Northern Ohio Geological Society, pp. 321–338.

Piggott. J., and Eynon, P., (1977) 'Ground Movements Arising From the Presence of Shallow Abandoned Mine Workings,' *Large Ground Movements and Structures: Proceedings Conference at University of Wales Institute of Science and Technology,* Cardiff, Wales, J.D. Geddes, ed., Wiley, New York, pp. 749–780.

Prakash. A., Saraf, A.K., Gupta, R.P., Dutta, M., Sundaram, R.M., (1995). Surface thermal anomalies associated with underground fires in Jharia Coal Mines, India. International Journal of Remote Sensing. 16 (12), 2105–2109.

Prakash. A., Gupta, R.P., Saraf, A.K., (1997). A Landsat TM based comparative study of surface and subsurface fires in the Jharia Coalfield, India. International Journal of Remote Sensing 18 (11), 2463–2469.

Prakash. A .,and Gupta. R.P., (1998), Land-use mapping and change detection in a coal mining area – a case study in the Jharia Coalfield, India, *International Journal of Remote Sensing* 19(3):391-410.

Prakash. A., Gens. R., Vekerdy. Z., (1999). Monitoring coal fires using multi-temporal night-time thermal images in a coalfield in northwest China. International Journal of Remote Sensing 20 (14),2883–2888.

Prasad. S.N., Rao. M.N.A., Mookerjee.A., (1984) Mine planning- A step towards modernisation of coal mining in India, Coal Mining in India, CEMPDIL, Ranchi, 73-85

Rathore .C.S., and Wright. R., (1993). Monitoring environmental impacts of surface coal mining, *International Journal of Remote Sensing* 14(6):1021-1042.

Raucoules. D., Colesanti. C., Carnec. C., (2007) Use of SAR interferometry for detecting and assessing ground subsidence. C. R. Geoscience 339 289–302

Reddy, C.S.S., Srivastav, S.K., Bhattacharya, A., (1993). Application of thematic mapper short wavelength infrared data for the detection and monitoring of high temperature related geo-environmental features. International Journal of Remote Sensing 14 (17), 3125–3132

Rosen. P. A., Hensley. S.H., Zebker. A., Webb. F. H., and Fielding. E., (1996). Surface deformation and coherence measurements of Kilauea volcano, Hawaii, from SIR-C radar interferometry, *J. Geophys. Res*., *101*(E10), 23,109 –23,125.

Rosen. P.A., Hensley. S., Joughin. I.R., Li. F.K., Madsen. S.N., Rodriguez. E., Goldstein. R.M., (2000). Synthetic Aperture Radar Interferometry. Proceedings of the IEEE, vol. 88, pp. 333–37.

Rellensmann. O., and Wagner. E., (1957), "The Effect on Railways of the Ground Movements Due to Mining," *Proceedings European Congress on Ground Movement,* University of Leeds, Leeds, UK, pp. 74–82.

Saraf. A.K., Prakash. A., Sengupta. S., Gupta. R.P., (1995). Landsat TM data for estimating ground temperature and depth of subsurface fire in Jharia Coalfield, India. International Journal of Remote Sensing 16 (12), 2111–2124.

Saxena. N.C., and Singh. B., (1980), "Investigations into the Safety of the Railway Line Against Ground Movement Due to Extraction of Two Thick Seams in India, *Proceedings, 21st US Symposium on Rock Mechanics,* University of Missouri, Rolla, MO, Sep., pp. 345–354.

Schori, A., Scrymgeour, A.H., Munshi, P.L., (1997). Environment management plan for the Jharia Coalfield. Proceedings 14th Annual Meeting of the American Society for Surface Mining and Reclamation, Austin, TX, May 10–15.

Sengupta. N.,(1980). A revision of the Geology of the Jharia coalfield with particular reference to distribution of coal seams, Ph. D thesis, Indian School of Mines, Dhanbad.

Singh. M.M., and Kendorski. F.S., (1981). "Strata Disturbance Prediction for Mining Beneath Surface Water and Waste Impoundments," *Proceedings 1st Conference on Ground Control in Mining,* West Virginia University, Morgantown, WV, pp. 76–89.

Singh. M.M., (1985), "Review of Coal Mine Subsidence Control Measures," *Transctions SME-AIME,* Vol. 278, Littleton, CO, pp. 1988– 1992.

Sinha.P.R., (1986). Mine fires in Indian coalfields. Energy,2,11/12,pp. 1147-1154.

Srivastava.V.K., Yadav. R., and Sadhu. P., (1989). Status of environmental hazard in Jharia coalfield. Journal of Engineering Geology 18.1& 2, pp 65-73.

Srivastava. P.K., Gopala Krishna. B., Srinivasan. T., Amitabh. Trivedi. S., Nandakumar. R., (2006). Cartosat-1 data products for topographic mapping. International Archives of Photogrammetry, Remote Sensing and Spatial Information Sciences 37 (Part 4), 1357–1362.

Srivastava. P.K., Srinivasan. T.P., Gupta. A., Singh. S., Nain. J.S., Amitabh. P.S., Kartikeyan. B., Gopala. K.B., (2007). Recent advances in CARTOSAT-1 data processing. International Archives of the Photogrammetry, Remote Sensing and the Spatial Information Sciences 36

Strozzi. T., Wegmüller. U., Tosi. L., Bitelli. G., and Spreckels. V., (2001) Land subsidence monitoring with differential SAR interferometry. *Photogrammetric Engineering and Remote Sensing* 67(11): 1261−1270

Strozzi. T., Wegmüller. U., Werner. C.L., Wiesmann. A., and Spreckels. V., (2003) JERS SAR interferometry for land subsidence monitoring. *IEEE Transactions on Geosciences and Remote Sensing* 41(7): 1702−1708

Usai. S., (2001) A New Approach for Long Term Monitoring of Deformations by Differential SAR Interferometry, Delf University Press, The Netherlands

Wells. D.E., Beck. N., Delikaraoglou. D., Kleusberg. A., Krakiwsky. E.J., Lachapelle. G., Langley. R.B., Nakiboglou. M., Schwarz. K.P., Tranquilla. J.M., and Vanicek. P. (1986), *Guide to GPS Positioning*, Canadian GPS Associates, Fredericton

Xia. Z.G., and Henderson. F.M.,(1997). Understanding the Relationship Between Radar Response Patterns and The Bio- and Geophysical Parameters of Urban Areas. *IEEE Transactions on Geoscience and Remote Sensing* 35(1): 93-101.

Zebker.. H.A., Goldstein. R.M., (1986). Topographic mapping from Interferometric Synthetic Aperture Radar observations. Journal of Geophysical Research 91 (B5), 4993–4999.

Zebker. H.A., Villasenor. J., (1992). Decorrelation in Interferometric Radar Echoes. IEEE Transactions on Geoscience and Remote Sensing 30, 950–959

Zhang, X., Van Genderen, J.L., Kroonenberg, S.B., (1997). A method to evaluate the capability of Landsat-5 TM band 6 data for sub-pixel coal fire detection. International Journal of Remote Sensing 18 (15), 3279–3288.

Zhang, J., Wagner, W., Prakash, A., Mehl, H., Voigt, S.,(2004). Detecting coal fires using remote sensing techniques. International Journal of Remote Sensing 25 (16), 3193–3220.